University of Cyprus

DEPARTMENT OF ELECTRICAL AND COMPUTER ENGINEERING

DC ORIENTED PHOTOVOLTAIC (PV) INTERFERENCE ON UNDERGROUND METALLIC PIPELINE SYSTEMS

DOCTOR OF PHILOSOPHY DISSERTATION

ANDREAS DIMITRIOU

2020

DEPARTMENT OF ELECTRICAL AND COMPUTER ENGINEERING

DC ORIENTED PHOTOVOLTAIC (PV) INTERFERENCE ON UNDERGROUND METALLIC PIPELINE SYSTEMS

ANDREAS DIMITRIOU

A dissertation submitted to the University of Cyprus in partial fulfillment of the requirements for the degree of Doctor of Philosophy

April 2020

Validation Page

Doctoral Candidate: *Andreas Dimitriou*

Doctoral Thesis Title: *DC Oriented Photovoltaic (PV) Interference on Underground Metallic Pipeline Systems*

The present Doctoral Dissertation was submitted in partial fulfillment of the requirements for the degree of Doctor of Philosophy at the ***Department of Electrical and Computer Engineering*** *and was approved on the 24th of April by the members of the* ***Examination Committee.***

Examination Committee:

Research Supervisor:

_____

(Dr. Charalambos A. Charalambous, Associate Professor)

Committee Member:

_____

(Dr. George Georghiou, Professor)

Committee Member:

_____

(Dr. Julius Georgiou, Associate Professor)

Committee Member:

_____

(Dr. Pantelis Mikropoulos, Professor)

Committee Member:

_____

(Dr. Ioannis Gonos, Associate Professor)

Declaration of Authorship

The present doctoral dissertation was submitted in partial fulfillment of the requirements for the degree of Doctor of Philosophy of the University of Cyprus. It is a product of original work of my own, unless otherwise mentioned through references, notes, or any other statements.

……

Andreas Dimitriou
Department of Electrical and Computer Engineering
University of Cyprus
April, 2020

Περίληψη

Η διατριβή πραγματεύεται ένα νέο θέμα που λαμβάνει σταδιακά την προσοχή της βιομηχανίας φωτοβολταϊκών (ΦΒ) εγκαταστάσεων και των διαχειριστών κρίσιμων υποδομών. Πρώτα από όλα, η διατριβή παραθέτει το θεωρητικό υπόβαθρο που υποστηρίζει την καθιέρωση μιας καινούργιας ιδέας που αφορά στην εμφάνιση διαβρωτικών διαφυγόντων ρευμάτων από ΦΒ συστήματα. Εισάγεται συγκεκριμένα η έννοια των "τυφλών σημείων διάβρωσης από διαφυγόντα συνεχή-ρεύματα (ΣΡ)" τα οποία είναι συνυφασμένα με τα ΦΒ συστήματα γείωσης και τους μηχανισμούς αναγνώρισης σφαλμάτων. Τα τυφλά σημεία προκύπτουν ως συνέπεια των παγιωμένων πρακτικών προστασίας οι οποίες οριοθετούν το μέγεθος των επιτρεπόμενων ρευμάτων διαρροής βάσει κριτηρίων, τα οποία βασίζονται σε θέματα όπως η έκρηξη πυρκαγιάς και ηλεκτροπληξίας. Χρησιμοποιώντας το έδαφος ως αγώγιμο μέσο, τα ρεύματα διαρροής μπορούν να ξεφύγουν από την περιοχή των ΦΒ εγκαταστάσεων και να δημιουργήσουν προβλήματα παρεμβολών σε τρίτες υποδομές κρίσιμης σημασίας. Η ενεργοποίηση της ΦΒ παρεμβολής στις υποδομές αυτές επεξηγείται ηλεκτρικά, παρέχοντας πληροφορίες για το σχηματισμό των διαφυγόντων ΣΡ ρευμάτων.

Δεύτερον, επιτυγχάνεται η ανάπτυξη κατάλληλων τεχνικών μοντελοποίησης οι οποίες βασίζονται στη θεωρία που αναδεικνύει τα επικρατούντα ηλεκτρικά χαρακτηριστικά των ΦΒ συστημάτων - υπό κανονικές και εσφαλμένες συνθήκες λειτουργίας – τα οποία προξενούν παρεμβολές και προβλήματα διάβρωσης σε υπόγειες κρίσιμες υποδομές. Οι τεχνικές μοντελοποίησης αναλύονται και επαληθεύεται η ικανότητά τους να αναπαράγουν τα αναμενόμενα διαφυγόντα ρεύματα μέσω μιας εμπορικά διαθέσιμης πλατφόρμας λογισμικού. Αναπτύσσονται τοπολογικά-ακριβή μοντέλα προσομοίωσης ρεαλιστικών περιπτώσεων, για την εξέταση της ΦΒ παρεμβολής σε υπόγειους σωληναγωγούς αξιολογώντας τη διαφορά δυναμικού μεταξύ εδάφους και σωλήνας. Οι κρίσιμες παράμετροι επηρεασμού της ΦΒ παρεμβολής αποκαλύπτονται μέσω πολλαπλών αναλύσεων ευαισθησίας και εναλλακτικών σεναρίων. Όπως επισημαίνεται από τα αποτελέσματα προσομοίωσης, η ΦΒ παρεμβολή παρουσιάζει ένα δυναμικό προφίλ, καθώς επηρεάζεται από τις περιβαλλοντικές συνθήκες σε ωριαία-, ημερήσια-, εποχική- βάση. Ιδιαίτερα η παρουσία μη ανιχνευμένων σφαλμάτων ως προς γη, επιδεινώνει δραματικά το πρόβλημα.

Επιπλέον, έχουν πραγματοποιηθεί δυναμικές προσομοιώσεις, προκειμένου να επιτευχθεί εις βάθος κατανόηση της ΦΒ παρεμβολής σε σωληναγωγούς κάτω από πραγματικές συνθήκες. Οι δυναμικές προσομοιώσεις παρέχουν πολύ σημαντικά συμπεράσματα καθώς και χρήσιμες

πληροφορίες που μπορούν να αξιοποιηθούν κατάλληλα στην αναγνώριση και τη μέτρηση της ΦΒ παρεμβολής σε υφιστάμενες εγκαταστάσεις. Τα μοναδικά χαρακτηριστικά της ΦΒ παρεμβολής επισημαίνονται και συγκρίνονται με άλλους τύπους συστημάτων / πηγών παρεμβολής ΣΡ. Έτσι, αναδύεται η ανάγκη ανάπτυξης μιας ειδικής μεθοδολογίας για τη μέτρηση της ΦΒ παρεμβολής. Για το σκοπό αυτό, παρέχονται κατευθυντήριες γραμμές για την αναγνώριση και μέτρηση της ΦΒ παρεμβολής σε τμήματα αγωγών που γειτνιάζουν με ΦΒ εγκαταστάσεις.

Τέλος, οι ερευνητικές προσπάθειες αυτής της εργασίας έχουν αναδείξει την ύπαρξη ενός υφέρποντος προβλήματος σχετιζόμενο με την διαβρωτική ΦΒ παρεμβολή που οφείλεται στη λειτουργία των ΦΒ εγκαταστάσεων. Υπό αυτό το πρίσμα, η σύσταση κανονισμών/οδηγιών ή υπηρεσιών για τη διαχείριση των κινδύνων διάβρωσης και πρακτικές μετριασμού της, είναι απαραίτητες για τη αρμονική και μακροχρόνια συνύπαρξη κρίσιμων υποδομών που βρίσκονται κοντά σε ΦΒ εγκαταστάσεις.

Ως πρώτη αναγνώριση του συνόλου των ερευνητικών εργασιών, μέρος του περιεχομένου που περιλαμβάνεται σε αυτή τη διατριβή συμπεριλήφθηκε κανονιστικά και ενημερωτικά στο πρότυπο ISO 21857 [FDIS] standard **"***Petroleum, petrochemical and natural gas industries — Prevention of corrosion on pipeline systems influenced by stray currents*", που θα εκδοθεί το Σεπτέμβριο του 2020.

Abstract

The thesis elaborates on a new issue that progressively receives attention by the photovoltaic (PV) installation industry and critical infrastructure's operators. First of all, the thesis provides the theoretical background that supports the idea of a novel concept regarding the emergence of corrosive stray currents from PV systems. It specifically introduces "DC stray current corrosion blind spots" that are inherent to PV systems' earthing and associated DC ground fault detection mechanisms. Blind spots arise as the existing protection thresholds for DC leakage currents have been based on other issues, such as fire or personnel safety. Using the soil as a conductive medium, DC leakage currents can stray from the area of PV installations and interfere with nearby third-party critical infrastructure. The PV interference mechanism on third-party infrastructures is electrically explicated, by providing insights for the formation of DC stray currents.

Secondly, the formulation of appropriate modelling techniques to further elaborate on the theory that describes the prevailing electrical characteristics of PV systems' -normal and faulty operation - that lead to interference and corrosion concerns on underground critical infrastructure is accomplished. The modelling techniques are analyzed and their ability to reproduce the expected stray currents in a commercially available software platform is verified. Topologically accurate simulation models of realistic case studies are developed to examine the PV interference on buried pipeline systems in terms of their spatial pipe-to-soil potentials. The critical parameters affecting the PV interference are revealed through multiple sensitivity analysis and *what-if* scenarios. As highlighted from the simulation results, PV interference has a dynamic profile since it is affected by environmental conditions in hourly-, daily-, seasonal- bases. Particularly, the presence of undetected ground faults dramatically exacerbates the problem.

Moreover, to acquire knowledge on realistic PV interference situations on pipeline systems, dynamic simulations have been performed. The dynamic simulations provide very important conclusions as well as useful insights that can be appropriately used in the identification and field-measurement of PV interference on pipeline systems. The unique characteristics of PV interference are highlighted and are compared with other types of DC interference systems/sources. Thus, the need for developing a special methodology for measuring PV interference emerges. To this end, guidelines are provided for the identification and measurement of PV interference on pipeline sections neighboring with PV plants.

Finally, the research efforts of this thesis have evidently introduced a hidden problem regarding the corrosive (stray current) PV interference due to the operation of PV plants. To this extent, the development of documentation or services for corrosion risk-management and mitigation practices is necessary for a harmonised and long-term coexistence of critical infrastructures located in proximity to PV plants.

As a first recognition of the whole research work, part of the contents described in this thesis has been normatively and informatively included in the ISO 21857 [FDIS] standard "*Petroleum, petrochemical and natural gas industries — Prevention of corrosion on pipeline systems influenced by stray currents*", that will be issued in September 2020.

Acknowledgments

First of all, I would like to express my heartfelt thanks to Dr. Charalambos A. Charalambous who stand by my side as a mentor, advisor as well as a friend throughout this journey. Your constant support, academic approach and high expertise in the field of stray current interference were instrumental in the completion of my postgraduate studies. It has been a great honor to be a member of PSM Lab for the last six years.

Also, I would like to thank my colleagues Antonis Lazari, Alexandros Nikolaidis and Christos Melios who have helped me a lot through their knowledge and skills. Our collaboration and friendship these years have been transformed into invaluable memories.

Finally, I would like to thank my family: my father Alexandros, my mother Kyriaki, my sister Fotini and brother my George for their unlimited and unconditional love. Your encouragement and support in various ways were significant to achieve the completion of this dissertation.

Contents

List of Figures

List of Tables

Chapter 1

Introduction

1.1 Introductory Remarks

It is well established that direct current (DC) systems can generate currents (intentional or unintentional) that flow through the earth or any other electrolyte. Such systems include DC traction systems [1], [2], cathodic protection systems [3], photovoltaic (PV) power systems [4] and high voltage DC (HVDC) transmission systems [5], [6]. Consequently, DC interference is a disturbance, provoked by DC systems' normal and/or faulty operation, that affects buried metallic infrastructures primarily by conduction that occurs through the earth or any other electrolyte. With regard to buried or immersed pipeline systems, the disturbance may take the form of accelerated corrosion on their external metallic surfaces [7].

To this extent, various international standards [1], [2], [5], [7], [8] dictate that all current-carrying conductors of DC power systems shall be insulated from earth. In exceptional cases, where earthing - of current currying conductors - is required, i.e. for personal safety, special care shall be taken in order to limit DC leakage to earth, as this may be leading to accelerated corrosion on third-party metallic infrastructures in the nearby vicinity of these DC systems [7]. However, leakage current from DC systems cannot be avoided since it is an inevitable consequence of their operation principles and the finite insulation properties of their energized components. Under some circumstances, the DC leakage currents will leave their intended conductive path, effectively taking the form of stray currents that will flow through the earth or other conductive paths (e.g. metallic infrastructures) to find their way back to the energy source. This circulation of DC leakage current outside of the intended conductive path is called "DC stray current" [9], [10].

Assessments of the DC stray currents' corrosion-impacts on metallic infrastructures are currently made as qualitative assessments using a mix of engineering judgment and simple spreadsheet applications of Faraday's laws [9], [10] to assess the cumulative mass of metal loss over the target operating period. Application of Faraday electrolytic law requires consideration of anodic-current flows to estimate the mass of metal loss depending on the kind of metallic element. In addition, standardised field testing/measurements can be performed to estimate stray current corrosion risk [7], [11]. The most common site validation tests are intended to measure the DC stray current interference in terms, of electrochemical corrosion potential variations on the interfered structure, voltage gradients in the soil and fluctuations of stray currents on the interfered structure. The state-of-the-art modelling techniques to predict and assess the impact of DC stray current induced corrosion across infrastructures are reported in [12]–[16]. The application of modelling techniques is a

necessity since: a) the size of the associated infrastructure enforces logistic restrictions for large-scale experiments, b) maintenance and management of critical infrastructures must be achieved with fewer resources and c) to minimize investment/financial risks.

1.2 PV Interference on buried Pipeline Systems

In recent years, the photovoltaic energy industry has spread rapidly as a means to meet carbon-emission reduction targets. In fact, large-scale commercial PV plants can produce electric energy from tens to several hundreds of megawatts (MWs). Taking into account the global trend in PV power generation, in the future, large areas of land are expected to host PV plants. To this end, it is highly probable (if not almost certain) that large-scale PV plants would be located in close proximity to other critical infrastructures, such as pipeline systems. This practice comes in response to minimizing environmental impacts (i.e. through the formation of joint energy corridors). However, the co-existence of PV plants and buried pipeline systems has not been evaluated with regard to DC interference and corrosion concerns. In fact, DC interference may be sourced both, by the normal or undetected fault conditions of PV systems.

1.2.1 DC leakage currents in PV systems

PV generators are classified as DC power systems. All conductors and elements of direct current systems should be insulated from earth. The limited insulation resistance of the energized components as well as the occurrence of undetected ground faults may generate considerable leakage currents to earth. It should be noted that commercial PV plants consist of a large volume of modules connected by several kilometers of DC cables to the PV inverters. To this extent, even a small amount of leakage current from each constituent component will result in a significant cumulative leakage current. For a certain voltage level, this leakage current is dependent on the effective insulation resistance that is known as R_{ISO} (see Fig. 1-1). The effective insulation resistance can be measured by the PV inverter before connecting the PV system to the grid [4][17] and this measurement provides an indication of the magnitude of the anticipated leakage currents to ground.

The operational level of (i.e. operational current and voltage) as well as the effective insulation resistance of PV generator are the critical parameters which control the conductive nature of the leakage current to earth. More explicitly, the level (magnitude) of DC leakage current is affected by external factors [18], [19] such as solar irradiance, ambient temperature, soil resistivity, moisture ingress at the modules' level, etc. For instance, usually

in the winter days the leakage current at morning hours - when PV plant starts its operation - is relatively high because the solar heat liquefies the frost on the back surface of modules [18]. The liquefied frost reduces the value of R_{ISO} of PV modules, as moisture penetrates in the insulation material, resulting in a significant increase of the leakage current magnitude.

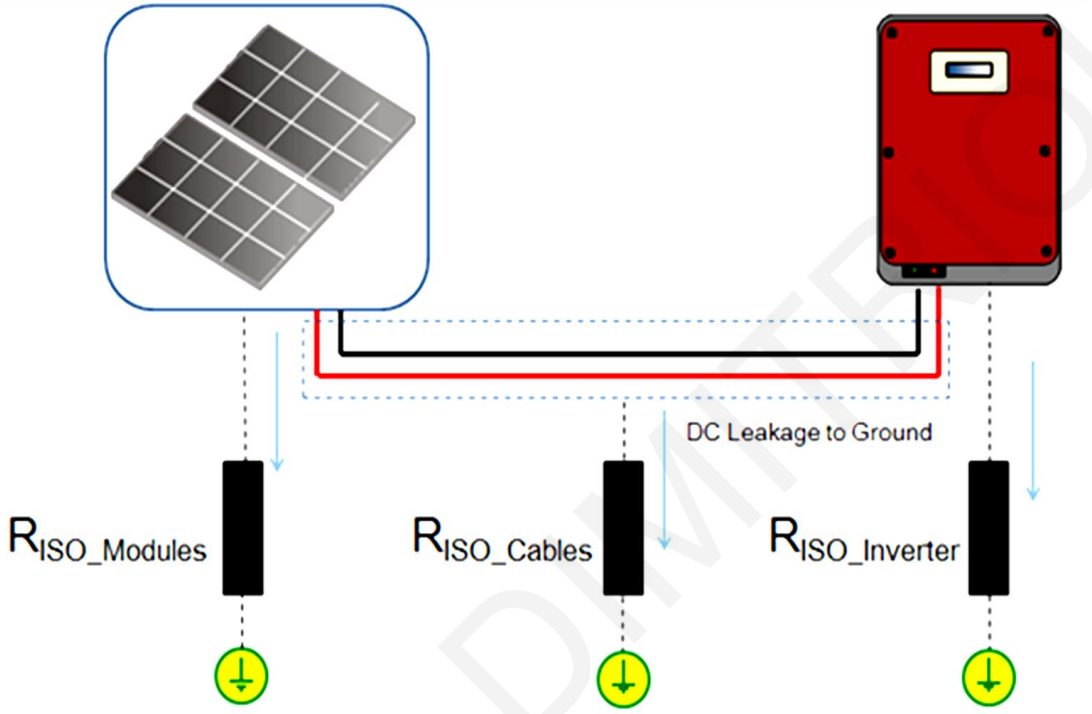

Figure 1-1: Effective Insulation Resistance (R_{ISO}) of a PV System Decomposed in Constituent Elements

Moreover, in the presence of DC ground faults, the DC leakage activity can be increased considerably. Ground faults in PV systems occur when there is an unintentional connection between energized components (i.e. cable's conductor) with a grounded surface or earth [20]. The detection mechanisms of these faults depend upon the DC grounding characteristics and are inevitably different for earthed and floating PV systems' configurations [4], [21]. However, since the existing thresholds for permissible DC leakage currents from PV systems have been based on other issues (i.e. fire prevention) the amounts of DC leakage may be adequate to cause stray current corrosion problems. It is worth noting that the threshold levels are set by taking into account the highest expected leakage activity which would be temporary (i.e. last for a few minutes) to avoid unwanted/undesirable operation of any fault detection schemes. In addition, a common practice followed by PV systems' operators is to alter fault detection thresholds at higher levels. This is done to avoid lost production due to false detections or "nuisance" trips from regular and inevitable leakage currents. This practice inevitably increases the DC leakage activity.

1.2.2 Corrosive activity under PV Interference

The mechanism of PV interference on buried pipeline systems can be summarized as follows. The leakage current, from PV modules and buried DC cables experiencing a fault or deteriorated insulation, will flow into the soil and may subsequently flow along parallel circuits either directly through the soil or buried metallic structures (see Fig. 1-2), before returning to the energy source. To this extent, the formation of a current loop is established. For example, if a section of a metallic pipeline falls into the established current loop, the pipeline can provide a convenient parallel conductive corridor for the leakage current to return back to the energy source.

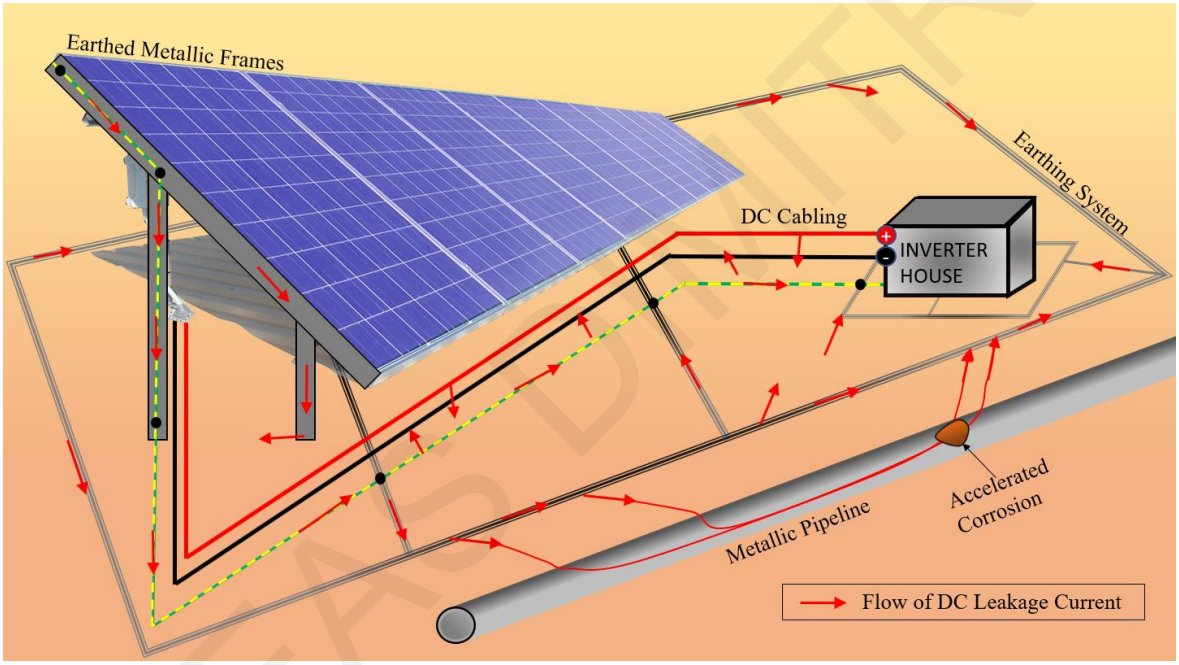

Figure 1-2: Graphical Illustration of PV induced DC Stray Current Corrosion

At the area where current is injected into the pipeline, a cathodic reaction takes place at the surface of the metal. The cathodic reaction results in a reduction of the corrosion rate which otherwise would be higher due to the corrosive influence of the surrounding environment [9], [10]. At this point, it should be noted that if a metal structure is surrounded by an electrolyte (i.e. soil), in the absence of an external source, an inevitable natural corrosion process established due to the electrochemical nature of the metal.

On the contrary, at the area where stray current discharges back to the soil, an anodic reaction takes place at the surface of the metal. The anodic reaction results in an acceleration of the natural corrosion process. The corrosion rate is usually pronounced as the mass of corroded metal [9], [10]. It can be calculated from the magnitude of anodic current (i.e. the

discharge current) and the duration of the interference activity, through Faraday's electrolytic law (see Appendix A).

It should be kept in mind that modern underground metallic pipelines are usually coated by a suitable anti-corrosion layer. Since the coating prevents the pipeline's metal to come in contact with an electrolyte (i.e. soil) the natural corrosion is avoided. By extension, the high insulation resistance of the coating material blocks the intrusion of stray currents into the metallic body of the pipeline.

The presence of coating holidays (i.e. defects on a protective coating at which metal is exposed to the environment) is inevitable and may cause local corrosion issues. In this case, PV interference can facilitate some corrosion damage at any existing coating holidays points. With reference to Figure 1-3, the mechanism that describes the corrosion concerns at coating holidays is as follows: Stray currents are inserted and collected into the soil through multiple points of the PV plant's components (i.e. buried cables, metallic frame extended into the soil, earthing system). The flow of stray currents through the earthing system can be characterized by a voltage drop on the earthing conductors with respect to a reference earthing point. Moreover, the stray current activity initiates variations of soil potential in the region of the PV plant. Depending on the pipeline's routing it is possible that some pipeline's sections can be influenced by the earth's potential variations. If the pipeline is well coated, then the variation in the earth's potential can significantly stress the coating material. This is because of the potential difference that is established between the pipeline's metallic wall and the adjacent soil. In particular as shown in Figure 1-3, at the area where soil presents an earth potential rise (EPR) the stray currents are forced into the pipeline's metallic wall through distributed coating holidays. Normally the collection of stray currents from the pipeline results in a reduction of the corrosion rate. Inversely, at the areas where soil exhibits an earth potential fall (EPF) stray currents are discharged back to the soil through distributed coating holidays. This accelerates the corrosion rate at the coating holidays' spots.

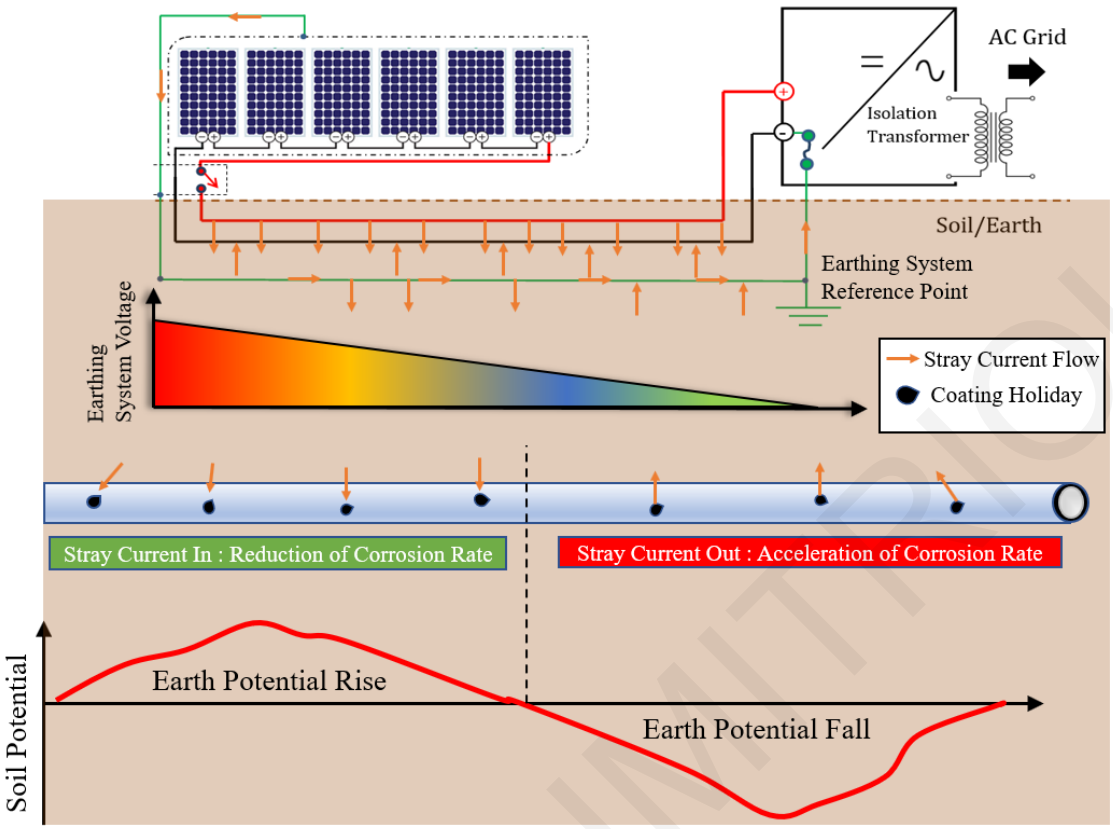

Figure 1-3: Soil Potential variations due to stray current flow

In order to avoid corrosion activity through the pipeline's coating holidays, supplementary protection against corrosion can be provided via cathodic protection (CP) system. The CP system controls the corrosion at the exposed metallic surface by making it the cathode of an electrochemical cell [3], [22]. A simple technique of protection connects the metal to be protected to a "sacrificial metal" (higher tendency to corrosion) to act as the anode while the protected metal becomes a cathode [10], [23]. Consequently, the sacrificial metal is corroded instead of the protected metal. This method is based on the generation of a galvanic current due to the potential difference (between the two metals) [24] which is established among dissimilar metals. In many cases where the galvanic current from sacrificial anodes is not adequate, it is recommended the use of an external DC source to provide an impressed current to the pipeline in order to reduce the corrosion rate. Impressed current anodes can deliver a much higher cathodic current providing cathodic protection of long pipeline segments where the use of sacrificial anodes is not practical, since for an equivalent current would require a large number of sacrificial anodes [10], [23]. In impressed current CP systems, the pipeline is connected on the negative pole of DC source (i.e. DC rectifier) while the anodes are connected on the positive pole. The generated cathodic current flows from anodes into the pipeline's surface resulting in a reduction of corrosion rate. Guidelines and criteria for an effective (CP) system are given in [3].

1.3 Research Innovation and Contribution

1st Contribution beyond the State-of-Art: *theoretical establishment of the prevailing electrical characteristics of PV systems' -normal and faulty operation - that lead to interference and corrosion concerns on underground critical infrastructure.*

The first contribution pertains to the formal theoretical establishment of the following:

DC leakage currents from PV systems to the ground may be sourced:

- by virtue of the distinct potential of the system against the ground and the potential difference between active system elements, and
- from undetected DC ground faults.

Ground faults in PV systems occur when there is an unintentional connection between any current-carrying conductor with a grounded surface or earth. Faults on the DC side can be found in both earthed and floating PV systems. The detection mechanisms of these faults depend upon the DC earthing characteristics of the PV system and are inevitably different for earthed and floating configurations. These faults can remain undetected since the allowable DC fault detection thresholds can be set high, to avoid lost production from false detections or "nuisance" trips from regular and inevitable leakage currents. The undetected DC faults arise as the existing detection thresholds for permissible DC leakage from PV systems have been based on other issues such as fire prevention or personnel safety.

2nd Contribution beyond the State-of-Art: *application of modelling techniques that are suitable for assessing PV systems' (grounded and floating) interference on underground pipeline systems.*

The second important contribution of this thesis is the formulation of appropriate simulation models to further elaborate on the theory that describes the prevailing electrical characteristics of PV systems' -normal and faulty operation - that lead to interference and corrosion concerns on underground critical infrastructure. This was achieved through a significant intervention with a simulation platform. Within this platform, the electrical circuit behavior of PV systems with respect to the DC leakage current (under normal and fault conditions) was transferred in an object-based graphical environment that is able to examine PV interference of pipeline systems in a topologically accurate representation. Some important features that were taken into account into the modelling process were:

- Actual size and positioning in three-dimensions of: a) PV plant's constituent components and b) interfered pipeline system

- Insulation and material characteristics of PV power equipment, supporting infrastructure and pipeline system
- Integration of undetected fault conditions
- Reproduction of the operational currents and voltages of PV plant's energized components under steady-state conditions and fault conditions. Compliance of modelled network of conductors with Ohm's and Kirchhoff's laws
- Realistic representation of fault current return paths through the earth, for floating and earthed PV systems.
- Spatial and time-varying monitoring of PV interference in terms of pipe to soil potentials

3nd ***Contribution beyond the State-of-Art:*** *proposed techniques for the identification and analysis of PV interference in the fields*

PV interference is time-variant and will normally follow the changing solar irradiance (i.e. the power per unit area received from the sun). It is therefore expected to be more pronounced during the daylight. However, the way that is pronounced on interfered structures is very different than other time-variant interference sources as for example DC traction systems. Therefore, the identification techniques described in international technical standards cannot directly be applied for the evaluation and mitigation of PV interference on pipeline systems. To this end, the thesis provides guidelines for the identification and measurement of PV interference that are tailored towards its unique characteristics. The proposed methods can be applied by practising engineers in their desk-based and field related assessments.

Formal Acknowledgment on the Impact of Research

By virtue of the active participation of our Research Group (PSM Laboratory) in the ISO/TC 67/SC 2/WG 24 'DC Stray Current Committee', part of the research described in this thesis has been normatively and informatively included in the new ISO 21857 [25] standard "*Petroleum, petrochemical and natural gas industries — Prevention of corrosion on pipeline systems influenced by stray currents*". In particular, Annex H in ISO 21857, describes the potential impact of PV interference on pipeline systems. Moreover, two IEEE Transactions papers that have resulted from this thesis are cited in the Bibliography of this new ISO 21857 standard. It should be noted that it is the first time that the impact of PV interference on pipeline systems is addressed in technical standards.

1.4 Thesis Outline

The technical work of this Thesis has been thoroughly described in five (5) Chapters. The contents of each structure are briefly described below:

Chapter 2- ***Elaboration on PV Interference Mechanisms and Impacts*:** This chapter specifically introduces stray current corrosion blind spots that are inherent to PV systems' grounding and associated DC ground fault detection mechanisms. These blind spots arise as the existing thresholds for DC leakage currents have been based on other issues, such as fire or personnel safety. Leakage currents may cause accelerated corrosion on PV supporting metallic structures as well as on third-party metallic utilities that may be present in the vicinity of PV installations. The impact of DC stray current corrosion is recognized by the stakeholders across the world in the DC traction community and codes and standards have been developed to provide designers and utility companies with a corrosion-management strategy that defines a level of corrosion risk which is acceptable across infrastructures. This chapter outlines the theoretical background that will assist the understanding of stray current corrosion by PV plant developers, designers, and owners and raise awareness with the utility distribution network owners.

Chapter 3- ***Development of Modelling Techniques to Address PV Interference on Pipeline Systems from Earthed PV Systems:*** In earthed PV systems, DC leakage to earth is formed by the contribution of the PV modules, inverters, and DC circuitry. Ground faults in such systems occur when there is an unintentional connection between any DC carrying conductor with a grounded surface or earth. On the occurrence of ground faults, DC leakage will be intensified and will flow through the earth or other conductive paths, before returning back to the source. Thus, it is highly probable that some portion of the DC leakage will attempt to return to the source through any low-resistance paths that exist in the nearby vicinity. For example, through nearby buried pipelines. Therefore, unattended DC leakage may induce stray current corrosion concerns on these pipelines. To this extent, this chapter presents a detailed DC interference modelling for assessing the DC leakage activity in PV systems - particularly under undetected fault conditions. Firstly, the modelling carried out embraces the topologically accurate consideration of all sources of DC leakage that are associated with grounded PV systems. A second feature presented in the paper is the modelling of blind-spot DC faults and their impact on third party infrastructure.

Chapter 4- ***Development of Modelling Techniques to Address PV Interference on Pipeline Systems from Floating Isolated PV Systems:*** In floating isolated PV systems there is no direct bonding to earth with regard to the PV arrays' current currying conductors. In addition, galvanic isolation, between the AC and DC side, is provided with the use of isolation transformer. Since the floating PV array is isolated any leakage currents are driven by the potential difference that arises between the active elements. The magnitude of leakage current depends on the effective insulation resistance and the operational level (i.e. Voltage, Current) of the PV system's DC side. Moreover, the circulation of leakage currents through the soil may interfere with a nearby metallic pipeline system resulting in an acceleration of their corrosion rate. This chapter develops a dedicated modelling technique to address the problem of PV interference on pipeline systems located in a vicinity with Floating Isolated PV Plants. Furthermore, a series of sensitivity analysis is performed on a realistic case study to identify the factors affecting the PV interference situation.

Chapter 5- ***Identification of PV Interference on Pipeline Systems:*** The level of PV interference is influenced by various parameters that rely on the PV systems' operational characteristics as well as on weather and environmental conditions. To this extent, the magnitude of PV interference may vary considerably within the course of a day and year. Consequently, the need for dynamic simulation arises for the true visualization of PV interference on pipeline systems. Firstly, in this chapter dynamic simulation of PV interference is performed. The unique characteristics of PV interference are highlighted and are compared with the most common types of DC interference systems. Secondly, based on the important conclusions and useful insights, guidelines for the identification and measurement of PV interference on pipeline systems are provided.

Chapter 6- ***Conclusion:*** The final chapter presents the main conclusions and the contributions of this research work. Also, future work related to the PV interference research area is proposed.

Chapter 2

Elaboration on PV Interference Mechanisms and Impacts

2.1 Introductory remarks

Leakage currents in Photovoltaic (PV) systems come as a result of a fault or from the systematic and inevitable flow of direct current (DC) through non-ideal materials of the cables, PV modules, and other PV array components. The Solar America Board for Codes and Standards (Solar ABCs) has issued a white-paper—"*Ground-Fault Protection Blind Spot*" [26], to raise the awareness of PV System Owners to appraise both the benefits of system retrofits and the risks associated with not implementing any strategies for the early detection of PV ground faults and leakage currents. The safety issue associated with the non-detection of PV ground faults has been highlighted after the two known PV system fires in Bakersfield, California (2009) and in Mount Holly, North Carolina (2011). The official reports, based on evidence collected from these two fire-events, are given in [26], [27]. The conclusion of the two case studies was that some ground fault protection schemes may not detect certain common ground faults in PV systems. These undetected faults—as termed by Solar ABCs—fall within detection "blind spots", intrinsic in the design and installation of PV systems (mainly earthed PV systems).

Nonetheless, one challenge for PV systems' inverters is that they should reliably disconnect under real fault conditions, without experiencing "nuisance" trips from regular and inevitable leakage currents. The arising question is however, how well defined or understood is the threshold for regular and inevitable leakage currents? Should it be defined based on an acceptable energy loss performance of PV Systems? Or alternatively, should it be dependent on safety issues related to fire ignition or humans' protection against electric shock [28]? To what extent is this threshold affected by weather conditions [18]?

This chapter theoretically supports that, under certain conditions, PV DC leakage currents, if left unattended, or not detected at all, may cause accelerated stray current corrosion on metallic structures (e.g., racks, joints, conduits, enclosures-boxes) or on metallic underground infrastructure (e.g., metallic pipelines) buried in the vicinity of utility-scale PV systems.

2.2 PV Systems' DC Earthing Configurations

Photovoltaic (PV) systems are no different from other electrical power systems and therefore they should be earthed to provide protection to personnel against critical electric shocks [29], [30]. Furthermore, the earthing system ensures the uninterrupted operation of services by reducing the risk of overvoltages. In addition, the earthing system is important for lightning

protection [31]. Finally, in some cases, the earthing system serves as the "functional earthing-grounding" of the PV inverters' current-carrying conductors [32].

Specifically, the DC side of PV systems (DC PV arrays) should be earthed and based on their type of earthing topology, the systems are classified as earthed (grounded) or floating (unearthed) [4], [21], (see Fig. 2-1). An earthed PV system has either the positive or negative DC-carrying conductor connected to the earth. The earthing of the DC current-carrying conductors facilitates the proper function of the protection schemes incorporated by PV inverters. To this extent, a live conductor on the DC side of the inverter is often connected to ground through a fuse, circuit breaker, resistance device, or through other electronic means that fall part of a ground-fault protection device (GFPD) [33]. Conductors in these systems that are normally at ground potential may exhibit a distinct voltage, relative to the ground during fault conditions.

In contrast, a floating PV system has neither the positive nor the negative DC current-carrying conductor connected to the earth. The inverters in floating PV systems may have a transformer, providing galvanic isolation between the DC and AC side or alternatively, it may be transformerless (non-isolated) [4]. A common misunderstanding about floating PV systems is that they lack all connections to ground, including the bonding to ground of exposed metal (e.g., metal frames of the PV modules, supporting infrastructure, combiner boxes) that could become energized in a fault situation or under normal operation due to capacitive-coupling mechanisms [28], [34]. However, this perception (i.e., lack of all connections to the ground) is not true. It is imperative that both earthed and floating PV systems must have their metal equipment grounded to earth (see Fig. 2-1) to maintain the electrical potential of any exposed metal parts at zero volts. That is to facilitate the operation of protection devices to assist in keeping systems and people safe.

In general, a global earthing system of a utility-scale PV plant embraces the Medium Voltage (MV) substation's grounding system [35], the inverters' housings (AC) grounding provisions as well as the PV generators' earthing system (including lightning protection additional earthing electrodes) composing an interconnected enhanced earthing system. The technical standards [21], [32] highlight that the metallic structures supporting the PV modules shall be bonded and connected to a suitable earthing terminal. Furthermore, PV parks' fences should be appropriately earthed, depending on the specific risks and hazards identified in [35].

The applied earthing/grounding configuration is dictated by national regulation and adopted standards. It should be noted that the earthed configuration is commonly used in U.S large scale PV Plants while the floating configuration is most frequently used in Europe. An assessment of protection against electric shock in the DC side of a PV plant is provided in [28] by adhering to the requirements of the IEC [29], [32] for LV electrical installations. The assessment is based on a theoretical and experimental study of the electrical behavior of a photovoltaic generator and its protection system against electrical shock. Moreover, the work reported in [34] presents and analyzes the possible issues associated with PV energy sources by considering the earthing configurations of earthed and floating systems. In addition, some research works have identified that the PID (potential-induced-degradation) phenomenon - on the PV modules – can be affected by the grounding configuration of the DC side of the PV system [36]–[38]. To this end, several studies have analyzed the design of earthing systems of PV plants with an emphasis on the protection against electric shock [28] and on the protection of PV equipment against lightning strikes [39], [40].

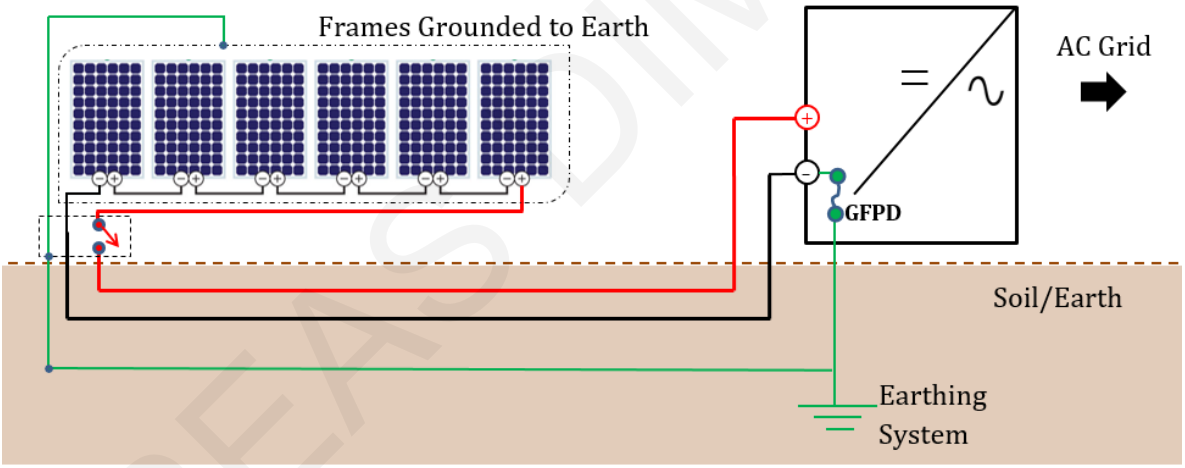

2-1a. Negative-earthed DC system

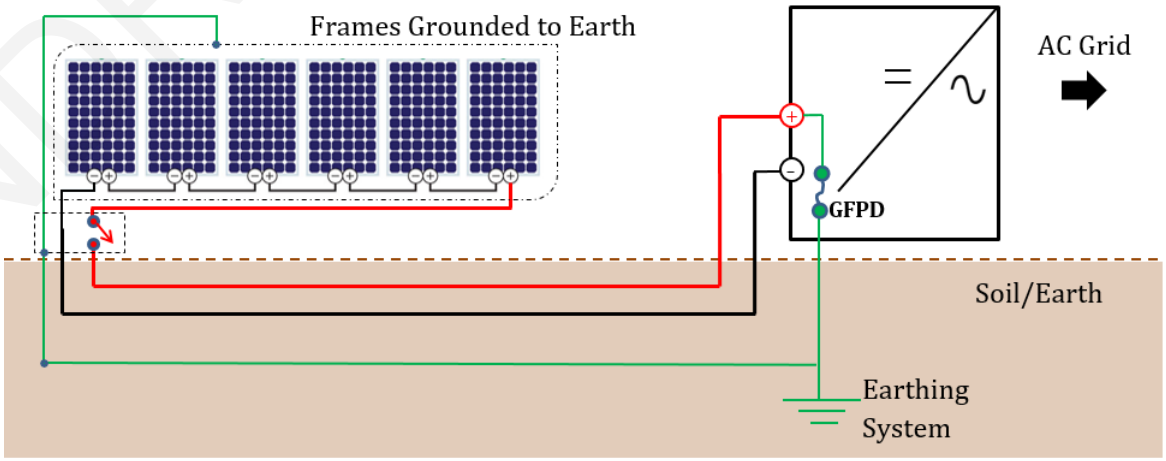

2-1b. Positive-earthed DC system

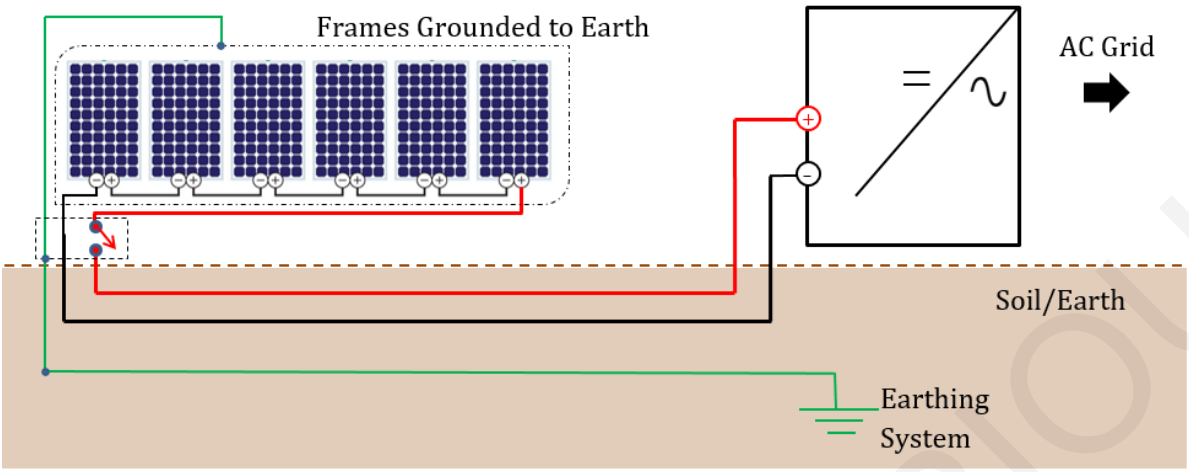

2-1c. Floating DC system

Figure 2-1: Types of PV Systems Earthing

2.3 Defining the sources of Leakage Currents in large-scale PV Systems

Since PV generators are classified as DC power systems, all live conductors and elements of direct current systems should be electrically insulated from earth. However, since the insulation is not perfect, an amount of generated current can leak into the earth. The total ground leakage current is formed by the contribution of all system energized DC components (e.g., PV modules, DC cables, inverters) when taken together. For a certain voltage level, this leakage current is dependent on the effective insulation resistance of PV array that is known as R_{ISO} (see Fig. 2-2). The effective insulation resistance can be defined as the ohmic resistance in Ohms between energized components and earth. To this extent, an indication of the magnitude of the anticipated leakage currents to earth is provided by the effective insulation resistance. More information is provided below on the description of the main components, which constitute a PV system and can have an impact on the DC leakage activity.

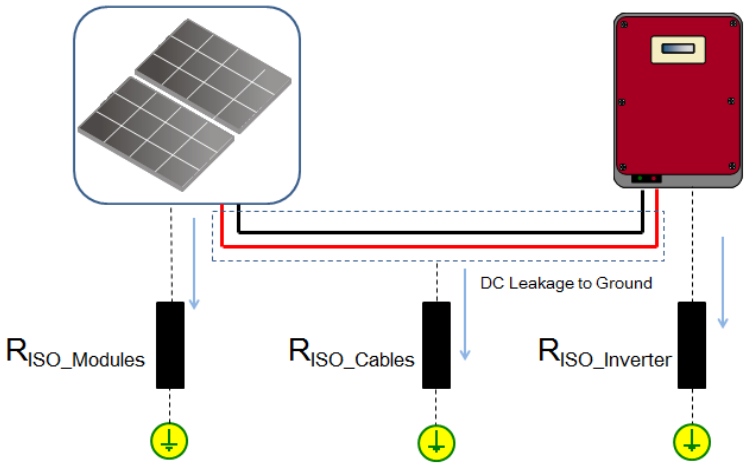

Figure 2-2: Effective Insulation Resistance (R_{ISO}) of a PV System Decomposed in Constituent Elements

2.3.1 PV modules

PV modules are the most crucial elements in a PV plant since they convert sunlight directly into electricity. For the understanding of leakage current activity of PV modules is necessary the identification of their assembly components. The individual elements which assemble a PV module are shown in Figure 2-3. The generation/energized unit comprises a group of PV cells which are connected in series to reach the desired voltage level that typically ranges between 35-45 Volts (in open-circuit condition) depending on the PV technology (e.g. mono-crystalline, poly-crystalline silicon cells). PV cells are encapsulated via cross-linkable ethylene vinyl acetate (EVA) that provides tightness against moisture and electrical insulation. The integrity of the insulation material is a crucial parameter regarding leakage activity. Potential degradation may increase leakage currents and reduce power performance [19]. In addition, a low iron glass is applied in the upper front to protect cells from damage and to provide UV screening. Also, plastic backing and aluminium frames improve mechanical integrity. The back sheet of a standard PV module is generally a thin opaque film, such as Tedlar (a film of polyvinyl fluoride, PVF), polyethylene terephthalate (PET) or metal. Last but not least, a junction box [41] is fitted in the back sheet to collect the electric contacts from the positive and negative terminals of the PV cells' series. Moreover, to avoid potential electric-shock hazards, the backside (i.e. aluminium frame) of PV modules are in electric contact with the supporting infrastructure either directly, or via an equipment grounding conductor (EGC) as required by [17], [42]. EGC bonds the metallic frames of PV modules with the metallic supporting infrastructure while its far end is connected to an earthing terminal. To this extent, any leakage from the PV modules can flow to earth through the metallic supporting infrastructure.

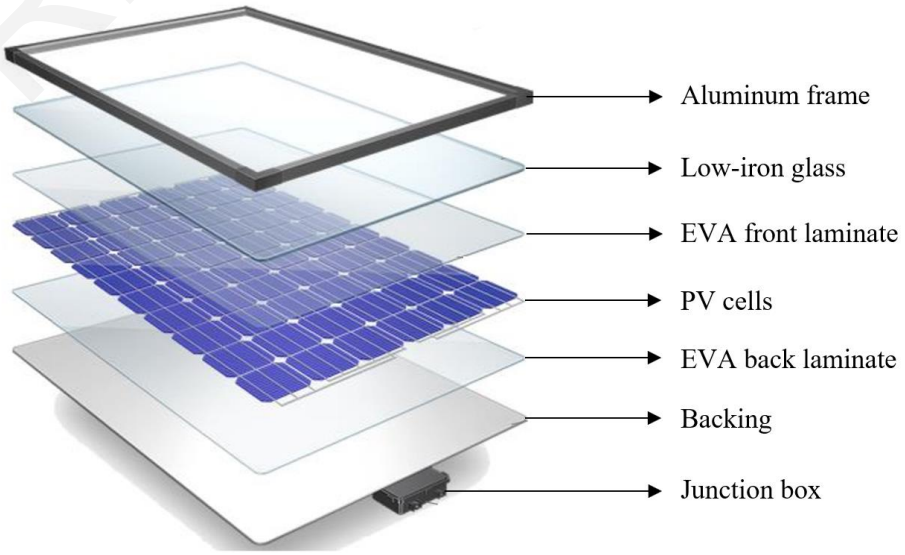

Figure 2-3: Assembly elements of a PV module

Large metallic structures host the PV modules which are used in a PV plant (see Fig. 2-4). The PV modules are mounted with precise tilt and orientation to reach a maximum solar gain and power performance [43] - through an orthogonal mesh consisting of vertical and horizontal linear rails while the whole structure is supported by posts which are extended into the soil. The framework is highly conductive because it utilizes specific grades of structural steel for a range of industry-standard requirements.

Figure 2-4: Metallic supporting infrastructure of PV modules

Moreover, the PV modules are collectively wired in series strings, e.g., the positive terminal of one module is connected to the negative terminal of the next module through connection cables. This results in a cumulative voltage output without altering the current. A set of PV modules connected in series is called *PV string*. Depending on inverter's characteristics the *PV string* nominal voltage can range between 800-1500 V. The output cables from multiple *PV strings* (positive and negatives) are subsequently grouped in parallel within combiner boxes via appropriate busbars. This parallelism of identical *PV strings* constitutes a *PV array*. The standard industrial practice suggests that combiners are used to eliminate running multiple DC cables from the PV arrays to the inverter as a means to reduce cabling costs and possibly installation costs. There are commercially available combiner boxes, which are providing in addition, protection (overcurrent, surge, etc.) and performance monitoring of the PV arrays. The connection of the PV strings on busbars as well as the installation of

surge protection devices such as SPDs may add an additional portion of leakage current [44]. Subsequently, the total produced power leading to the corresponding combiner box is distributed to the central inverter using DC cables.

2.3.2 PV Cables

Regarding DC cabling, PV cables are suitable for permanent outdoor use throughout the lifetime of the PV plant under variable demanding climate conditions and their characteristics should meet the requirements specified in [8]. DC cables are consisting of a copper core conductor coated with insulation material (i.e. XPLE) and an over jacket-sheath made of similar polymeric material (i.e. XLPE, PE). Despite strict standard specifications, the leakage activity from DC cabling is inevitable. Since the potential difference between cable's conductor and earth can high enough (e.g. 1000 Volts), leakage current can occur along the entire length of a cable [45] especially if the cable is aged [46] or has defects on its insulation [47].

PV designers are thoroughly assessing the optimal size of DC cables (by virtue of their duty), particularly those that run from combiner boxes to the location of the inverters. The assessment largely pertains to avoiding the increase of conductors' power losses since these losses may erode the percentage of the potential solar energy harvest. However, if the conductors are over-specified to minimize the power losses, the overall system costs will escalate, and unavoidably, the levelized cost of solar energy will rise. To this end, the manufacturers of DC cables - suitable for PV installations - specify a range of technical characteristics, which include the following: 1) electrical parameters (e.g., rated voltage, ampacity, insulation, etc.); 2) thermal parameters (e.g., ambient temperatures, maximum permissible conductor operating temperature, short-circuit temperature, etc.); 3) mechanical parameters (e.g., tensile rating, minimum bending radius, etc.); and 4) chemical parameters (e.g., acid and alkaline resistance, ammonia resistance, and environmental condition resistance). It should be highlighted that those PV cables that are directly buried into the ground may follow some installation guidelines such as the ones given in [48].

2.3.3 PV Inverter

Commercially available PV central inverters can manage an input power of some megawatts. They incorporate several DC inputs that benefit from suitable ground-fault protection devices [4], [49]. The nominal DC input voltage typically ranges between 800-1500 Volts. The output voltage is adjusted on grid frequency with a magnitude of some hundreds of

volts. In addition, an external step-up transformer is interposed between the inverter and the power network to transform the output low voltage current of the inverter into the nominal high voltage of the power grid. PV plants are connected either on the medium-voltage grid either on the high voltage grid.

The insulation withstand capability as well as the general requirements that should be fulfilled by the PV inverters are specified in [4]. Concerning earthed inverters, the leakage currents can circulate via the earthed current currying conductor while for floating transformerless inverters the leakage currents can circulate between the PV array and the grid (e.g. grounded neutral of distribution transformer). Moreover, the presence of common-mode voltage CMV due to modulation may generate leakage currents in transformerless systems [50]–[52].

2.4 Magnitude of DC leakage Current

The minimum insulation resistance for the PV modules is defined at 40 MΩ/m^2 for all commercially available PV technologies [53]–[56]. Consequently, the total insulation resistance to ground of each PV string is inversely proportional to the number of PV modules connected in series [18], [57]. To this extent, the high voltage level appearing on a series string in conjunction with insulation resistance's limitations entails an inevitable flow of DC leakage current. The experimental work carried out in [19] examines the leakage current from PV modules under different parameters such as modules surface temperature, surface wetting, salt and dust accumulation and ageing condition by exposed PV modules in high voltage stress. It is shown that the leakage current exponentially increases with ageing. The long-term field ageing downgrades the encapsulant material resulting in the reduction of the effective insulation resistance which in turn amplifies leakage current activity. In particular, the study reported in [58] states that under normal operating conditions the estimated maximum leakage current from crystalline Si PV modules could reach 11 μA/kW per module in 500-kWp array operating at 600 Volts. Within [58], the cumulative total leakage current from the 500-kWp array is reported to be about 56 mA. A field test [18] performed in an operational PV plant of 68 kWp reveals a strong correlation of R_{ISO} value with the relative humidity and modules' temperature. In fact, the R_{ISO} value can vary by several orders within the course of a day [18]. Regarding PV cables, laboratory experiments reveal that insulation materials (e.g. XLPE) increase their conductivity with the increase of temperature [59], [60]. The temperature of buried cables under operation may increase considerably due to the limited thermal dissipation of the resistive power losses. To this extent, the level of leakage

currents from PV cables can be affected considerably. Nevertheless, it should be born in mind that DC leakage currents will inevitably increase with PV system size, as the system ages or in the event of unidentified DC ground faults.

It should be also noted that the magnitude of the DC leakage has a time-varying profile. This is because a PV system is a current-limited source and the level of PV current and associated leakage current are thus dependent on external factors such as solar irradiance and other environmental conditions which include ambient temperature, soil resistivity, etc. [18], [28]. Consequently, the magnitude of leakage current can vary on a daily basis as well as on a seasonal basis.

2.5 PV Ground Faults and Detection Mechanisms

In PV systems, DC leakage currents to ground may be sourced: a) by virtue of the distinct potential of the system against ground and/or the potential difference between active system elements [18], [58], [57] and b) from DC ground faults [20], [61]. Ground faults in PV systems occur when there is an unintentional connection between any current-carrying conductor with a grounded surface or earth. Faults on the DC side can be found in both earthed and floating PV systems. The detection mechanisms of these faults depend upon the DC grounding characteristics and are inevitably different for earthed and floating configurations.

A thorough literature review reveals that the related to this work, research efforts have been merely concentrated in demonstrating and characterizing various types of faults on PV arrays [20], [62], [63]. The common objective of these works lies in maintaining human hazards to a safe level. More explicitly, the work described in [61], examines the protection challenges in PV arrays due to the existence of line-line faults and their time evolution under varying solar irradiance conditions. Other similar works propose algorithmic techniques for the detection of various types of faults [64], [65] while other works propose relevant mitigation techniques [20], [66]. In terms of experimental investigations of the DC leakage issue in PV systems, the work reported in [57] discusses some measurement-related implications, by mainly focusing on the steady-state operating conditions of small and large PV arrays. Moreover, a specialized field testing program for DC ground faults investigation on large PV arrays has been reported in [26], [58], [67], [68]. Briefly, the main objective of this program was, by creating intentional blind-spot ground-faults, to evidently demonstrate and characterize the effective ground fault detection thresholds of the inverters. The main conclusion was that the sustained operation of the inverters, in the presence of non-zero ohm

ground faults, is evidently true. For example, a 500kW inverter continued its operation under a 3 A ground fault current measured at the array, when the ground fault resistance introduced had a value of 1 Ω.

2.5.1 Leakage Currents and Fault Detection in Earthed PV systems

In earthed PV systems, it is possible to have DC leakage current to frames emanating from the PV modules. This is an unavoidable phenomenon comprising very minor amounts of current leaking from the cells to the module frames [57], [58] and may be significantly increased due to degraded sealants and water ingress [18], [28], [19]. More explicitly, the leakage current flow is exacerbated when moisture penetrates the module glass and as a result, the resistance between the active module circuitry and the frame diminishes. Since the frame is grounded, the leakage current moves from the frame to ground circuit and return via the grounded polarity conductor and/or through the ground to the inverter modules. The location and number of inverters will vary, but for most large-scale PV systems, the DC cabling is distributed within a field resulting in significant length of cable (this can be estimated at 2.5 km in a 1 MW PV plant). Damage during installation could generate a fault and it is also possible to have DC leakage currents from those portions of DC cables that are laid underground (e.g., cables between combiner boxes and inverter). This latter type of leakage will become more apparent in case of ground faults that can happen when the insulation of buried DC cables is ineffective or deteriorated due to moisture ingress, freeze/thaw cycles or accidental damages. In such cases, the leakage currents will flow through the earth or other conductive paths before returning back to the energy source—also through the grounded polarity conductor (see Fig. 2-5).

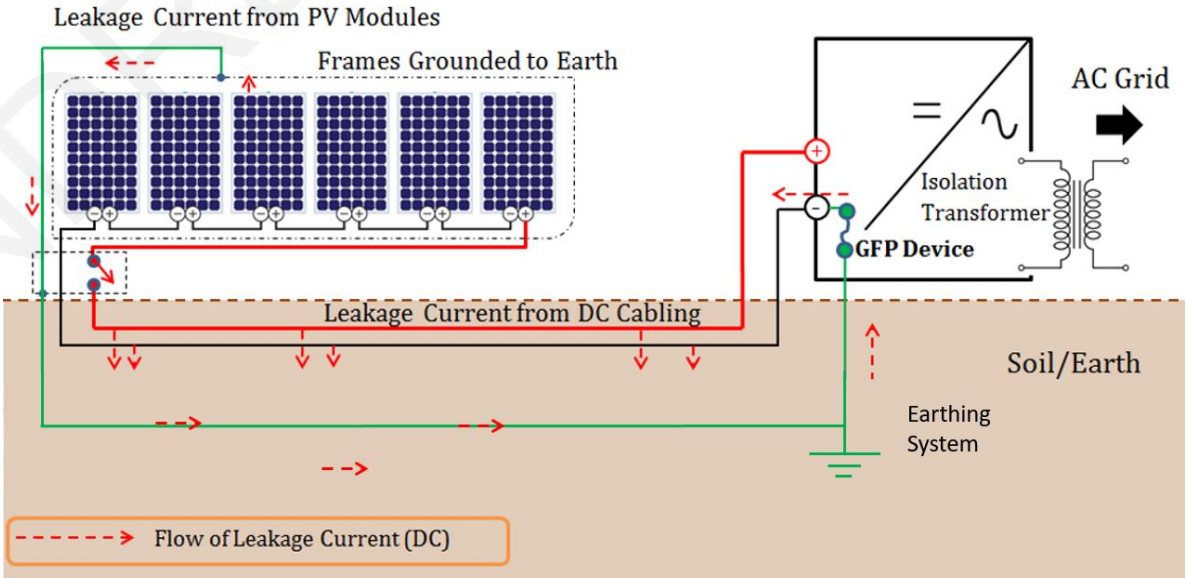

Figure 2-5: DC Fault/Leakage Currents Paths for Earthed PV Systems

For detecting DC leakage faults in earthed PV systems (mostly used in the USA) the UL 1741 [21] and the NEC [42] require the installation of a Ground Fault Protection Device (GFPD).The GFPD could be a fuse-type, circuit breaker, resistance device or other electronic means that is part of a listed ground-fault protection system [33]. These devices are designed to interrupt the flow of DC fault currents and also to alert about fault occurrences. To visualize the current detection process, one should recall the fundamental grounding configurations of an earthed PV system. For example, if the negative current-carrying conductor is grounded, this implies that the negative conductor has a connection to the grounded parts of the PV system through a fuse-type GFP device that is embedded in the inverter. If there is a fault (e.g., excess current leakage between a grounded conductor and ground), the fault current will flow from the fault location in a parallel ground circuit (i.e. EGC) or via the earth, through the GFP fuse and back through the negative conductor to complete the circuit (see Fig. 2-5). The magnitude of the fault current, returning through the GFP device, will be largely dependent on the impedance path formed by both the fault and earth return path [58]. Generally, high ground fault impedance would result in lower ground fault currents flowing in the ground circuit return paths and this may limit the type of fault that can be sensed by the GFP device. A ground-fault current that falls below the detection level of GFP devices may subsequently lead to a permanent reduction of operation output [61], which could provide an indication of the fault occurrence if the power monitoring systems have adequate sensitivity.

However, once the GFP fuse's current rating is violated, the fuse will blow to isolate the system ground. To this extent, the selection of the fuse rating should be high enough to avoid nuisance tripping due to leakage and transient currents but not as high as to let harmful leakage currents undetected [20]. The ground fault interruption requirements and thresholds for earthed PV systems can be found specified in the UL 1741 [21]. The level of current thresholds tabulated in the standard is given according to the size of PV systems and the respective size of the inverters (see Tab. 2-1). The thresholds shown in Table 2-1 are partly dependent on: a) the anticipated leakage currents from PV arrays and cabling under normal operating conditions and b) the contribution of other factors in the ground leakage detection processes, such as AC noise, radio frequency noise within the array and inverter [58]. However, it should be appreciated that these standardized thresholds are universal for all PV systems, regardless of their individual technical specifications and installation/location conditions. Thus, they should be regarded as conservative figures to avoid catastrophic fire failures. The currently applied detection thresholds may prevent to a large extent "nuisance"

trips from regular and transient leakage currents which are possibly fueled by harsh environmental/soil conditions. Nonetheless, there is always the underlying risk that the inverters maintain the normal operation of a PV system, despite the presence of a considerable amount of leakage current flowing to ground [27], [20], [58].

Table 2-1: Ground Fault Detection Thresholds (UL 1741)

Inverter DC Rating (kW)	Ground Fault Current Threshold (A)
0-25	1
25-50	2
50-100	3
100-250	4
>250	5

2.5.2 Leakage Currents and Fault Detection in Floating PV systems

As previously noted, a floating DC system may have galvanic isolation between its DC and AC side or alternatively it may be non-isolated. The galvanic isolation is achieved by the use of isolation transformers compliant to the minimum insulation requirements—defined by the leakage current testing endeavors (for fire and shock hazards) described in [4]. Moreover, it is important to acknowledge that floating systems are not ideally isolated from the ground due to the presence of resistive leakages paths to ground and distributed capacitance between active elements (PV modules, positive—negative DC cabling) and ground [34], as will be further explained in detail.

By definition, a floating isolated PV system does not have a distinct potential to ground. However, it is still possible to have DC leaking from the cells to the grounded metallic parts of the system. This leakage may be driven by the potential difference that arises between two remote active elements; for example, the first and the last PV module of a PV string. Furthermore, DC leakage activity can also take place where buried underground DC cables are laid due to their inherent potential difference (i.e., current from positive conductor to negative conductor) and/or deteriorated insulation properties.

In fact, the DC leakage activity in the cable circuitry of a floating isolated system, may exhibit the illustrative behavior shown in Figure 2-6. Take for example the DC leakage activity of a pair of buried DC cables emanating from a combiner and leading to a central inverter. The potential difference between cables equals to the cumulative voltage of PV strings and depends on the incident solar irradiation. Along the positive DC cable, the current

leaking out while along the negative DC cable the current leaking back into the cable, thus completing the current return path. The leakage activity may be higher in those sections of buried DC cables that are faulted or have deteriorated insulation.

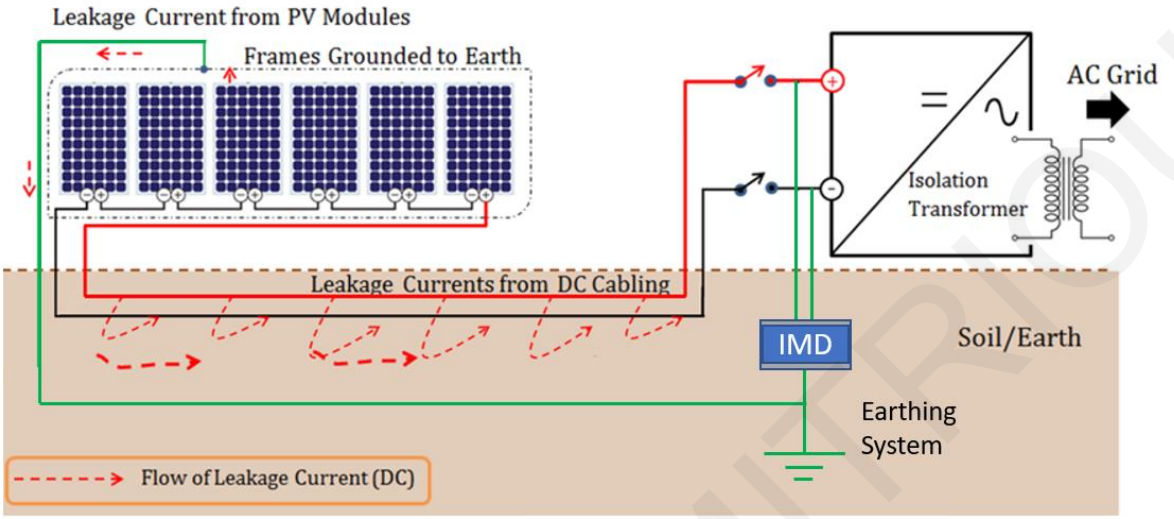

Figure 2-6: DC Fault/Leakage Currents Paths for Floating Isolated PV Systems

Special attention, however, should be given in floating PV systems that have no galvanic isolation (i.e., non-isolated) where even the first ground fault in a PV array can create a hazardous potential [17]. This is because the fault or leakage current is allowed to be sourced on the AC side of the system [17], as illustratively shown in Figure 2-7. (Note: the grounded neutral on the AC side will provide a return current path for the fault current). Thus, a floating non-isolated PV system will have a reference potential to earth provided by the AC neutral that is grounded [27]. Therefore, the magnitude of the potential between the PV array and ground will be influenced by the topology and the switching operation of the inverter [69]-[70].

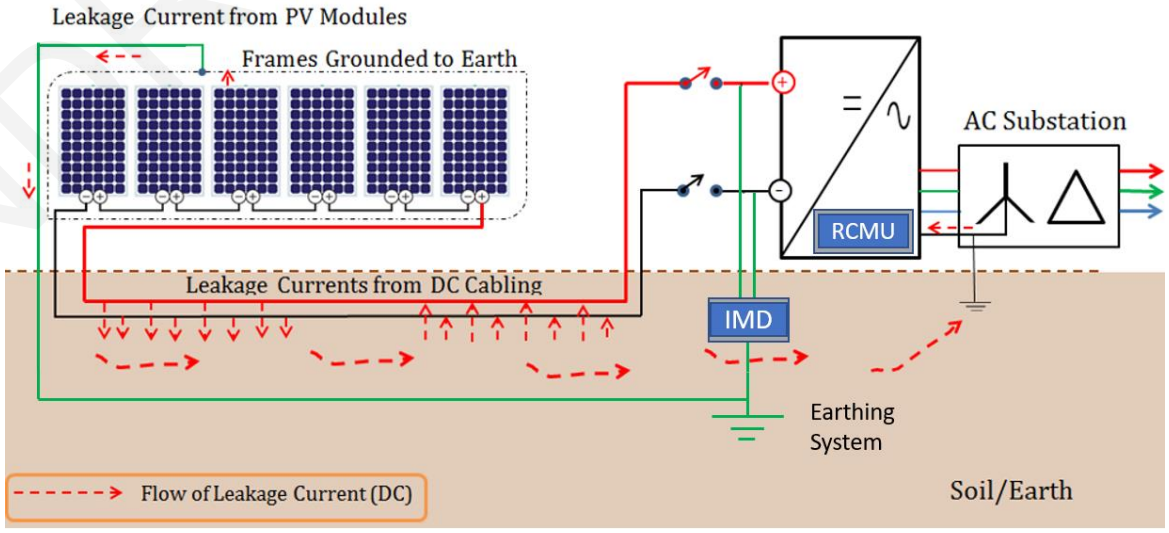

Figure 2-7: DC Fault/Leakage Currents Paths for Floating non-Isolated PV Systems

The above described principles dictate that both the ground fault tolerance practices and the detection of DC leakage currents are inevitably influenced by whether a PV system is galvanically isolated or not.

Primarily, ground fault detection in floating PV systems (isolated & non-isolated) is typically achieved by monitoring the DC insulation resistance from the PV input (array) to ground [4]. The measurements are typically achieved by monitoring the insulation impedance of each pole (positive and negative) relative to ground [18], [57],[28], [58] as shown in Figure 2-6 & Figure 2-7. They are achieved by the use of embedded insulation monitoring devices (IMDs) [71] and they usually take place before inverter starts operation [4]. This type of monitoring is commonly referred to as R_{ISO} measurements. The IMDs are connected between the live DC conductors and the earthing terminal and superimposing an auxiliary voltage. Most IMDs work by injecting low level DC on the energized circuit and detecting. Some manufacturers use a patented AMP-monitoring principle (Adapted Measuring Pulse [72].

The IMD setpoint should be in accordance with the minimum insulation resistance of PV array under some worst meteorological conditions to avoid nuisance tripping events [20], [28]. The minimum permissible value of insulation resistance is defined in [4] and its dependence on the maximum array voltage (V_{max}) is given in Equation (2-1).

$$R_{ISO\_min} = \frac{V_{max}}{30\ mA}\Omega \qquad (2\text{-}1)$$

However, a clear distinction between the floating isolated and non-isolated PV systems should be made when it comes to IMD measurements, as follows. Firstly, it should be borne in mind that in floating isolated configurations a single ground fault will not cause fault currents to flow, but a second ground fault in conductors will allow fault currents to circulate through the circuits associated with the two faults—i.e., due to the potential difference established between the faults' location [34], [58]. In floating isolated PV systems, a leakage activity to the ground can be detected when the measured impedance to ground of either the positive or the negative conductor pole drops to a low level (faults of about one kΩ or less can be almost certainly detected by the IMDs). The inverter should indicate a fault; however, its operation would not necessarily be prevented [4].

In floating non-isolated systems, if the IMDs detect a fault (i.e., low insulation resistance) the inverter should indicate a fault and would prevent its operation (i.e., not connect to the mains) because even the first ground fault will cause large fault currents to flow (due to the fact that the system is effectively grounded, by virtue of its non-isolating nature, via the AC side/grid). In such systems, it is therefore advocated to include an array residual current detection mechanism that would trip the inverter to automatically disconnect from the mains: a) in the event of a fault on the DC side that is not detected by the IMD or b) in the event of a fault that may appear during the operation of the inverter—(Note for (b): IMDs' measurements are obtained before the inverter starts its operation).

The use of a residual current detection mechanism is considered adequate since, as noted above, the fault current is allowed to be sourced on the AC side through the grounded neutral on the AC side. This transition of current on the AC side can create an imbalance in current going in (neutral) as opposed to the current going out (ac line conductors that are routed to substation) of the inverter. Therefore, the formed imbalance will indicate the presence of faults within the inverter as well as any ground faults (i.e., leakage currents) occurring in the DC side of the system.

The residual current detection mechanism could be an RCD (residual current device) with an interruption threshold setting of 30 mA, located between the inverter and the mains. A type B RCD is required in order to respond to both residual sinusoidal alternating currents and residual direct currents [73]. Alternatively, in order to avoid unwanted trips, the inverter could benefit from an array Residual Current Monitoring Unit (RCMU) that is capable of detecting: a) continuous excessive residual currents and b) the sudden changes in residual currents. The RCMU shall measure the total RMS current of both AC and DC components. It should be noted that the thresholds for excessive residual currents are dependent on the inverter's size (e.g., 300 mA RMS for inverters with rated continuous output power ≤ 30 kVA). These are reproduced from IEC 62109-2 [4] in Table 2-2 and are meant to indicate that beyond these values, a major failure risk such as fire-ignition risk is highly probable.

Table 2-2: Ground Fault Current Interruption Thresholds for Floating (Non-Isolated) PV Systems

Description	Threshold Currents
For inverters with rated continuous output ≤ 30 kVA	300 mA rms
For inverters with rated continuous output > 30 kVA	10 mA rms per kVA rated continuous output power

The threshold for excessive residual currents during the operation of the inverter (i.e., 300 mA) is inevitably higher than the 30 mA threshold used to determine the minimum acceptable value of R_{ISO_min} in Equation (2-1)—applied before the inverter is set to operation. This is because during the operation of the inverter there is additional leakage current activity through the inverter [57] and cables [8]. It is also possible to have "normal" capacitive leakage currents flowing through distributed capacitances formed between the solar cells and the grounded metallic frames [50], [69]. In fact, a floating non-isolated (i.e., transformerless) system could suffer from noticeable capacitive leakage currents. This is due to the lack of galvanic isolation, a fact that allows for a variable voltage level between the DC PV array and ground. That is, while the DC side of the PV array is floating, its voltage relative to the AC ground fluctuates by virtue of the inverters' high-frequency switching process. In a floating isolated (with transformer) PV system capacitive leakage currents are negligible because the system is galvanically isolated. Thus, any circulation of leakage currents between the AC and DC side of the inverter is avoided. It should be noted that no flow of capacitive leakage currents is anticipated in earthed PV systems, since the voltage of the DC PV array relative to the ground is stable [34].

2.6 PV interference leading to DC Stray Current Corrosion

As illustrated in Section 2.5 the leakage current activity as well as the presence of permanent fault currents to earth is defined by the threshold levels of embedded fault detection devices. The detection mechanisms of these faults depend upon the DC earthing characteristics of the PV system and are inevitably different for earthed and floating configurations. These faults can remain undetected since the allowable DC fault detection thresholds can be set high, to avoid lost production from false detections or "nuisance" trips from regular and inevitable leakage currents. The undetected DC faults arise as the existing detection thresholds for permissible DC leakage from PV systems have been based on other issues such as fire prevention or personnel safety. Nevertheless, the presence of permanent leakage/fault currents to earth can cause corrosion issues on nearby metallic infrastructures.

2.6.1 General Remarks

So far, the ground fault "*blind spot*" in earthed PV systems has been used to describe the presence of undetected, permanent ground leakage currents (i.e., a ground fault on earthed conductors) that can result in some sort of arcing or ignition should a subsequent ground fault occur on an ungrounded conductor of the PV system. The Solar America Board for Codes and Standards (Solar ABCs) [26], [58], [67], [68] has described the "*blind spot"*

problem as "*not an inherent limitation in the earthed/isolated configuration but rather an unintended consequence of the prevailing Ground Fault Detector/Interrupter (GFPD) method used to deal with multiple faults".*

At the same time, the board has correctly acknowledged that the so called "*blind spot"* phenomenon (i.e., ground fault in the earthed conductor) is not applicable in floating isolated systems since they have no grounded current-carrying conductors. However, excessive leakage currents due to various faults do exist in both earthed and floating configurations and if they are left undetected or unattended may facilitate serious failures in either of the two configurations.

To this extent, the leakage current detection thresholds tabulated in the UL 1741 [21] and in IEC 62109-2 [4] are set to protect the PV systems against serious failures. Nevertheless, the conclusion that can be drawn is that any DC leakage activity that falls below these thresholds may go undetected by the protection devices or mechanisms. Apparently, there will be no problem for disastrous failures if the fault level remains below the recommended threshold settings. Consequently, the presence of permanent DC leakage/fault currents below the threshold level is technically acceptable in large scale PV systems. However, should we, under certain conditions, worry about DC stray current corrosion that can happen in underground metallic structures that are laid nearby a large-scale PV system? More explicitly, are there any stray current DC corrosion blind spots?

It is worth reiterating at this point that stray current corrosion refers to corrosion damage resulting from direct current (DC) flow other than in the intended circuit. The first prerequisite to facilitate stray current corrosion is a leakage current that falls within the undetected threshold zones defined by the inverters (see Sec. 2.4). The second prerequisite is, for the faulted leakage current flowing into the earth to be persistent.

The formation of DC stray current interference can appear on PV plants, which are located in close vicinity to pipeline systems (see Fig. 2-8). At this point, it should be noted that when considering stray current corrosion, the location where the current first enters the ground will most likely be the PV module frame or buried cabling, where the insulation is damaged. If the damage is severe, rapid failure would be expected. Stray current corrosion at secondary locations is also possible. Large scale PV plants are often installed in rural areas and many such sites are remote from buried utility services, however, the sites may be near to metallic infrastructures, such as national networks of buried gas and oil pipelines, or even irrigation pipelines. To this end, let us consider the case where a faulted DC buried cable (that may act

as the source of stray leakage current into the soil), shares a parallel corridor with some buried metallic infrastructure (e.g., gas pipelines) located within or near the PV plant. It is highly probable, a proportion of the stray leakage current from the faulted DC cable is picked up on the nearby metallic infrastructure and travels for some distance before discharging back to the soil, to subsequently return back to the energy source. The latter rationally assumes that the stray current will attempt to return to the energy source through any low-resistance paths that exists within the soil. An analogy to the principle described above can be found in the Stray Current Control and Corrosion literature related to DC Mass Transit Systems [54]–[58]. These low resistance paths can be inherently given by metallic structures, especially when these structures are bare or not perfectly insulated. Thus, severe damage can occur on the metallic structures at the location where the current discharges back to the soil for its return to the energy source.

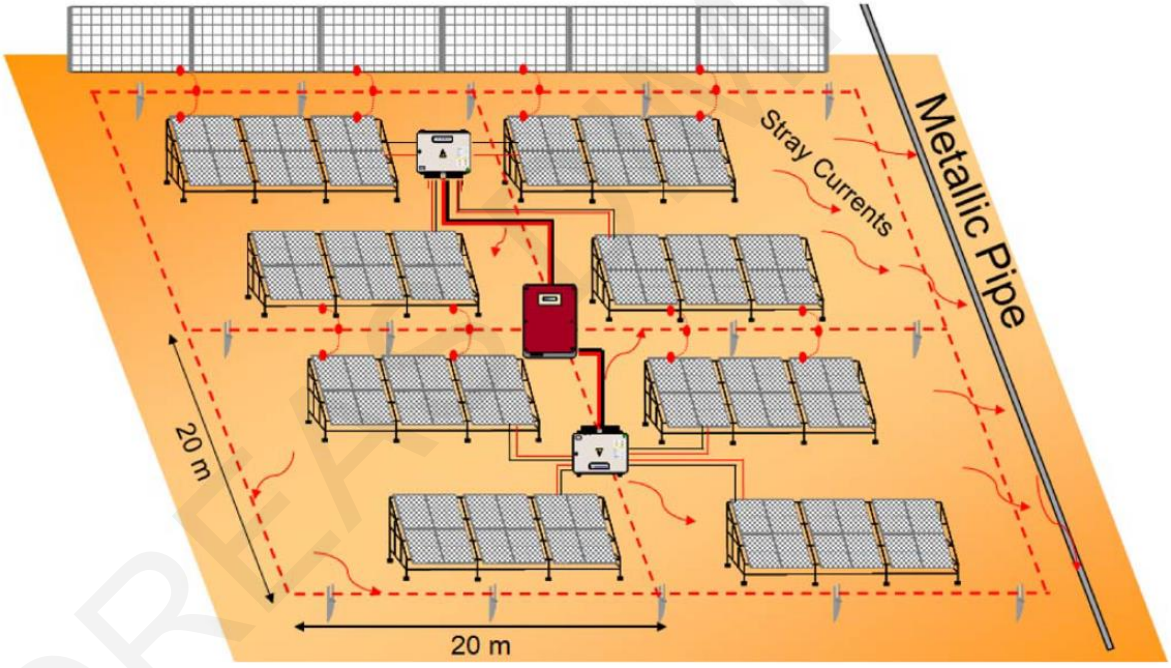

Figure 2-8: Stray current interference on pipeline system due to PV Plant operation

More explicitly, the mechanism of stray current corrosion in large-scale PV applications can be briefly summarized as follows: The leakage current (from PV modules and buried DC cables experiencing a fault or deteriorated insulation) will flow into the soil and may subsequently flow along parallel circuits either directly through the soil or through buried metallic structures, before returning back to the energy source. To this end, a current loop is formed. Thus, any nearby metallic structures that provide a convenient (mainly) parallel conductive corridor can be very good candidates to provide a path for ground-fault leakage currents to return to the energy source. Given that current flow in a metallic conductor is

electronic, while that through electrolytes such as the soil, concrete, etc., is ionic, it follows that there must be an electrochemical reaction (involving either ion to electron transfer as current enters a metallic conductor or electron to ion transfer as current discharges to earth) [10]. Therefore, where the current leaves metallic-pathways to earth (i.e., to return to the energy source) there will be an oxidation, or electron-producing, anodic reaction (see Eq. (2-2)). This reaction is visible after time as corrosion damage [9], [10].

$$General\ anodic\ reaction\ equation: M \rightarrow M^{n+} + ne^{-} \quad (2\text{-}2)$$

Accelerated corrosion on metallic objects will, hence, occur from each point that current transfers from a metallic conductor to an electrolyte. One should note that for pipelines or structures with cathodic protection applied, stray current may not always generate corrosion, and low levels of interference may be tolerated.

The above conceptual analysis dictates that it is equally important to consider/examine the DC leakage currents return path to the energy source, in both earthed and floating PV systems configurations.

2.6.2 PV Interference in Earthed PV systems

As previously described in Section 2.5, in earthed PV systems, it is possible to have DC fault/leakage current to frames emanating from the PV modules. It is also possible to have DC leakage currents from those portions of DC cables that are laid underground and are connecting, for example, any combiner boxes to the inverter. This type of PV system is usually grounded through the use of the Equipment Grounding Conductors (EGCs) which ensures that all metallic infrastructures (e.g., frames, metal frames, conduits, junction boxes, and inverter) are equipotentially bonded.

Thus, any leakage current flowing to ground should ideally be captured by the EGCs and should return via the grounded polarity conductor to the modules. However, the conductive ability of the EGCs may be limited or deteriorated by a number of factors such as: a) loose joints, b) resistance increase of grounding connections due to galvanic incompatibility and thus corrosion of different metals (e.g., modules, rails, grounding conductors), c) damp heat ageing, d) salt mist ageing and e) mechanical damage or failure of EGCs.

Under these conditions, it is highly probable that some portion of the leakage current will attempt to return to the energy source through any other low-resistance paths that exist in the nearby vicinity. For example, through the soil and metallic structures such as pipelines.

Consequently, at pipelines' locations where the current discharges back to the soil for its return to the energy source an acceleration of corrosion rate is expected. The concept described, is shown in Figure 2-9. It is noted that Figure 2-9 should be regarded as merely illustrative and the direction of stray current flows indicated by the arrows is a simplistic illustration to visualize the concepts verbally explained.

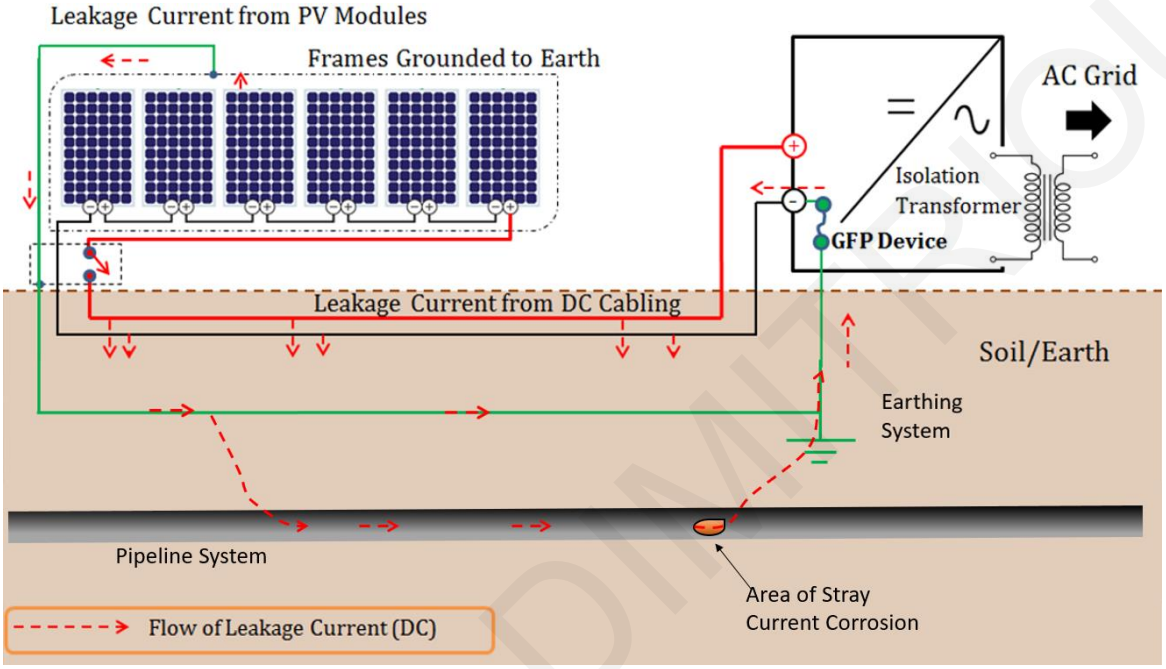

Figure 2-9: Graphical illustration of PV interference in Earthed PV Systems

2.6.3 PV Interference in Floating PV Systems

It should be reiterated from Section 2.5 that DC leakage currents are also present in floating systems due to the presence of resistive leakage paths to the ground (i.e., between the PV array and ground).

The extent of DC stray current corrosion concern in floating PV system configurations will be dictated by the current return path to the energy source which in turn depends on whether the system is galvanically isolated from the AC side or not. In isolated floating PV systems, the leakage currents may emanate both from the modules or the underground portions of DC cables (which have finite insulation) and will circulate through the soil and buried metallic infrastructure. As shown in Figure 2-10 by means of a merely illustrative example PV interference can lead in an accelerated DC stray corrosion on a nearby pipeline system.

The issue of leakage current flow from floating isolated PV systems can be exacerbated when the impedance formed by the circuit associated with a double fault is high. This

condition may allow not only a persistent flow of undetected (by IMDs) but also a corrosive leakage current to the earth.

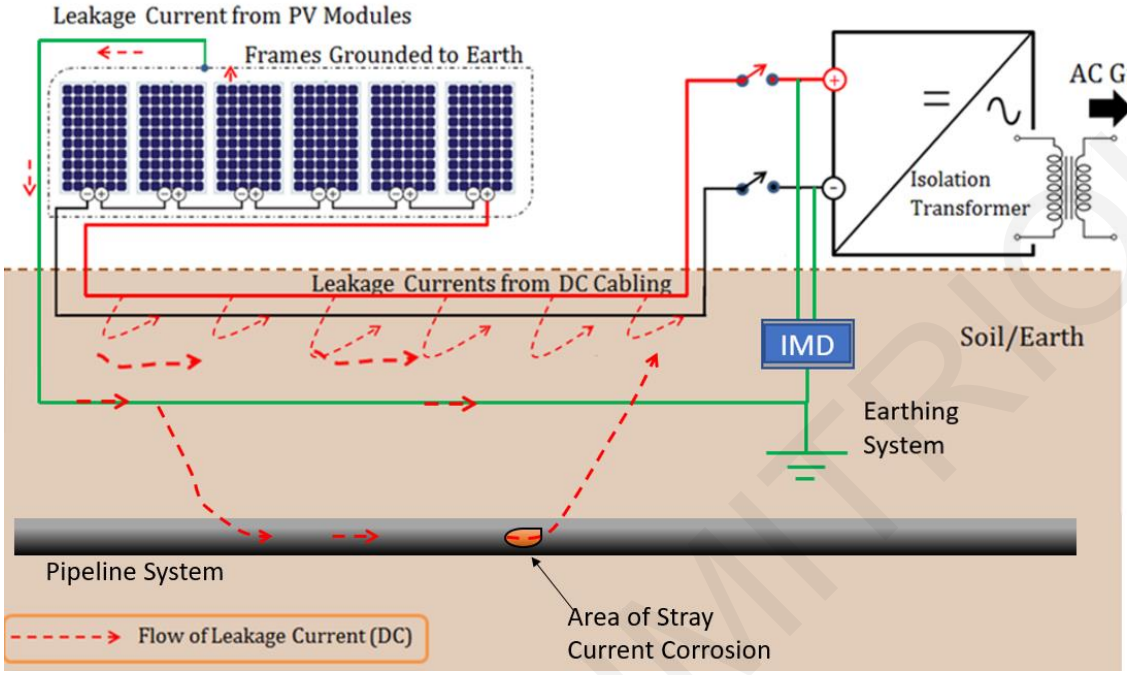

Figure 2-10: Graphical illustration of PV interference in Floating Isolated PV Systems

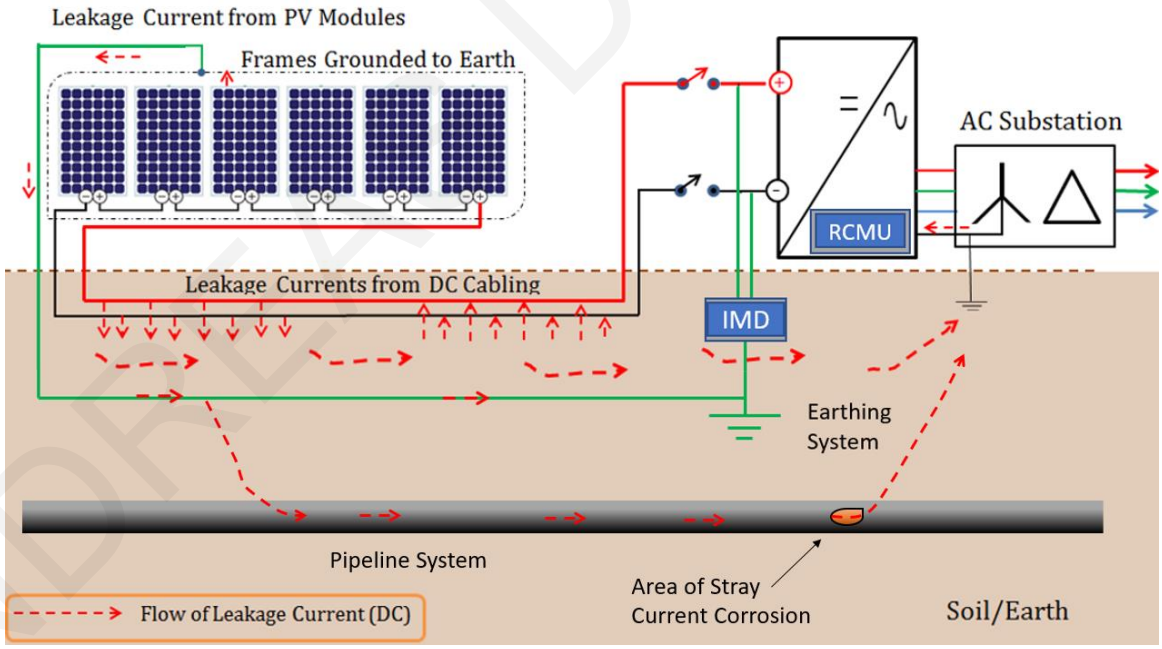

Figure 2-11: Graphical illustration of PV interference in Floating Non-Isolated PV Systems

Moreover, in floating PV systems (non-isolated) one should bear in mind that some DC leakage current would be allowed to return to the source via the AC side through the grounded neutral on the AC side (i.e., substation) as shown in Figure 2-11. If the substation is remotely located then the leakage current flowing into the earth may travel a considerable

distance to reach the grounding neutral of the substation in order to find a return point for the energy source.

It is therefore more probable to use any metallic low resistance paths (e.g., pipelines) that exist in the nearby vicinity, thus increasing the risk of stray current corrosion of these metallic paths at the location where the current will discharge to flow in the grounded neutral of the substation.

2.6.4 Towards Defining the Associated Corrosion Risk

The impact of stray current corrosion has been thoroughly assessed in DC traction systems (EN 50162 [7] & EN 50122-2 [2]) and a fair analogy can be drawn when assessing the impact resulting from large PV plants. Stray current interference from DC traction systems is characterized by repeated relatively short duration fluctuations, with rapid corrosion potential changes. Any interference from solar farms is more likely to be associated with the intrinsic characteristics of PV current generation that affects over a longer time period.

Faraday's electrolytic law (see Appendix A) is a useful application that correlates the current of an electrochemical reaction with the number of moles of the element being reacted and the number of moles of electrons that are participated in reaction process [9], [10]. Indicatively Faraday's law, for steel give a relationship where 1 amp.year of current will corrode approximately 9.1 kg (for lead the value is 33 kg). The above relationship implies that a constant flow of 20 mA DC would corrode 0.18 kg of steel in the course of a year. This amount of metal loss, if restricted to a localized area, could result in the loss of pipeline integrity. These figures highlight the severity and risks of the issue for unprotected assets. Such risks are at their highest in locations where there are densely-packed buried utility services.

In PV installation industry, the DC leakage-related research efforts have also been concentrated in demonstrating and characterizing the DC ground fault or quantifying allowable DC injection level into low voltage AC networks [27], [61], [74]–[76]. The ultimate objective of these efforts was to reduce PV systems' susceptibility to legitimate DC ground faults and to quantify the effect of DC injections on distribution transformers and on power quality issues. However, to appropriately calibrate the settings of the monitoring devices to detect legitimate DC faults entails the understanding of the typical leakage currents' level under normal operating conditions. In many occasions, however, the owners of utility-scale PV systems are concerned about lost production from false detections or

"nuisance" trips from regular and inevitable leakage currents. For this reason, a common practice followed by PV owners is to raise the current leakage detection thresholds higher, to maintain their systems' operation and availability. In fact, their most preferred option is to respond to a detected fault by triggering an alarm rather than immediately seizing the operation of the inverter. This practice, however, suggests the sustained operation of PV inverters in the presence of non-zero DC ground faults, which further entails the constant flow of leakage/stray currents through unintended return paths such as the soil or other conductive pathways.

To assess the stray current corrosion concern further, let us consider the standards' DC leakage detection thresholds for earthed and floating PV systems (described Section 2.4). For instance, in an earthed 300kWp PV system, the fault current detection threshold to prevent catastrophic failures is 5 A. On the other hand, if the system is floating the threshold is approximately 30 mA (R_{ISO} measurement dependent) before the inverter is operating, reaching the value of 3000 mA (in case of non- isolated PV systems) during the operation of the inverter. To this extent, we note that a practical criterion for characterizing the corrosion on metallic infrastructure "moderate to high" is for the estimated corrosion penetration rate to be approximately 10-100 μm/year [77]. This penetration range corresponds (according to Faradays' electrolytic law for Fe) to corrosion current density, at the discharge location. These figures highlight the severity and risks of the issue for unprotected assets. Such risks are at their highest in locations where there are densely-packed buried utility services or unprotected metallic infrastructures. Nonetheless, the up to date threshold levels [4], [21] of the leakage current detection devices for both floating and earthed PV systems are only calibrated to detect faults that their magnitude may exceed some hundreds of milliamps as discussed in the 300 kW example above. The latter implies the presence of undetected faults/ leakage currents that may result under certain conditions, in DC stray current corrosion on metallic infrastructure that is laid nearby large-scale PV applications [78].

However, in practice, the stray current corrosion risk is estimated by performing field measurements of voltage and current variations on interfered structures [7]. The methodology for capturing measurements depends on the nature of stray current interference. To this extent, it is necessary to interpret the PV interference mechanism in order to establish a tailor-made methodology for testing procedures regarding the stray currents originated from PV systems. The latter is thoroughly addressed in Chapter 5.

Chapter 3

Development of Modelling Techniques to Address PV Interference on Pipeline Systems from Earthed PV Systems

3.1 Introductory Remarks

As conceptually elucidated in Chapter 2, the DC leakage currents from PV plants can take the form of stray currents that subsequently interfere with nearby buried metallic infrastructures such as metallic pipeline systems. In Earthed Photovoltaic (PV) systems, DC leakage to earth comes as a consequence of the finite insulation withstand of energized components. However, on the occurrence of undetected blind spot faults, the DC leakage can be intensified. To this extent, this chapter presents a detailed PV interference modelling for assessing the impact of DC leakage activity of PV systems - particularly under undetected fault conditions, on a buried Gas pipeline system.

Specifically, this chapter elaborates on how an equivalent electric circuit of an earthed PV system is modeled in an object-based graphical environment of commercial software [79] (see Appendix C). This is achieved through the development of networks of conductors. The conductors are modelled in such a way to reflect on: a) the equivalent electric circuit of the PV system, b) all the electrical and insulation elements of the PV system and c) on the true installation topology of the PV modules, inverters, and associated DC cables. Thus, this modelling approach ensures the correct representation of all sources of DC leakage from an earthed PV system, in terms of their magnitude and relative location - with respect to the supporting, earthing and nearby third-party infrastructure (i.e. pipeline system).

A second feature presented in this chapter is the modelling of DC blind spot faults in earthed PV systems [26], [58], [67], [68]. Capitalizing on this feature would allow for PV interference modelling evaluations to effectively account for the impact of any undetected DC leakage (due to the blind-spot DC faults) on susceptible nearby pipeline systems. Thus, this modelling approach allows the reproduction of the expected fault and its location, based on the actual topology of the system.

The chapter is organized as follows: Section 3.2 elucidates the fundamental principles of the proposed simulation model via a small-scale PV model. It specifically elaborates on: a) how the DC leakage activity of an earthed PV system can be facilitated in a model that accounts for the true installation topology of the PV modules, inverters and associated DC cables and b) how the theory of blind-spot faults is accounted for, in such a model. Section 3.3 builds on the principles described in Section 3.2. It specifically describes a complete case study simulation model of a large-scale 864 kWp earthed PV park, which its operation interferes with a nearby gas pipeline. Moreover, some sensitivity analysis, to quantify and elucidate

the competence of the model, is also presented. Within Section 3.4, the impact of PV blind-spot faults on the DC interference occurring on a nearby gas pipeline is explicitly discussed.

3.2 Description of Fundamental Modelling Principles

3.2.1 Topologically Accurate Modelling of PV systems' DC leakage sources

The equivalent electric circuit of an earthed PV system can be represented by the model shown in Figure 3-1. The earthed nature of this model is achieved through the grounding of the negative DC cable at the inverter's level via GFPD. Through this earthing, a distinct voltage between the PV system and the earth is established. At this point, it worth mentioned that GFPD is usually a fuse-type system with negligible resistance which is connected in series between the earthing terminal and the negative current-currying conductor.

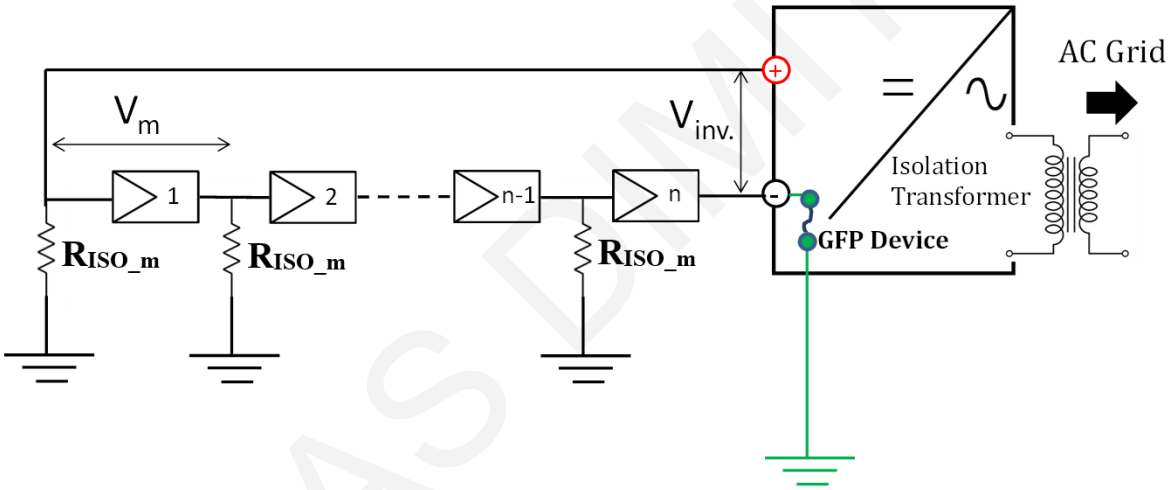

Figure 3-1: PV Array String of *n* Modules Connected in Series with Effective Insulation Resistance R_{ISO_m}

Thus, this simple system is effectively utilized to compute the leakage current emanating from the PV modules [18], [19]. With reference to Figure 3-1, V_m is the operating voltage of each PV module and R_{ISO_m} is the corresponding insulation resistance to earth. By applying Kirchhoff's first and second law the total leakage current I_{leak}, originating from n modules connected in series, can be given as in Equation (3-1).

$$I_{leak} = n \times \frac{(n+1)}{2} \times \frac{V_m}{R_{ISO\_m}} = \frac{(n+1)}{2} \times \frac{V_{inv}}{R_{ISO\_m}} \quad (3\text{-}1)$$

However, Figure 3-2 illustrates how the true topology of the equivalent electric circuit of the earthed PV system shown in Figure 3-1, can be modeled in an object-based graphical environment of commercial software [79] (see Appendix C). In particular, the model in Figure 3-2 relies on a network of conductors. The conductors are calibrated and oriented, in

such a way, to reflect on: a) the electric circuit of the PV system (see Fig. 3-1), b) all the electrical and insulation elements of the PV system, c) on the true installation topology of the PV modules, inverters and associated DC cables and d) the soil conditions. In particular, the model embraces: a) the metallic frames hosting the PV modules which are connected in series, b) a set of buried, in a uniform soil model 100 Ω.m, DC cables (positive and negative) that are routed from the series-connected PV modules to a central inverter, and c) the Equipment Grounding Conductor (EGC) [42] that ensures the equipotential bonding of all PV metal frameworks as well as their connection to an earthing grid.

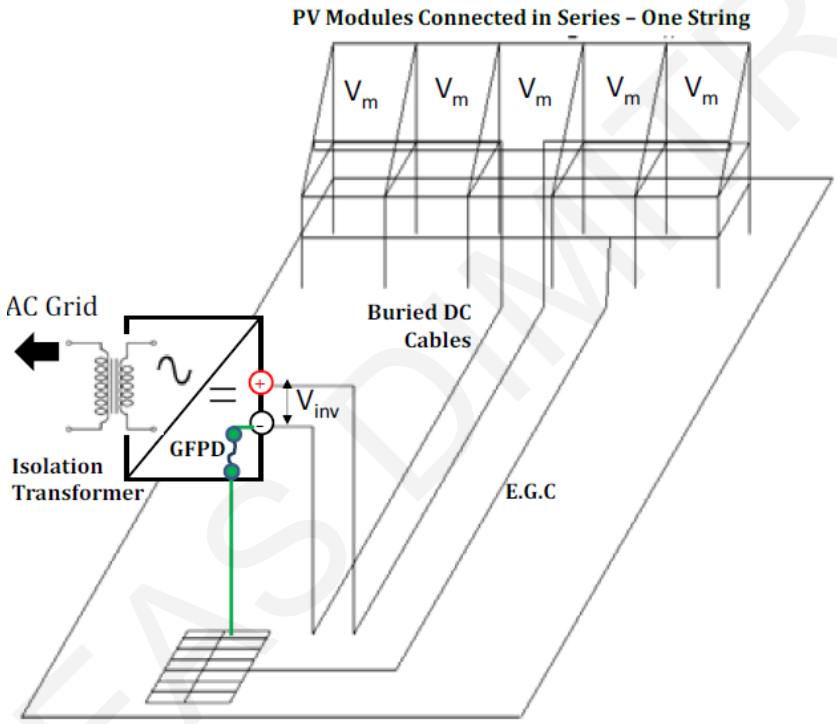

Figure 3-2: True topology of the equivalent electric circuit of the earthed PV system in CDEGS [79]

However, it should be kept in mind at this point that the primary objective, at this stage of work, is to calculate the DC leakage that is formed by the contribution of all the system's electric components (e.g. PV modules, DC cables, PV inverters). To reflect on this objective, the model shown in Figure 3-2 is transformed into the one shown in Figure 3-3. In particular, the simulation model shown in Figure 3-3 allows DC to be injected (*I*+) and collected (*I*-) at the modules' level (i.e. above the ground level). The energisation of the model is achieved through the use of a current source - to replicate the direction of flow for *I*+ and a sink to replicate the direction of flow for *I*-. This is an artificial component of the software [79] that allows an indirect snapshot of the DC circuitry's static power flow. Under this energisation principle, the model is subsequently able to compute the flow of DC through each individual

conductor that forms part of: a) PV metal frames and b) buried DC cables. This allows for the associated DC leakage activity to be topologically accurate, as thoroughly described below.

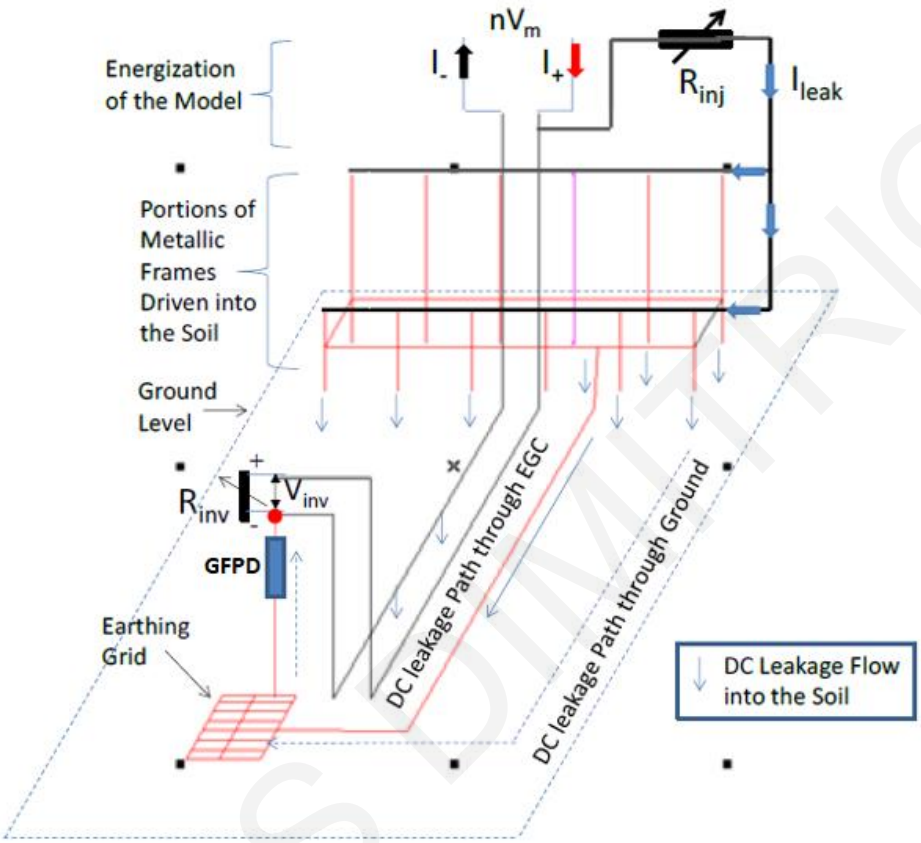

Figure 3-3: Topologically Accurate Model to Simulate DC leakage activity in a PV System

DC Leakage Activity Related to DC Buried Cables:

The DC leakage activity associated with the buried cables is directly controlled by: a) the cables' intrinsic insulation resistance to earth values and b) the potential difference that exists between cables' conductor and the earth. In particular, the potential difference between the DC cables is adjusted, in the model, through: a) a load resistance (R_{inv}) and b) the currents flowing in the DC cables ($I+$ & $I-$).

DC Leakage Activity Related to PV Modules:

The DC leakage that originates from the PV modules which subsequently streams through the metallic frames into the earth, has been modelled as follows:

1. The total leakage current (I_{leak}) originating from n modules connected in series is theoretically calculated using the equivalent electric circuit shown in Figure 3-1 and the equation described in Equation (3-1).

2. The corresponding I_{leak} value is integrated into the simulation model, as shown in Figure 3-3. This is achieved through the use of a lumped resistance R_{inj}. This resistance is interfaced between the positive DC cable (I+) and the metallic frames. Since the negative DC cable (I-) is grounded, the value of $R_{inj.}$ can be approximately calculated as the ratio of V_{inv} to I_{leak}. This ratio is effectively a function of R_{ISO_m} of the PV modules which are connected in series. The corresponding R_{inj} formulation is given in Equation (3-2). (Note: $R_{inj}>>R_{inv}$ therefore V_{inv} is exclusively controlled by R_{inv}).
3. Following the above two steps, the total leakage current (I_{leak}) is electrically and topologically divided in each portion of the metallic frame that is driven into the soil (see Fig. 3-3).

$$R_{inj} = \frac{V_{inv}}{I_{leak}} = \frac{V_{inv}}{\frac{n+1}{2}\cdot\frac{V_{inv}}{R_{ISO\_m}}} = \frac{2\times R_{ISO\_m}}{n+1} \qquad (3\text{-}2)$$

Return of DC Leakage to the Energy Source

With reference to Figure 3-3, the Equipment Grounding Conductor (EGC) is able to capture most of the leakage current emanating either from the PV modules or from the DC cables. Any remaining leakage current taking the form of stray current can return to the earthing grid through the soil, or through other conductive paths. The earthing grid however, is bonded to the negative DC cable at the inverter's terminal. This bonding allows the leakage current to return to the source.

Simulation Results of the Simple Case Study for Steady-State Conditions (SSC)

To illustrate the competence of the modelling technique described in Figure 3-3, the model is simulated as per the input particulars shown in Table 3-1.

Table 3-1: Input Parameters for Simulating Leakage Activity (SSC)

Description of Parameter	Value
V_module (V_m)	35,88 V
I_module (I_m)	6.9 A
V_inverter (V_{inv}) [5 modules in series]	179.4 V
R_{ISO_m}	10 MΩ
I leakage_modules (I_{leak})	53.82 μA (calculated as given in Eq. (3-1))
R_{inv}	26 Ω
R_{inj}	3333.3 kΩ (calculated as given in Eq. (3-2))

To this extent, Figure 3-4 illustrates the simulated current value (mA) as well as the direction of flow, in each modelled conductor.

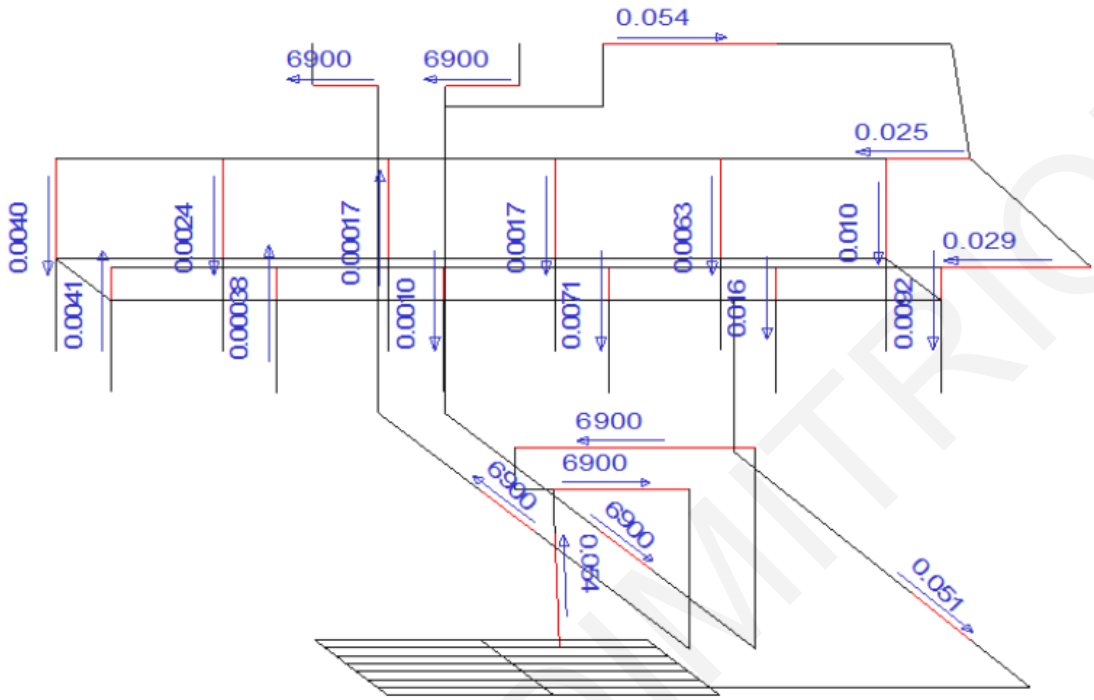

Figure 3-4: Calculated Current Flow in milliamps (mA) at the Origin of each Conductor Modelled – SSC

Table 3-2 summarises and confirms the expected/theoretical leakage performance of the system model (i.e. the calculated sum of currents leaking into the metallic frame (I_{leak}) equals the current flowing through GFPD (I_{GFPD}). In particular, 0.051 mA of leakage current is returning through the EGC and thus, 0.003 mA is returning through the earth.

Table 3-2: Summary of DC Leakage Activity (SSC)

Quantity Evaluated	Total Leakage Current (mA)
Calculated sum of currents leaking into the Metallic Frame (I_{leak})	0.054
Current flowing through EGC (I_{EGC})	0.051
Current Flowing through GFPD (I_{GFPD})	0.054
Current flowing through earth to return to the source (I_{Gr}) * $I_{Gr} = I_{GFPD} - I_{EGC}$	0.003

3.2.2 Modelling of DC Blind Spot Faults on Grounded PV systems

The equivalent electrical circuit shown in Figure 3-5 (a & b) serves to illustrate two separate blind-spot fault scenarios that may occur in an earthed PV system. In particular, the marked

fault (GF1) pertains to an accidental connection of the negative grounded DC cable with the grounded PV metallic frames at a combiner box (e.g. following a connector loosening). On the contrary, the marked fault (GF2) pertains to accidental insulation damage of a subarray grounded conductor. As shown in Figure 3-5 for both scenarios, some portion of the array current flows in the intended circuit and some portion flows in a parallel ground circuit, between the array and the negative-ground connection in the inverter. It should be highlighted that in the presence of a blind spot fault on a grounded conductor, a portion of the array current flows through the parallel circuit developed between fault location and inverter's earthing system. The magnitude of fault current depends on the fault resistance loop, which is established by the parallel circuit comprising fault impedance at fault point, EGC, soil, and the earthing system.

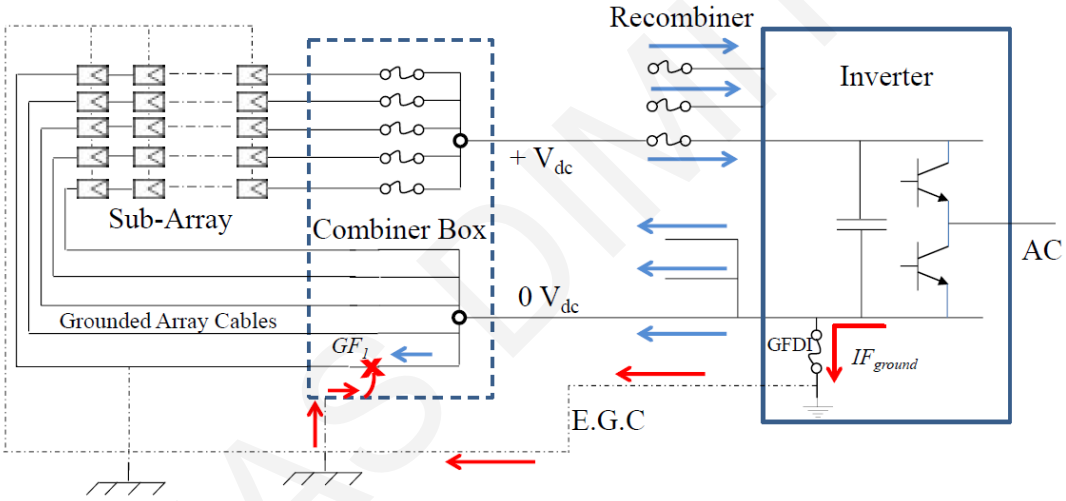

3-5 a. Blind-spot fault at a combiner box (GF1)

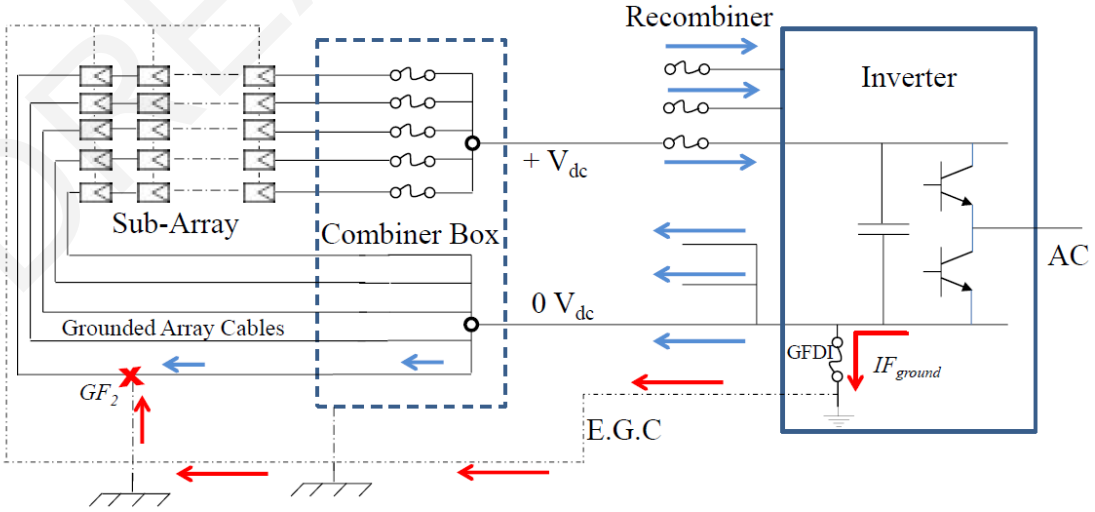

3-5 b. Blind-spot fault at a subarray conductor (GF2)

Figure 3-5: Equivalent Electrical Circuit to illustrate blind-spot faults

3.2.2.1 Integration of Blind Spot Ground Faults in the Model

Figure 3-6 illustrates the model that has been developed to simulate the impact of "*blind spot faults"* in the DC leakage activity of an earthed PV system. In particular, the model shown in Figure 3-6 is an extended version of that shown in Figure 3-3. The model embraces a conductor (R_{fault}) that bonds the grounded negative DC cable to the EGC. This allows for the modelling of a "*blind spot fault"*.

It should be noted that the "*blind spot fault"* has been simulated on the grounded negative cable, because of the low potential difference that exists between the negative cable and the earth. The latter may allow the fault current to remain below the threshold detection level, even in cases where the fault impedance is low. Within the model, the magnitude of the fault current is controlled by a load resistance R_{fault}. The value of R_{fault} is adjusted so that the fault current passing through the GFPD is lower than an interruption threshold level (e.g. < 5A). However, the magnitude of the fault current, returning through the GFPD, would be largely dependent on the fault return impedance path [62]. At the event of a fault, the fault current is allowed to flow from the inverter's grounded point to the earthing grid and it is subsequently returning to the fault spot through the EGC, the soil or any other high conductive paths in the nearby vicinity. The high conductive path, for example, can be offered by a buried gas pipeline that may be laid near the PV system.

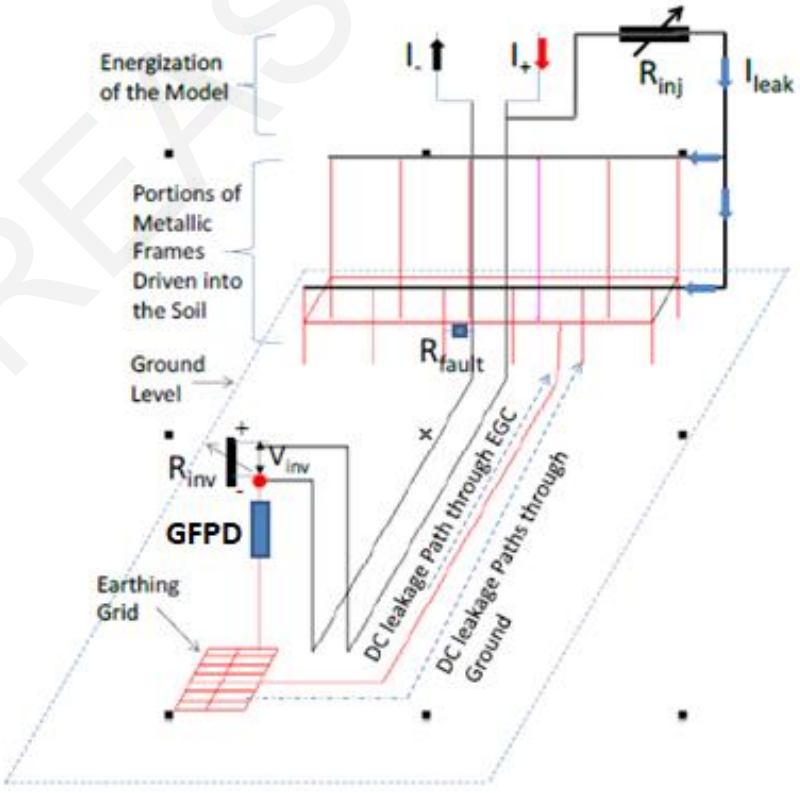

Figure 3-6: Topologically Accurate Model to Simulate DC leakage activity in a PV System under blind-spot fault conditions

3.2.2.2 Simulation Results of a Simple Case Study for Blind-Spot Fault Conditions (BSFC)

The competence of the BSFC model is tested under the input parameters shown in Table 3-3.

Table 3-3: Input Parameters for Simulating Leakage Activity (BSFC)

Description of Parameter	Value
V_module (V_m)	35.88 V
I_module (I_m)	6.9 A
V_inverter (V_{inv}) [5 modules in series]	179.4 V
R_{ISO_m}	10 MΩ
I leakage_modules (I_{leak})	53.82 μA (calculated as per Eq. (3-1))
R_{inv}	26 Ω
R_{inj}	3333.3 kΩ (calculated as given in Eq. (3-2))
R_{fault}	1 mΩ

Thus, based on the input parameters of Table 3-3, Figure 3-7 topologically illustrates the calculated current (mA) as well as its direction of flow, in each modelled conductor.

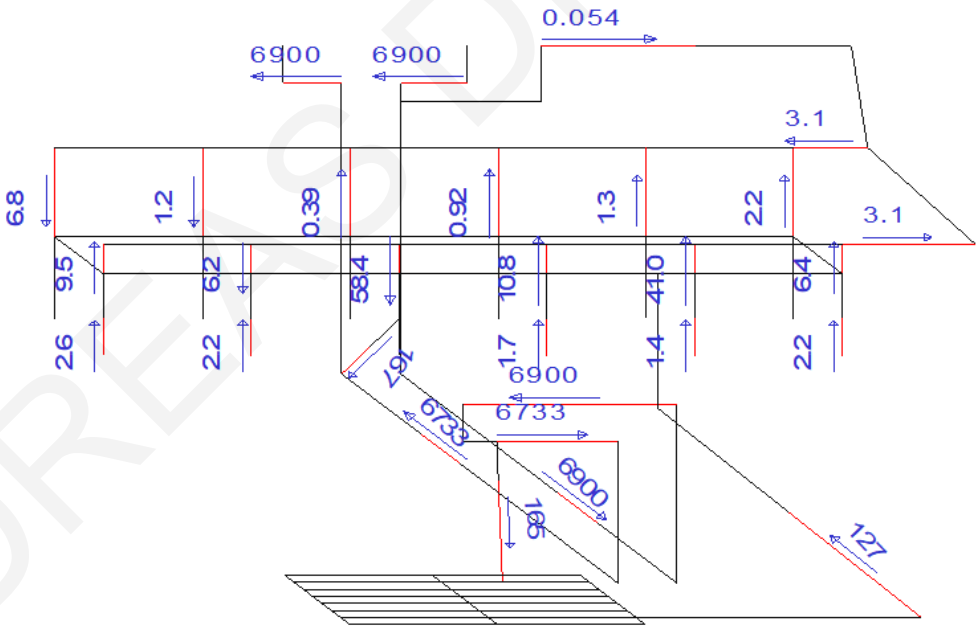

Figure 3-7: Calculated Current Flow in milliamps (mA) at the Origin of each Conductor Modelled - BFSC

Table 3-4 summarises and confirms that the circulation of current leakage in the various components of the model is accurate. In particular, because of the simulated fault, the total current returning to the source through the GFPD has been increased to 165mA. In fact, 23 % of the 165mA current is flowing through the soil while the 77% is flowing through the EGC, to reach the fault location.

Table 3-4: Summary of DC Leakage Activity (BSFC)

Quantity Evaluated	Total Leakage Current (mA)
Calculated Sum of currents leaking into the Metallic Frame (I_{leak})	0.054
Current flowing through R_{fault} (I_{RF})	167
Current flowing through EGC (I_{EGC})	127
Current Flowing through GFPD (I_{GFPD})	165
Current flowing through soil to return to the source (I_{Gr}) * $I_{Gr} = I_{GFPD} - I_{EGC}$	38

3.3 Case study of a utility-scale PV system and DC interference on nearby Gas Pipeline

The simulation principles and techniques described in Section above (Sec. 3.2) are applied to a realistic case study that involves a large-scale 864 kWp earthed PV park that its operation interferes with a nearby gas pipeline. The ultimate objective is the evaluation of PV interference under steady-state conditions and blind-spot fault conditions as well as the elucidation of parameters that influence the interference level.

3.3.1 Description of Physical System

Figure 3-8 illustrates the top plan view of an 864 kWp earthed PV park. The top plan view reflects on the actual topological arrangement of the PV arrays and on the dimensions of its constituent electrical components. In particular, the T-shape PV park consists of three identical PV arrays, each having a rated power of 288 kWp.

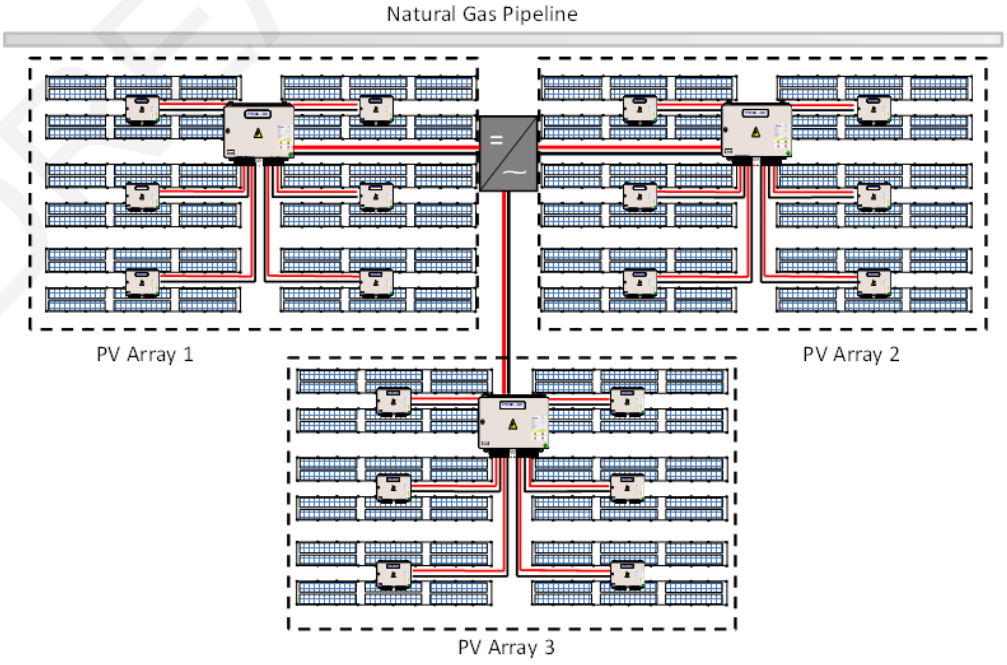

Figure 3-8: Topologically Accurate Top view of an 864kWp PV Park

Each PV array is occupying an area of 7875 m^2 by hosting 12 similar metallic structures of fixed inclination. Each metallic structure is supported by a group of 18 metallic poles which are extended into the soil at a depth of 0.9 m. Moreover, each structure comprises six PV-strings that are formed by the series connection of 25 PV modules. The nominal power of a single PV module is 160 W and at standard test conditions (i.e. 1000 W/m^2), I_{mp} is 4.53 A and V_{mp} is 35.3V. The dimensions of each PV module are 1m×1,3m and the rated insulation resistance (R_{ISO_m}) is 40 MΩ/m^2 [26]. The park's power production is controlled by a central inverter that hosts three main separate DC inputs, one for each PV array. More specifically, there exist 6 combiner boxes in each array and each box is consolidating the incoming power of 12 PV-strings into one feeder that is distributed via a pair of underground sub-array cables to a central combiner box.

The total produced power from each PV array is distributed from the corresponding central combiner box to the central inverter. This is achieved through a pair of underground array cables. Each pair is composed by one positive and one negative DC cable (i.e. current-carrying conductors).

3.3.2 Equivalent Simulation model

Using the topologically accurate design shown in Figure 3-8, an equivalent geometrically accurate model has been developed (see Fig. 3-9). In the interest of clarity, a portion (i.e. PV array 1) of the computer model formulated is also illustrated in greater detail in Figure 3-9.

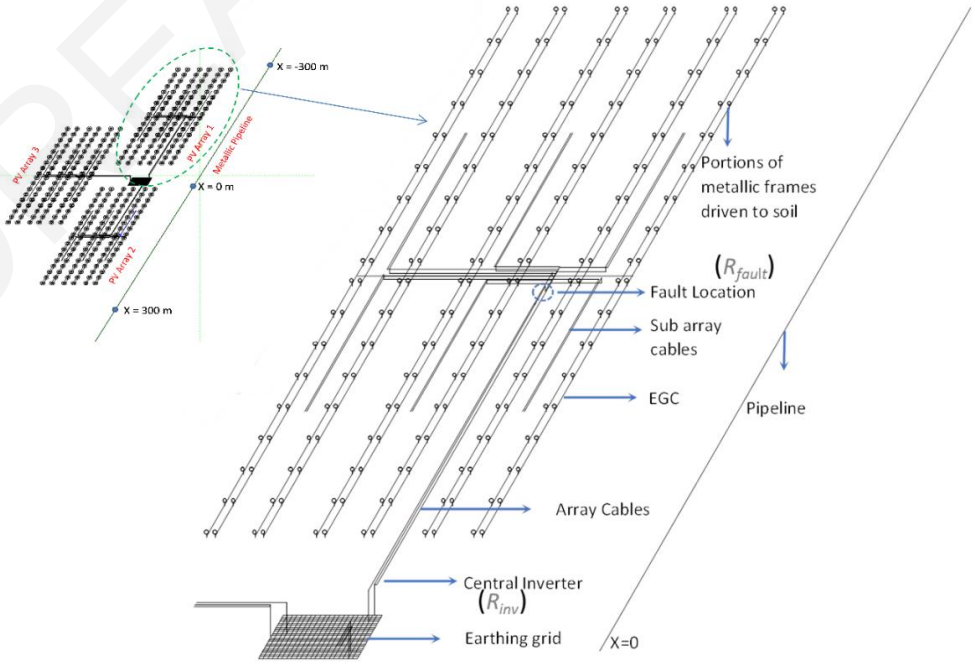

Figure 3-9: Design Detail of Full-Scale Simulation Model

With reference to Figure 3-9, the following items are described in more detail below:

Array cables and Sub-Array Cables: In PV systems, both the positive and the negative cables are current-carrying. Therefore, the size of the cable conductors (positive and negative) has been based on their required ampacity value [8]. In particular, the current-carrying requirements and insulation specifications, which are labeled in Table 3-5, are complying with standardized requirements [8]. Finally, in the simulation model, the cable conductors are buried into uniform soil (100 Ω.m), 0.25 m below the earth's surface.

Table 3-5: Specifications of Array and Sub-Array Cables

Specifications	Array Cables	Sub-Array Cables
Cross-sectional area of conductor (mm^2)	95	10
Current carrying capacity (A)	395	93
Thickness of insulation (mm)	1,1	0,7
Coating resistivity (Ω.m)	1.41×10^{16}	2.05×10^{16}
Insulation resistance (MΩ.km)	220	420

Central Inverter: As per the modelling principles described in Section 3.2, the central inverter is modeled as an ideal conductor having a lumped resistive load (R_{inv}) to control the operating voltage of the system.

Equipment grounding conductor (EGC): The conductor is made of copper with the cross-sectional area (CSA) of $6mm^2$ and ensures that all metallic infrastructures (e.g. frames, metal frames, conduits, junction boxes, and inverter) are equipotentially bonded [42].

Earthing Grid: The earthing grid (15m×15m) is modeled as a group of interconnected cylindrical conductors buried under the central inverter house. The dimensions of the cylindrical conductors as well as its buried depth were chosen to provide an equivalent 1 Ω earthing resistance in a uniform soil of 100 Ω.m.

Portions of Metallic Poles Driven to Soil: These are galvanized steel conductors that are modelled to replicate the portions of the PV façade frameworks driven into the soil. In total, 216 metallic elements have been modelled for each array section. The portions are driven into a depth of 0,9 m below the earth's surface. Each portion has an effective CSA of 141 mm^2.

Gas Pipeline: A Gas Pipeline has been modelled as a hollow metallic conductor of 10km (-5km to 5km) length with 0,6m diameter and 2 cm wall thickness. It is buried 1.5 m below the earth's surface. Moreover, the pipeline is coated with a layer that has 2 mm thickness and

a resistivity value of 10^8 Ω.m complying with [80]. As shown in Figure 3-9, the pipeline is running in parallel to PV Park from -300m to +300m, at a distance of 28m.

Blind spot fault: The blind spot fault has been modelled through the use of a high load resistance (R_{fault}) as per the principles described in Section 3.2. The location (see Fig. 3-9) of the fault is varied according to the simulation requirements, as will be further illustrated.

3.3.3 Simulation Results and Sensitivity Analysis.

A) Simulation Scenarios

This section hosts the simulation results of two reference scenarios that rely on the maximum power production operation of PV Park. The first scenario pertains to the case where PV Park operates under Steady-State Conditions (*SSC).* The second scenario pertains to the case where the PV Park operates under an undetected Blind-Spot Fault Condition (*BSFC)* by simulating a fault current of 4.8 A (i.e. just below the 5 A detection threshold).

B) Theoretical Benchmarking of Results (GPR)

Initially, the model is calibrated through R_{inv}, so that in conjunction with the cables' rated currents (see Table 3-5), the corresponding potential difference between the positive and the negative main (array) cables is established. To this end, Figure 3-10 plots the ground potential rise *(GPR)* of the main (array) cables associated with PV Array – 2. It is noted that similar behavior is observed for the *GPR* of the rest of cabling pairs; however, in the interest of space, only one pair is presented.

The results shown in Figure 3-10 reveal that under *SSC* the *GPR* of positive array cable (*SSC+ve*) is 889,8V near the central combiner. The *GPR* of the cable is gradually reducing to 883 V at the central inverter. Respectively, the *GPR*, of the negative cable (*SSC-ve)* ranges from -6,5V to -0,01 V. It should be noted that this small voltage variation along the cables' length, is due to their conductors' longitudinal resistance. As shown in Figure 3-10, the grounded end (i.e. at the inverter's location) of the negative cable is close to the earth's potential. However, this value is not zero because the leakage current from the PV modules and the cables, returns via the grounded conductor to the source. The return of this leakage current creates a local potential shift at the grounded terminals of the negative cable. Furthermore, the GPR of the cables under *BSFC* is marked in Figure 3-11.

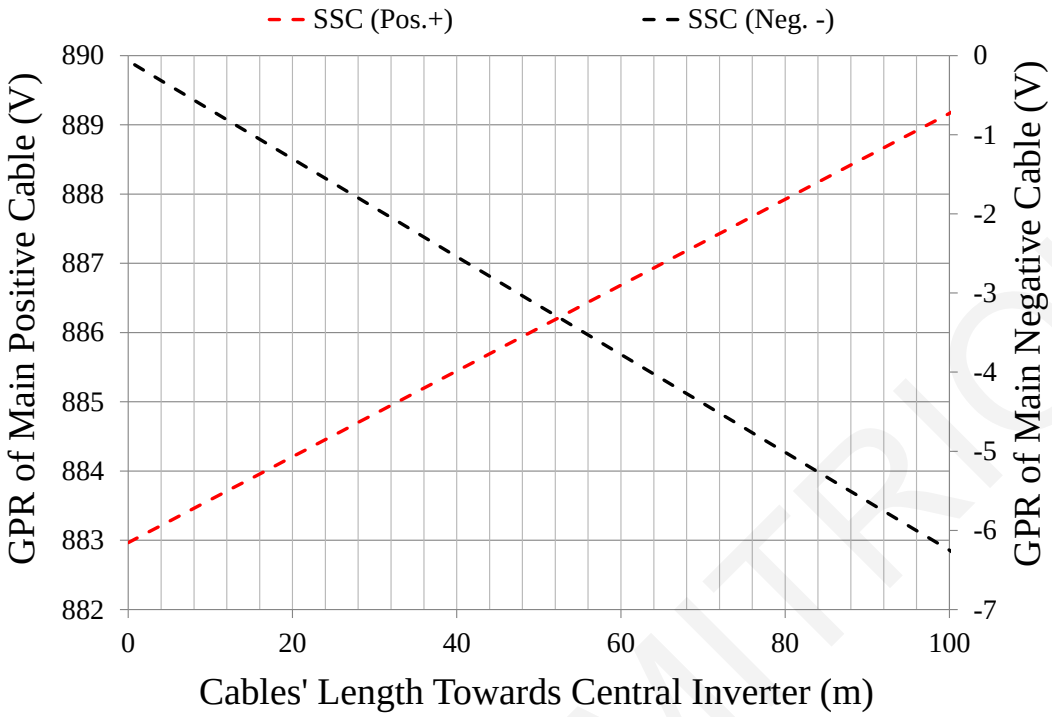

Figure 3-10: Ground Potential Rise of main Array Cables (SSC)

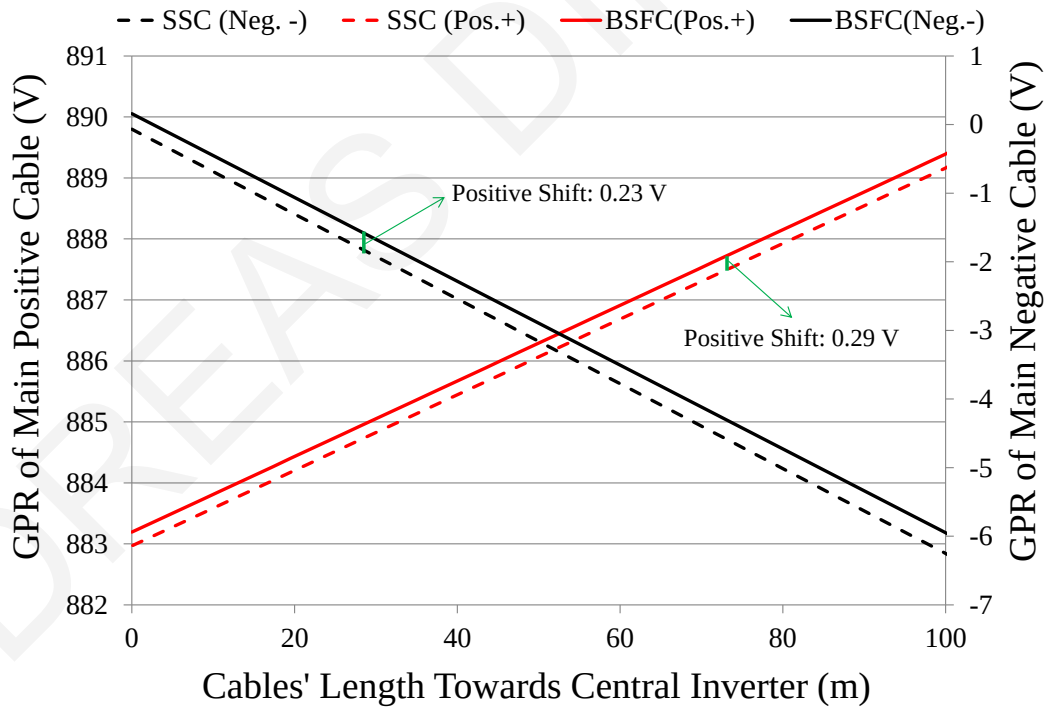

Figure 3-11: Ground Potential Rise of main Array Cables (BFSC)

In particular, when simulating a blind spot fault (4.8 A) on the negative cable, at a location near the central combiner (see Fig. 3-9), the fault current is allowed to flow from the inverter's grounded point to the earthing grid. From the earthing grid, it is subsequently returning to the fault spot through: a) the EGC, b) the soil and c) any other conductive paths such as the gas pipeline. Thus, the fault current flow produces a rise in the earth's potential.

As a consequence, a *GPR* shift on the positive (*BFSC+ve)* as well as on the negative (*BFSC-ve)* cable will take place. These shifts are benchmarked against the *SSC* GPR results and are clearly displayed in Figure 3-11.

C) Theoretical Benchmarking/Validation of Results (Current Flows)

With regard to the calculated current flows in the positive and negative cables, the simulated results for both scenarios are shown in Figures 3-12 and 3-13 respectively. Figure 3-12, in particular, shows a snapshot of the current flowing in both the positive and negative main (array) cables of PV Array 1 under SSC. The results displayed in Figure 3-12 confirm that the currents, flowing in both the positive and negative main (array) cables of Array 1, are equal in magnitude (i.e. 326 A) and opposite in direction. The total return current (i.e. from the earthing grid to the negative cable) is approximately equal to 30 mA (28mA). This current (~28 mA) confirms that the leakage from the PV modules (R_{ISO_m} = 40 MΩ/m^2, 12 structures with six PV-strings each, formed by the series connection of 25 PV modules) is returning to the PV source through the earth.

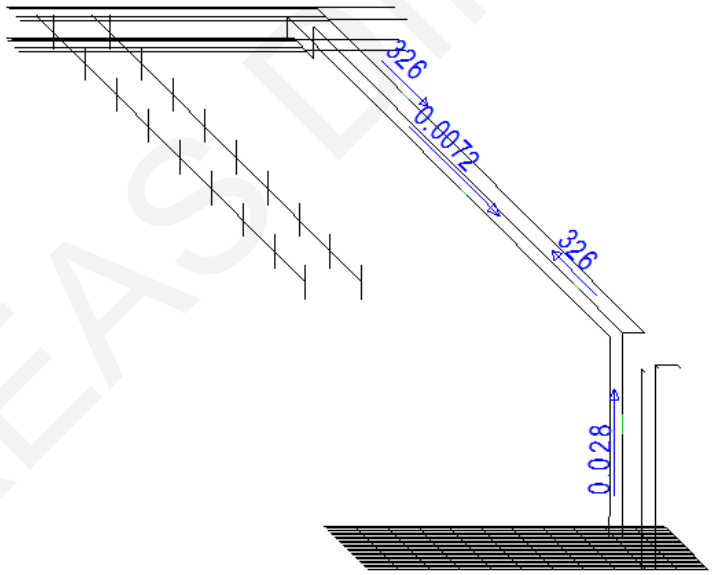

Figure 3-12: Currents flowing in the positive and negative main (array) cables of Array 1 (SSC)

Moreover, Figure 3-13 shows a snapshot of the current flowing in both the positive and negative main (array) cables of PV Array 1 under the *BFSC*. In this scenario, the results show a distinct difference between the current flowing in the negative cable (i.e. 321 A*)* and in the positive (i.e. 326 A*)* cable. This is because 4.8 A is allowed to flow from the inverter's grounded point to the earthing grid. From the earthing grid 4.7 A is returning to the fault spot through the *EGC*, while the remaining 0.1 A returns to the fault spot through the soil or other conductive paths.

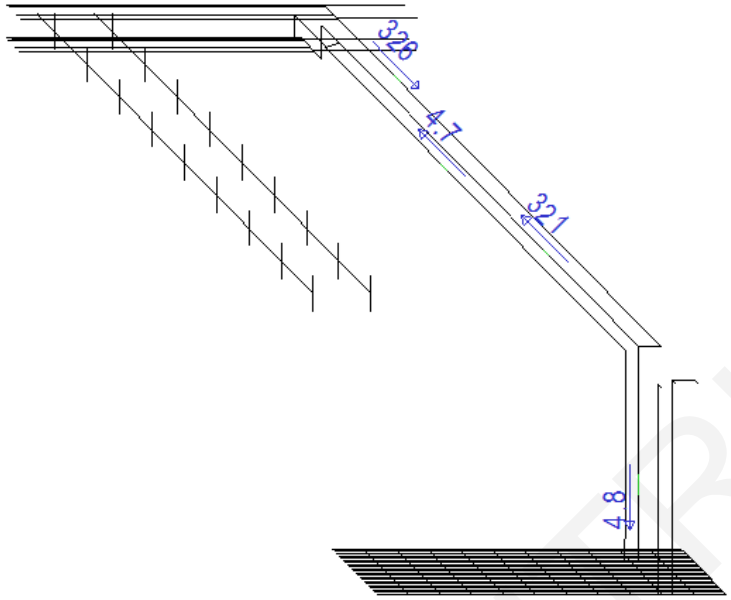

Figure 3-13: Currents flowing in the positive and negative main (array) cables of Array 1 (BFSC)

3.3.4 Sensitivity Analysis

The first set of sensitivity analysis serves to investigate the DC leakage performance of the main (array) cables of PV Array 1 under SSC. This is performed to highlight that when the insulation of buried main (array) cables becomes ineffective or deteriorated - due to moisture ingress, freeze/thaw cycles or accidental damages - the leakage currents flowing through the soil will be increased. In the simulation model, the level of leakage current flowing in the soil can be calculated through the total current returning from the earthing grid to the inverter. Thus, Table 3-6 illustrates how the level of leakage current is associated with the decreased insulation condition of the main PV array cables. The results are benchmarked against the leakage performance of the reference model, shown in Figure 3-12 (i.e. 28 mA when the insulation resistance of the main array cables is 220 MΩ.km). These results suggest that if the insulation resistance of the main array cables is reduced by three orders of magnitude, then the leakage activity through the soil is exponentially increased by ~529 %.

Table 3-6: Sensitivity Analysis for the Leakage Performance of Main PV Array Cables

Insulation resistance of Main Array Cables (MΩ.km)	Total return current from the earthing grid to the Inverter (mA)	% Increase relative to 220 MΩ.km
220 MΩ.km	28 mA	-
22 MΩ.km	31.5 mA	12.5 %
2.2 MΩ.km	41 mA	46.43 %
0.22 MΩ.km	176 mA	528. 57%

Moreover, it is important to note that in all the parameters detailed in the DC leakage/ stray current performance of the simulation model, the soil resistivity is likely to introduce the greatest source of uncertainty [81] into the analysis process. The soil resistivity (and structure) is, however, difficult to measure and will change as a function of the seasons/weather conditions. However, it is essential to highlight that the lowest the soil resistivity is, the more pronounced it would be the concern that in case of *BFSC* the increased leakage fault currents will flow through the soil, rather than through the intended paths (e.g. the Equipment Grounding Conductor –EGC). The latter is demonstrated through the sensitivity analysis summarised in Table 3-7. More explicitly this sensitivity analysis, serves to demonstrate how the DC fault flow (under *BSFC*) through the EGC is varied when the soil resistivity is different to that used in the reference model's results, shown in Figure 3-13 (i.e. 4.7 A when the soil resistivity is 100 Ωm). It should be mentioned, that the earthing resistance of the PV plant's global earthing system (i.e. interconnected inverters' earthing grid, EGC conductors and metallic posts) is allowed to vary, according to the soil resistivity value. The results reveal that when the soil resistivity is relatively low (i.e. 10 Ωm), then the fault current through the EGC is reduced by 16.56 %. In contrast, when the soil resistivity is relatively high (i.e. 1000 Ωm) then the fault current through the EGC is increased by 1.67 %. The essence of these results is that any stray current corrosion concerns - associated with PV interference investigations on nearby buried pipelines - would be more pronounced in low soil resistivity environments.

Table 3-7: Sensitivity Analysis for the Impact of Soil Conditions on the Efficiency of EGC Under BSFC

Soil Resistivity (Ωm)	Current through the EGC (A)	% Increase relative to 100 Ω m
10	3.93 A	-16.56 %
100	4.71 A	-
500	4.78 A	1.48 %
1000	4.79 A	1.67 %

3.3.5 PV Interference Evaluation on Gas Pipeline

The quintessence of the modelling technique described in Sections 3.2 and 3.3, rests with the ability of the model to evaluate the PV interference level on the buried gas pipeline system. As the PV stray current flows within the soil, it initiates local variations in the soil potential in the PV Park's area. Since the pipeline is coated with a high-resistance insulation material, a voltage potential difference is established between the pipeline's metallic wall and the adjacent soil. To this extent, in coated pipeline systems the PV interference can be

interpreted as a variation of pipe to soil potential (PSP) (see Sec. 1.2). The PSP equals to the voltage difference between the soil at the surface of the pipeline and its metallic wall. For the examined case study, the calculated PSP on the interfered section of the gas pipeline shown in Figure 3-14. This voltage potential basically indicates the stress voltage applied on the coating material along the length of the pipeline.

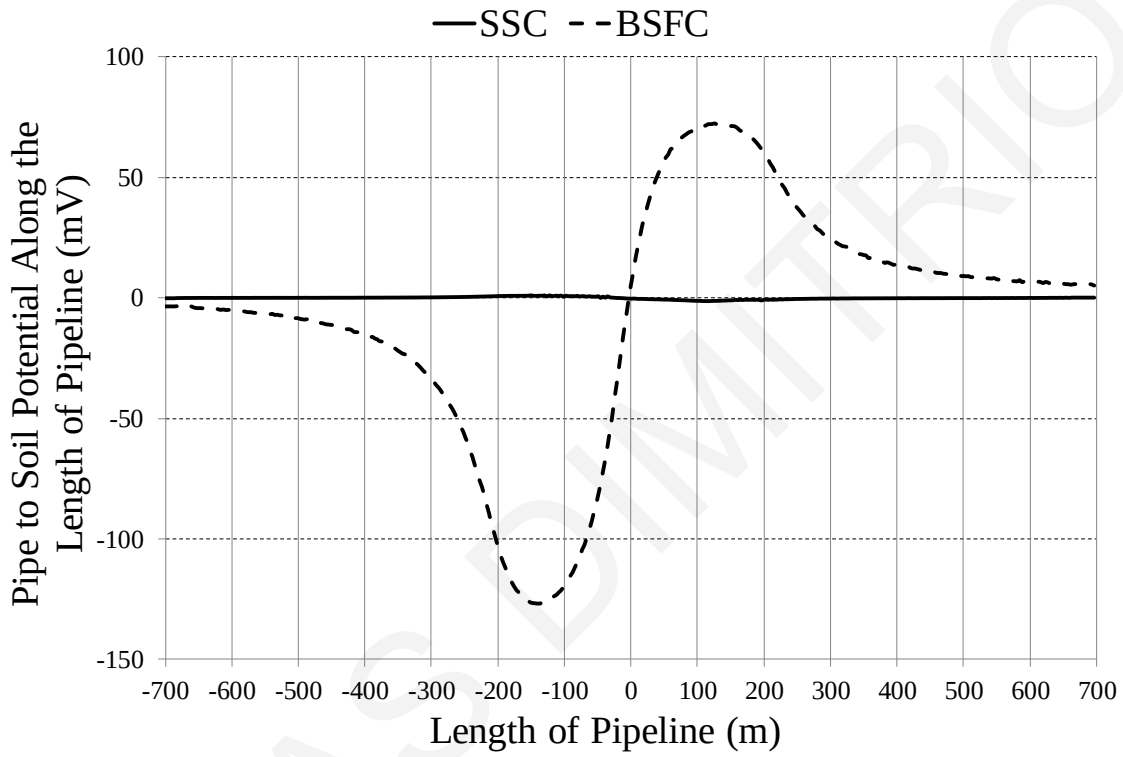

Figure 3-14: Pipe to Soil Potential Along the length of Pipeline under SSC and BSC

In particular, Figure 3-14 shows the calculated PSP on the interfered section of the gas pipeline, both under SSC and BFSC. Specifically, the results show that under SSC the impact of DC leakage activity on the gas pipeline is negligible. In contrast, under BSFC the calculated pipe to soil potential is much higher. The spatial results show that there is an anodic (negative values) and a cathodic (positive values) region. This entails that stray currents can enter the pipeline through coating defects where the voltage is positive (i.e. the earth's potential is higher than on the metallic wall) and where the voltage is negative (i.e. the earth's potential is lower than on the metallic wall) the currents will leave the pipeline to return to the energy source.

In practice, such field measurements (i.e. pipe to soil potential) are suffering from ohmic voltage drops - known as IR drops [7]. This is because it is not practical to place a reference electrode too close to the pipeline. Thus, the advantage of the developed model is its ability

to account for the local pipeline's potential shift at the coating / electrolyte interface, by excluding any IR drops. The calculation in the model, is achieved by computing the difference between the earth's scalar potential which is calculated at the surface of the pipeline's coating and the pipeline's metal GPR. This feature is particularly useful, since estimating the local PSP allows for the subsequent quantification of the DC current density through the coating defects of pipelines. In principle, the current density can be calculated by PSP with the ohmic resistance of the coating defect to earth (i.e. spread resistance) as per an assumed geometry of the coating defect, to estimate the metal loss on the pipeline and the subsequent reduction of its useful time [10], [23].

As per the Annex C of EN 50162 [7], the current density flowing through a circular coating defect is calculated via Equation (3-3) if the pipe to soil potential is known:

$$J = \frac{8(PSP)}{\rho \pi d} \qquad (3\text{-}3)$$

where ρ is the electrolyte resistivity (i.e. soil resistivity) and d is the exposed steel surface diameter. By integrating the current density for a certain period and by applying Faraday's electrolytic law a thickness of corroded metal can be deduced (see Appendix A).

With reference to Figure 3-15, if a blind spot fault occurs in a PV plant, then locally - at the area of inverter's earthing grid, an earth potential rise (EPR) is expected at the location where the fault current is injected into the soil. On the contrary, at the blind spot fault location, the fault current returns back to the energy source. The latter entails an earth potential fall (EPF) at the current's return location. Depending on the relative pipeline's routing, the pipeline may be influenced by these earth potential variations. Since the pipeline's metallic wall has a GPR close to zero, at the areas where the soil exhibits an EPR, stray currents are forced into the pipeline's metallic wall through coating holidays. Inversely, at the areas where soil exhibits an EPF stray currents are discharged back to the soil through remote coating holidays – thereby accelerating the corrosion rate locally.

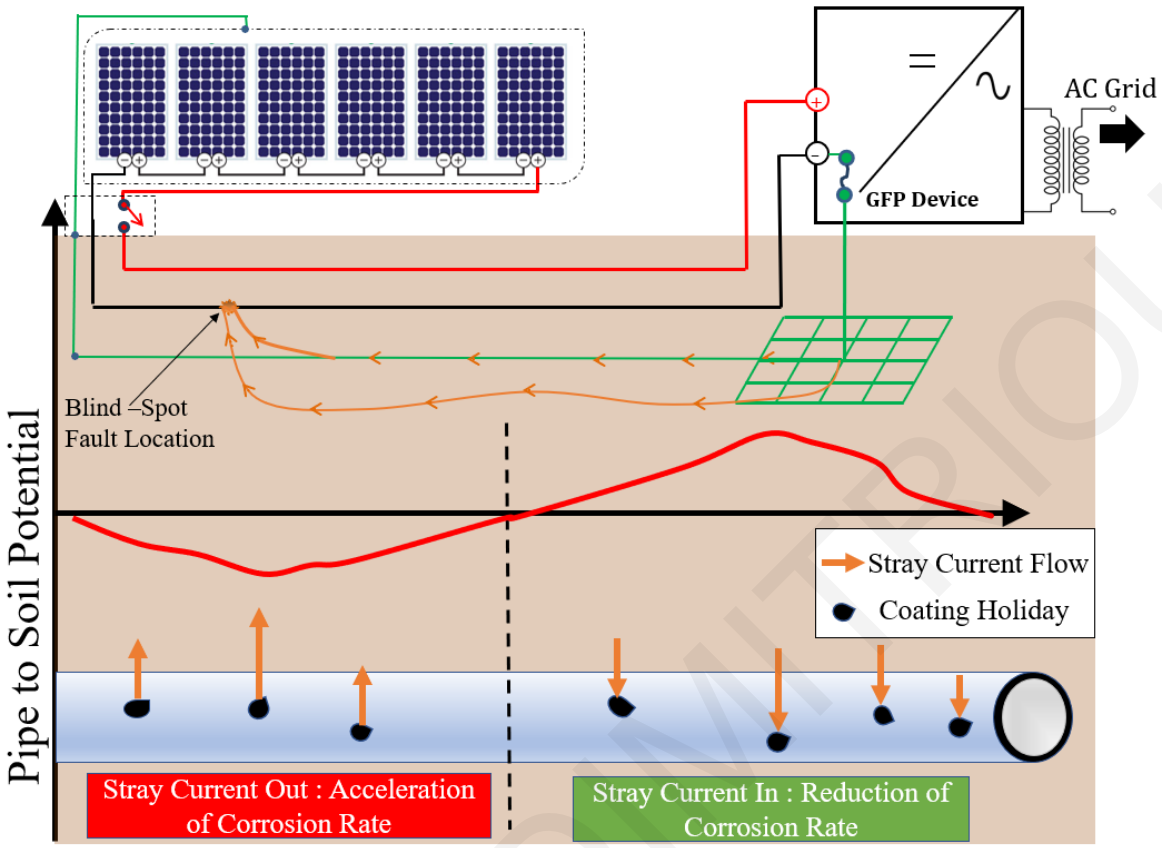

Figure 3-15: Interference of stray currents on the pipeline section under blind spot fault conditions

- ***Influence of Separation Distance Between PV Plant and Pipeline:***

Figure 3-16 illustrates some sensitivity analysis with respect to the variation of the PSP by changing the separation distance between the pipeline and the faulted PV Array. The results, in this occasion, show that PSP decreases as the pipeline's distance from PV Park increases.

Finally, it should become clear that the extent of any stray current corrosion damage on a third-party infrastructure would be specific to the characteristics and topology of each large-scale PV installation. It will also be specific to the relative position of any metallic infrastructure with respect to the blind-spot fault location that would occur on the PV system. The latter can be evidently assessed through the results shown in Figure 3-16.

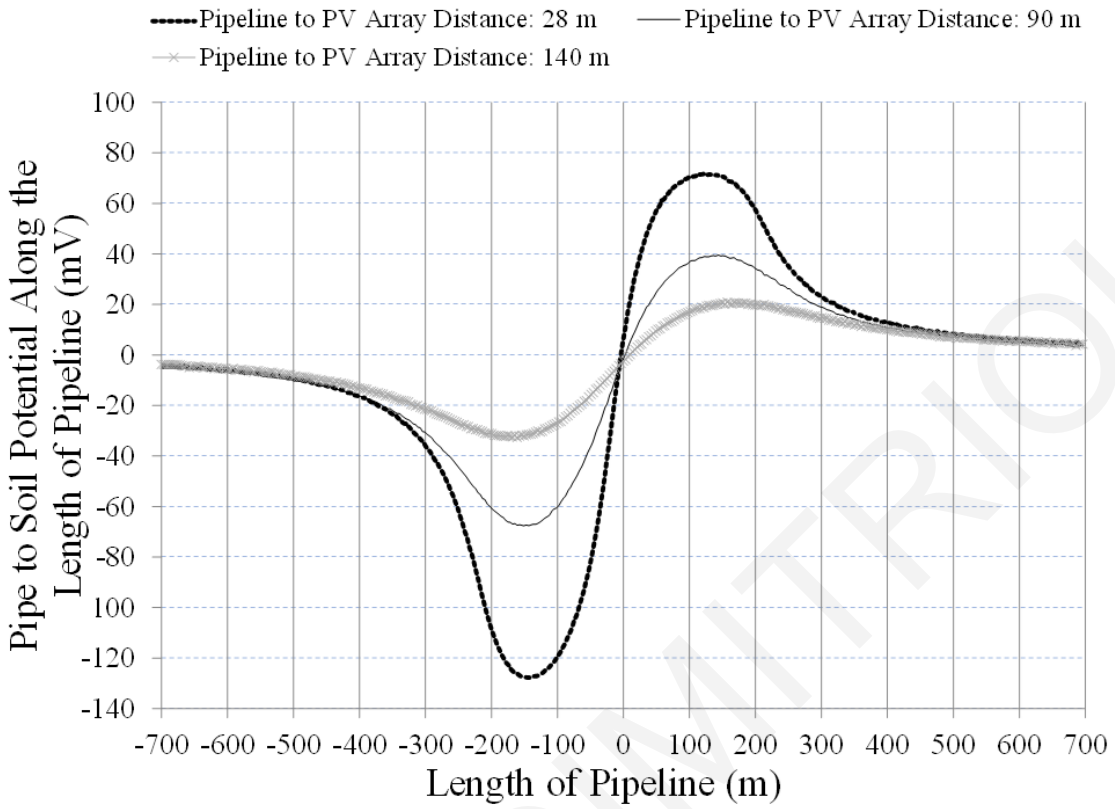

Figure 3-16: Sensitivity Analysis of PSP on the interfered section of pipeline under BSC for varying distances from Faulted PV Array

Influence of Blind Spot Fault Location: The results exhibited in Figure 3-17 show what would be the impact on the pipeline, should the blind-spot fault (i.e. 4.8 A) occur on PV-Array 1, PV Array 2 or PV Array 3 (See Fig. 3-8 and Fig. 3-9). In all cases, the blind-spot fault has been simulated on the grounded negative main array cable, near the central combiner. As expected, a blind spot fault on PV Array 3 has the less impact on the pipeline. Due to the symmetry of the system modelled, a fault on Array 2, would mirror the anodic interference section of the pipeline at X=0.

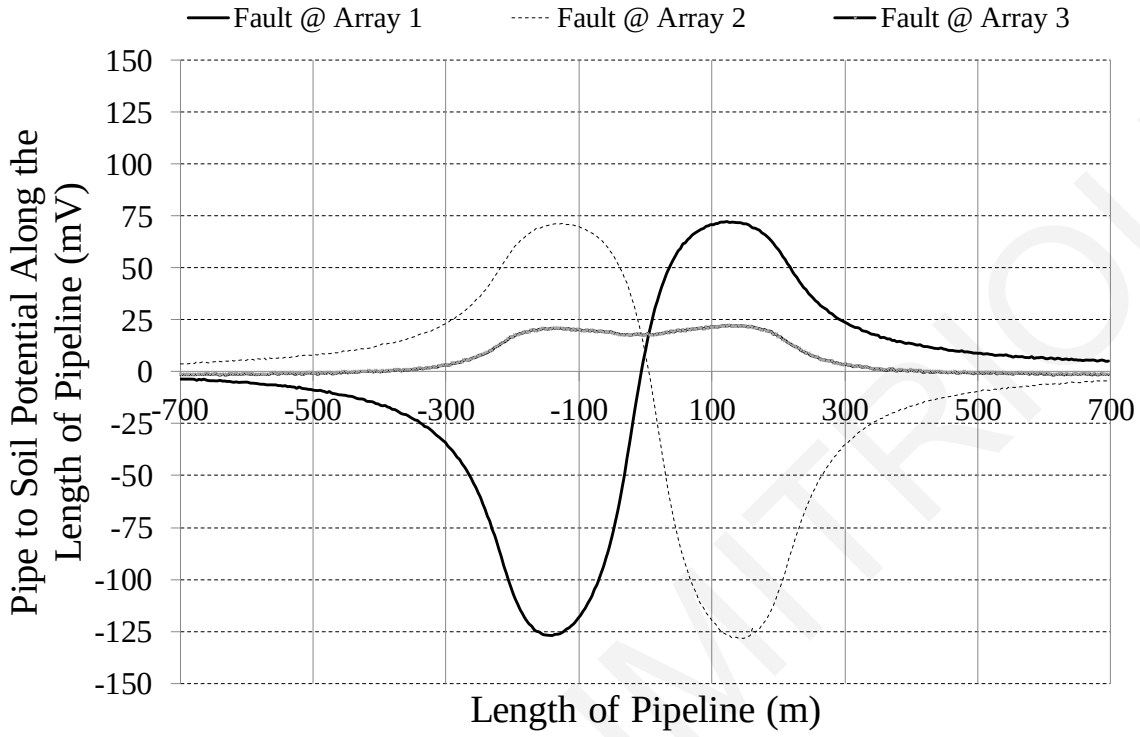

Figure 3-17: Pipe to Soil Potential Along the length of Pipeline for Different Blind Spot Fault Locations

- ***Influence of Blind Spot Fault Impedance:***

The magnitude of fault current under BSFC, depends on the fault resistance loop which is established by the parallel circuit comprising fault impedance at fault point, EGC, soil, and the earthing system (see Sec. 3.2.2). The fault impedance is the impedance that is established through the path connecting an energized component (i.e. negative current-carrying conductor) with an earthed component. Since the fault impedance value can vary depending on the conductivity of the established path, Figure 3-18 presents the PV interference by a) twice and b) four times the fault impedance in comparison to its initial value.

The level of PV interference is inversely proportional to the fault impedance value (see Fig. 3-18). This means that the fault impedance value is the dominant resistance in the overall fault resistance loop. In extension, the magnitude of fault current (which is the source of interference) is predominately adjusted by the fault impedance value. This can be justified by comparing the magnitude of the return current (see Tab. 3-8) flowing from the earthing point of the negative current currying conductor (see Fig. 3-13). The magnitude of the return current is inversely proportional to the fault impedance value.

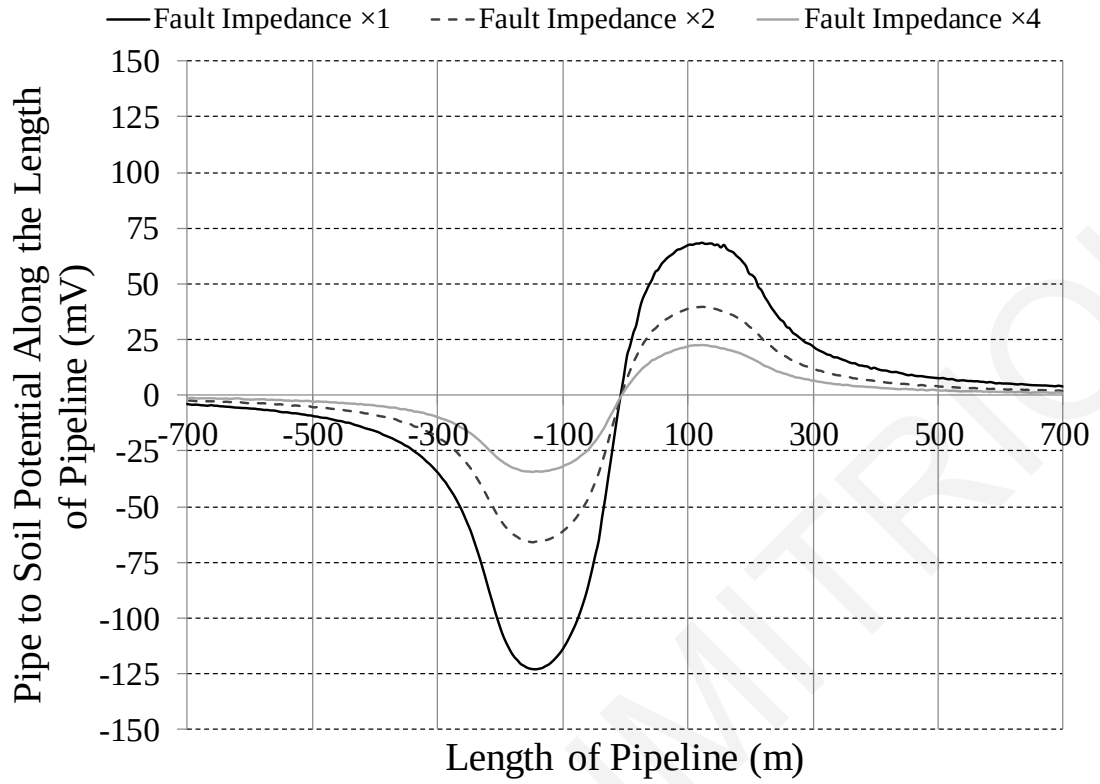

Figure 3-18: Sensitivity Analysis of PSP on the interfered section of pipeline under BSC for varying fault impedance value

Table 3-8: Sensitivity Analysis for the Impact of Fault Impedance Value on the magnitude of Fault Current Under BSFC

Fault Impedance Value	Current at earthing point of negative current currying conductor (A)
× 1	4.8
× 2	2.45
× 4	1.24

- ***Influence of Pipeline's Insulation Resistance:***

The insulation resistance of the pipeline systems depends on the thickness and the resistivity of the coating material. Always high resistivity insulation materials (i.e. polyethylene) are selected for coating buried pipelines. However, during the lifetime of the pipeline, the insulation resistance of the pipeline system may be downgraded by several orders due to the natural degradation of the coating material. To this extent, Figure 3-19 presents the PV interference under BSFC, by decreasing 10-fold (10^7 Ω.m) and 100-fold (10^6 Ω.m) the resistivity of the pipeline's coating material.

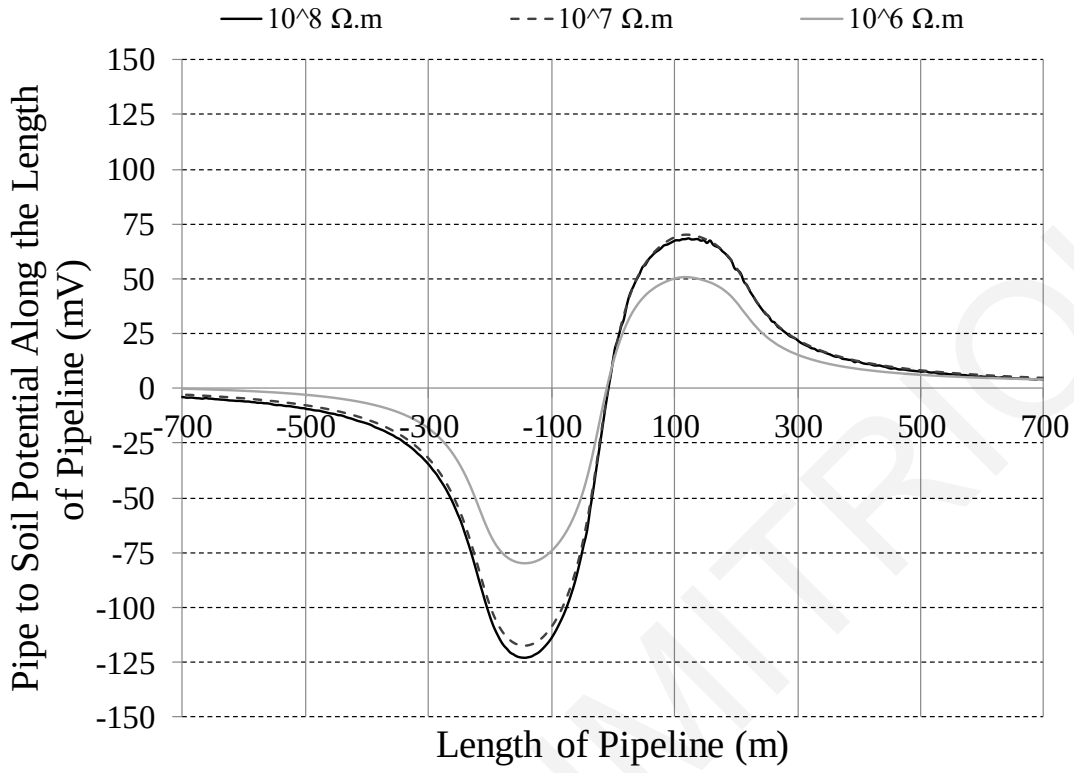

Figure 3-19: Sensitivity Analysis of PSP on the interfered section of pipeline under BSC for varying pipeline's coating resistivity value

Simulation results reveal that in the case where the coating resistivity is 10-fold decreased, the PSP remains almost unaffected. On the contrary, when the resistivity is 100-fold decreased, the PSP is reduced considerably. This practically means that in the case of a newly constructed pipeline (with a high coating resistivity) the current density at the surface of a coating holiday (see Eq. 3-3) would be higher in comparison to a pipeline with high degraded insulation (i.e. 100-Fold). In extension, the corrosion at holidays which fall within the area of anodic interference would be more severe. However, this conclusion should not be misinterpreted. Although the corrosion at a coating holiday of a newly constructed pipeline appears more severe, overall the corrosion on this pipeline would be much less. This is because a degraded pipeline exhibits a considerably higher number of coating holidays in comparison to a newly constructed. Moreover, the degradation of coating material practically implies the development of coating holidays. In conclusion, special attention should be given for the identification of the coating holidays in newly constructed pipelines since they may introduce severe corrosion locally at the surface of the coating holidays.

3.3.6 Conclusions

The developed model and the associated simulation results have evidently confirm that PV

interference is not only affected by the magnitude of leakage currents flow but is also affected from the topology of the involved systems (PV system & Pipeline system). This is due to the fact that PV interference is static in space (i.e. the dc source injections are fixed). The specific conclusions from this chapter are summarised as follows:

- The PV interference on a coated pipeline system can be defined as the alteration variation of PSP. This variation comes as a consequence of the soil gradients established by the leakage/fault currents circulation into the earth
- Under SSC the total leakage current originated from PV modules and DC cables is relatively low (i.e. ~30 mA per array). To this extent, no noticeable PV interference can be exhibited on a nearby pipeline system. However, this response is a consequence of the extremely high insulation levels considered in modelling representing a perfect condition of PV's assembly components. Lower insulation levels can result in higher values of interference.
- Under BSFC the PV interference is considerably higher in comparison to SSC. This is because in this case the total leakage current is higher by several orders (i.e. ~ 4,8 Amps). Consequently, PV interference is dominated by the fault current of the faulted array. This current level could result in a corrosion metal loss rate that deems unacceptable i.e. >10 μm/year.
- The PV interference is predominantly influencing the section of pipeline located at the area close to the PV plant. This is because of the conductive nature of the interference mechanism that involves the circulation of stray currents through PV plant's components (i.e. metallic post, earthing grid). As the distance between the pipeline and the PV plant increases the PV interference is reduced.
- The location and the magnitude of a blind spot fault influences the interference level. Depending on the fault location, both the profile and the magnitude of the PV interference on a pipeline may vary significantly. This inevitably entails difficulties to identify the interference using standard-based field tests, as will be discussed in Chapter 5.
- The resistivity of the pipeline's coating material influences the interference level. Simulation results reveal that high insulation materials could result in higher PSP variations. In extension, localized severe corrosion issues at the surface of coating holidays can occur in highly insulated pipeline systems.

Chapter 4

Development of Modelling Techniques to Address PV Interference on Pipeline Systems from Floating Isolated PV Systems

4.1 Introductory Remarks

In floating isolated PV systems there is no direct bonding to earth with regard to the PV arrays' current-currying conductors. In addition, galvanic isolation, between the AC and the DC side, is provided with the use of isolation transformer. Since the floating PV array is isolated any leakage currents are driven by the potential difference that arises between the active elements. For example, the potential difference between: a) the positive and the negative cabling and b) the first and the last PV module of a PV string. In extension, the magnitude of leakage current depends on the effective insulation resistance and the operational level (i.e. Voltage, Current) of the PV system's DC side. Moreover, the degradation of insulation materials can increase leakage activity. By incorporating an insulation monitoring device, the PV inverter may disallow the operation of the PV plant if the insulation level (i.e. R_{ISO} of the PV array) is relatively low [4], [17]. To this extent, the permissible leakage current is limited by the threshold level that is adjusted by the insulation monitoring device. As shown in Figure 4-1 the circulation of leakage currents through the soil may interfere with nearby metallic pipeline systems resulting in an acceleration of their corrosion rate.

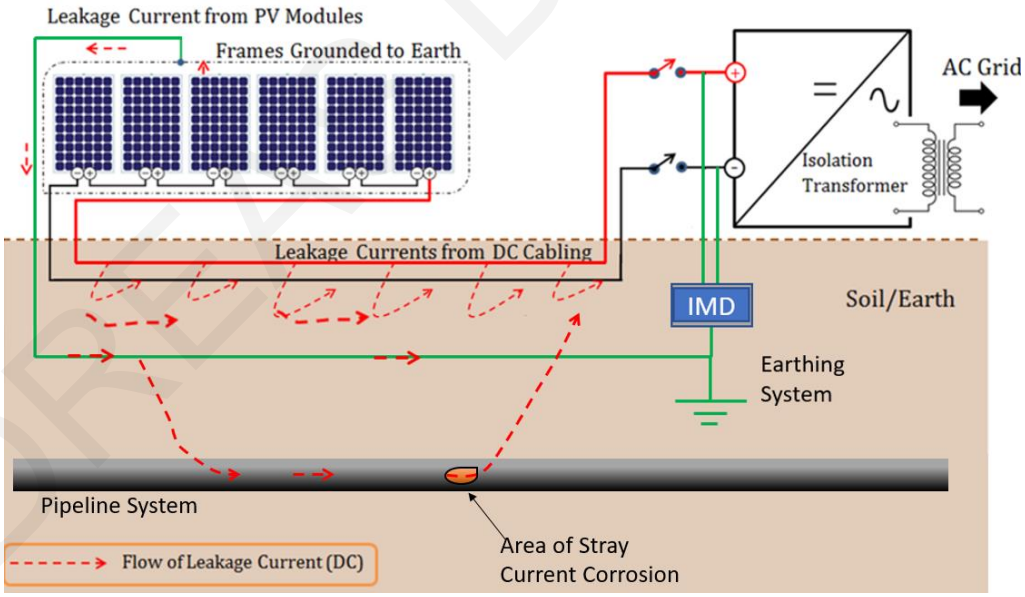

Figure 4-1: Graphical illustration of PV interference in Floating Isolated PV Systems

This chapter develops a dedicated modelling technique to address the problem of PV interference on pipeline systems located in a vicinity with Floating Isolated PV Plants by utilizing a specialized simulation software [79] (see Appendix C).

The modelling principles are developed initially on a simplified small-scale model (Section 4.2) and consequently are applied to a more realistic large-scale model (Section 4.3) in order

to examine the PV interference on a nearby buried pipeline system. Furthermore, a series of sensitivity analysis is performed to identify the factors affecting the PV interference situation (Section 4.4). Finally, some concluding remarks are provided (Section 4.5).

4.2 Description of Fundamental Modelling Principles

4.2.1 Topologically Accurate Modelling of PV systems' DC leakage sources

An electric equivalent circuit of a floating isolated PV system can be represented by the model shown in Figure 4-2. Since the system is floating, there is no reference point of the energized components with respect to the earth. In extension, there is no specified point for the return of leakage currents as is the case for an earthed PV system. Due to the lack of a distinct reference point to earth, the ground potential rise (*GPR*) of a floating PV string will exhibit the behaviour presented in the graph associated with Figure 4-2. Essentially, the *GPR* of a floating PV system is the result of the resistive leakage current paths established between the active elements and the ground. The node at the positive end of the PV string (leading to the positive terminal of the inverter) will exhibit a positive *GPR*, equal to half of the operating voltage of PV inverter ($V_{inv}/2$). The *GPR* along the PV string will decrease, with the value at the middle point node of PV string, diminishing to zero. The node at the negative end of the PV string (connected to the negative terminal of the inverter), will exhibit negative *GPR* equal to the half operating voltage of PV inverter ($-V_{inv}/2$). To this extent, at the section of PV string [1 - n] with positive *GPR*, leakage currents flow out of modules while at the section of PV string [1′- n′] with negative *GPR* the leakage currents return back to the modules.

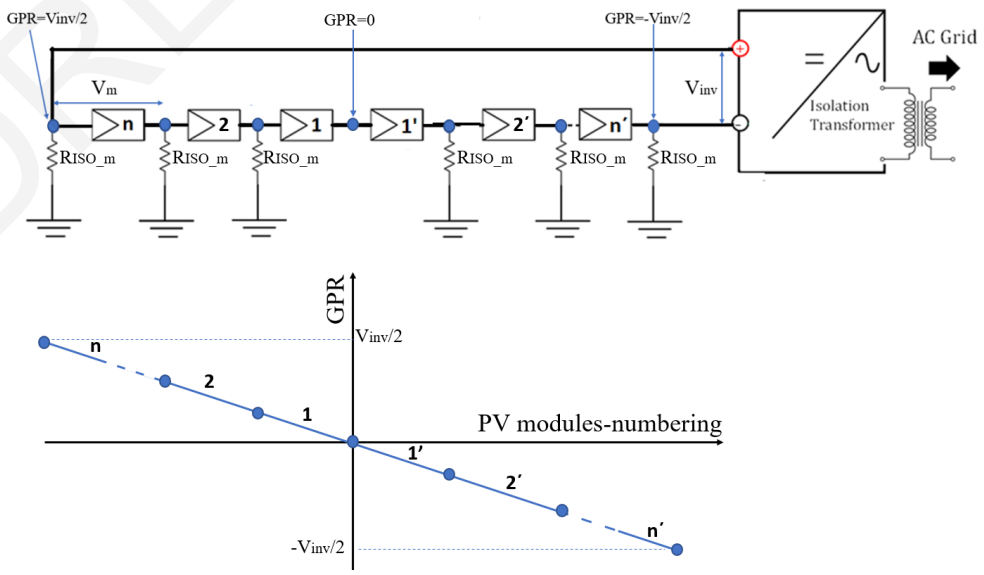

Figure 4-2: PV Array String of 2*n* Modules Connected in Series with Effective Insulation Resistance R_{ISO_m}

This simple approach is effectively utilized to compute the leakage current emanating from the PV modules. With reference to Figure 4-2, V_m is the operating voltage and R_{ISO_m} is the corresponding insulation resistance to the earth, of each PV module. The total number of the PV modules connected in series is 2×n. By applying Kirchhoff's first and second law, the leakage current (I_{leak_k}), originating from the module placed in *k* position (starting from the center of PV string), can be given as in Equation (4-1), if the PV module is connected to the section of PV string presenting positive *GPR*. On the contrary, if the PV module is connected into the section of PV string with the negative *GPR*, the leakage for the k'^{th} module is calculated via Equation (4.2).

$$I_{leak\_k} = k\frac{V_m}{R_{ISO\_m}} \quad (4\text{-}1)$$

$$I_{leak\_k}{}' = -k'\frac{V_m}{R_{ISO\_m}} \quad (4\text{-}2)$$

The total cumulative leakage currents produced by each semi-PV string can be given in Equation (4-3). However, the direction of leakage flow is opposite for the two semi-PV strings depending on the polarity of *GPR*.

$$I_{leak} = \frac{n(n+1)V_m}{2R_{ISO\_m}} \quad (4\text{-}3)$$

In contrast to the model shown in Figure 4-2, the model in Figure 4-3 illustrates how the equivalent electric circuit of the floating PV system, can be alternatively modelled in a topologically accurate manner [79]. In particular, the conductors are topologically directed in 3D and their intrinsic characteristics account for all the necessary power, electrical and material parameters comprising the PV system under study (i.e. PV modules, metallic frames, inverters, DC cables, the Equipment Grounding Conductor (EGC) and soil resistivity).

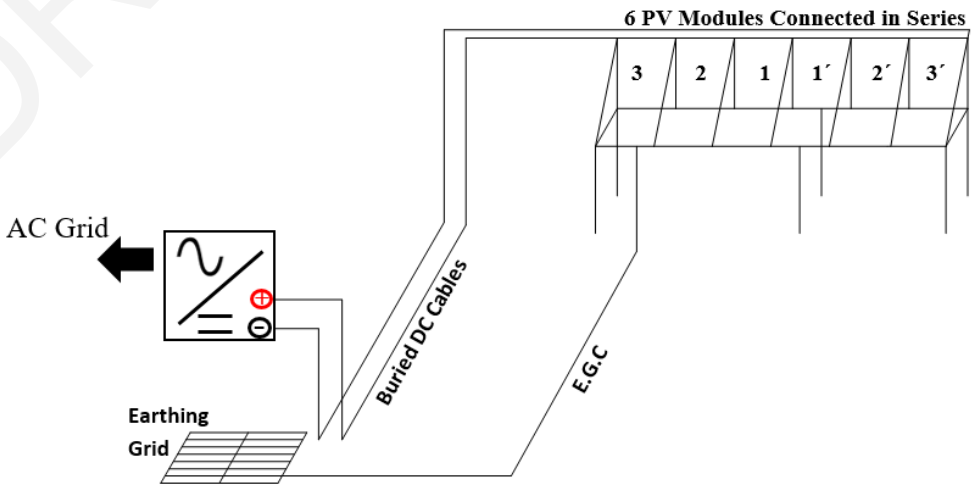

Figure 4-3: True topology of the equivalent electric circuit of the floating PV system in CDEGS [79]

However, it should be kept in mind at this point that the primary objective of this work is to reproduce the DC leakage from system's components as well as the points within the soil where the DC leakage is injected/ returned. To achieve this objective, the model shown in Figure 4-3 is transformed into the one shown in Figure 4-4. The updated model (see Fig. 4-4) using a current source and resistive components, implements an electric circuit that is able to reproduce the topologically accurate activity of leakage currents as well as the energization conditions of PV generators. More specifically, the simulation model shown in Figure 4-4 utilizes a current source (I_{inv}) at the inverter's level to replicate the current generated from PV modules. This is an artificial component of the software [79] that allows an indirect snapshot of the DC circuitry's static current flow. The PV cables allow the current I_{inv} (i.e. positive and negative) to be circulated through the PV string. Each PV module of the PV string is modelled as a conductor with an embedded series resistance (R_s) which its value can be adjusted in order to calibrate the operation voltage of PV module (V_m). As the current flows through $R_{s,}$ a voltage drop is produced, equal to the operating voltage of the PV module (V_m). Also, resistances (R_{ISO_m}) are inserted between PV modules to integrate their insulation resistance to earth. Each R_{ISO_m} is terminated at the metallic frames, allowing any leakages to flow via the metallic frames and soil. Under this energisation principle, the model is subsequently able to compute the flow of DC leakage through each individual conductor that forms part of: a) PV metal frames and b) buried DC cables. This allows for the associated DC leakage activity to be topologically accurate. (Note: $R_{ISO\_m} >> R_s$ therefore V_m is exclusively controlled by R_s)

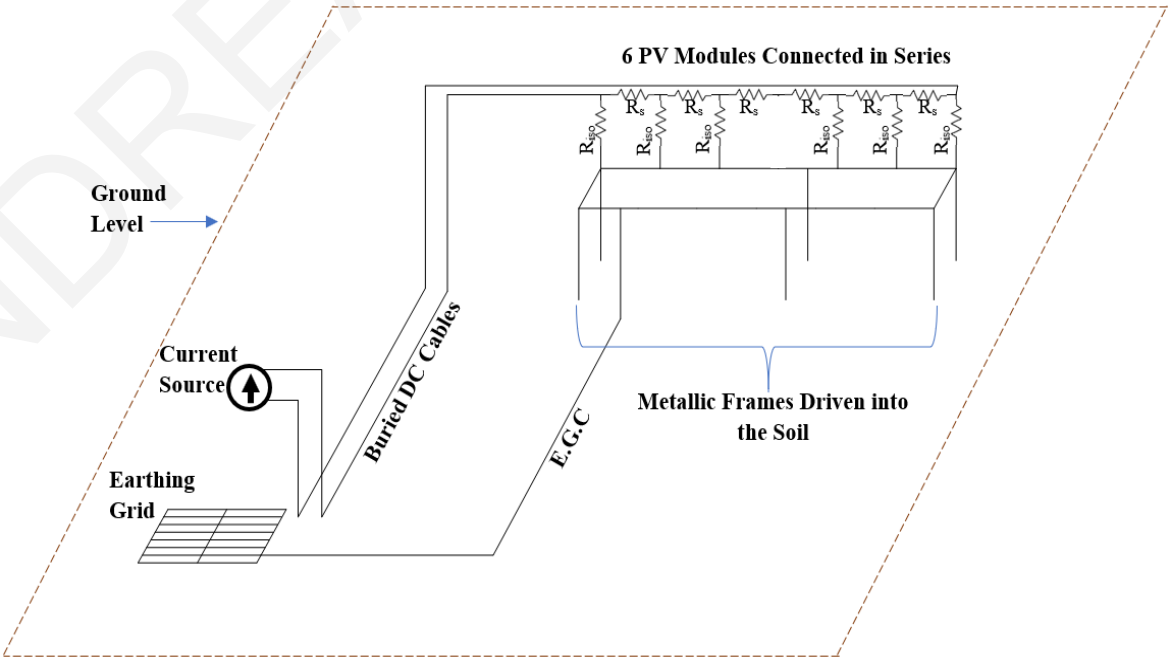

Figure 4-4: Topologically Accurate Model to Simulate DC leakage activity in a PV System

DC Leakage Activity Related to DC Buried Cables:

The DC leakage activity associated with the buried cables is directly controlled by: a) the cables' intrinsic insulation resistance to the earth and b) the potential difference that exists between the positive and the negative DC cable. In particular, the potential difference between the DC cables is adjusted, in the model, with the combination of: a) the modules' series resistance (R_s) and b) the current source of the inverter (I_{inv}).

DC Leakage Activity Related to PV Modules:

The DC leakage that originates from the PV modules, subsequently streaming through the metallic frames into the earth depends on the established *GPR* of each module and the R_{ISO_m}. The estimated leakage current of each module can be calculated theoretically via Equation (4-1) and Equation (4-2).

Simulation Results of the Simple Case Study for examining PV modules leakage activity

Firstly, the model is simulated as per the input parameters shown in Table 4-1 in a uniform soil model of 100 Ω.m. Initially, high insulation resistance of the DC cables was assumed in order to limit any leakage activity arising from the DC cables. This allows the leakage activity to be exclusively originated from the PV modules.

Table 4-1: Input Parameters for Simulating PV Modules Leakage Activity

Description of Parameter	Value
Module operation Voltage (V_m)	35.1 V
Inverter operation Current (I_{inv})	6.5 A
Inverter operation Voltage (V_{inv}) [6 modules in series]	210.6 V
Insulation Resistance of PV module (R_{ISO_m})	10 MΩ
Series Resistance of PV module (R_S)	5.4 Ω
PV Cable Conductor: Copper Conductor resistivity Cross-section area	 1.68×10^{-8} Ω.m 10 mm^2
PV Cable Insulation: Coating Resistance Thickness	 8,6 MΩ×m 1 mm

The results that are reported in Figure 4-5 show the simulated current value (in mA) computed by the software. By extension, Table 4-2 presents the leakage performance of the PV modules for the system modeled. The simulation results of leakages originated from PV modules are compared with the expected values calculated from Equation (4-1) and Equation (4-2). The validity of modelling technique is confirmed since the expected/theoretical leakage performance of the system model converges to the simulation results.

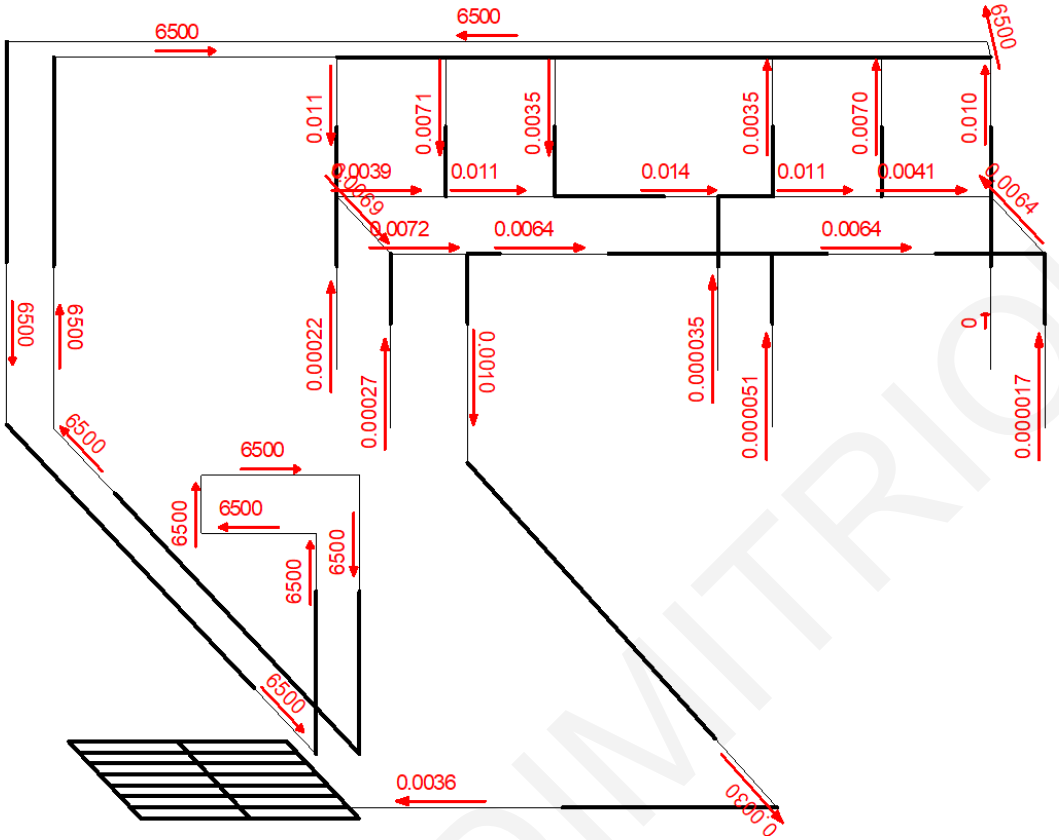

Figure 4-5: Calculated Current Flow in milliamps (mA) at the Origin of each Conductor Modelled

Table 4-2: Summary of DC Leakage Activity

Module number	Leakage Current (mA)	
	Simulation	Theoretical
1	0.0035	0.00351
2	0.0071	0.00702
3	0.011	0.01053
1′	-0.0035	-0.00351
2′	-0.007	-0.00702
3′	-0.01	-0.01053

With reference to Figure 4-5, the magnitude of the leakage currents is consistent with the theoretical analysis. Leakage currents from PV modules are circulating between the two semi-sections of PV string via the metallic frame. More importantly, part of the leakage current is captured by the EGC and returns to the modules through the conductive path established by the earthing grid, the soil and the metallic framework which is extended into the soil. This ability of the simulation model is especially important since it will allow the reproduction of the interfering stray currents on a pipeline system in the next section.

Simulation Results of the Simple Case Study for examining PV modules & PV cables leakage activity

Secondly, the simulation model is re-executed as per the input particulars shown in Table 4-1 with the exception that the insulation resistance of PV cables is decreased to 8,6 kΩ.m. Since the insulation resistance of PV cables is decreased 1000-fold in comparison to the previous case (where the insulation resistance of PV cables was 8,6 MΩ.m) an additional leakage activity is exhibited. By comparing the simulation results of Figure 4-5 with the obtained results of this case study (see Fig. 4-6) it is obvious that there is an additional leakage due to the lower coating resistance of the PV cables. The leakage current from the PV cables appears as a decrease in the current flowing through them. This is because a part of the generated current (I_{inv}) is circulating between positive and negative cables, due to their potential difference (i.e. 210 V). This activity is highlighted in Figure 4-7 where the leakage current from the PV cables is exclusively presented. As shown in this figure the portion of PV cables laying underground, exchanges leakage current through the soil, traveling from the positive to the negative cable. The indicated values are given in mA per square meter. It is worth noting that no leakage currents are observed in the above-ground section of PV cables.

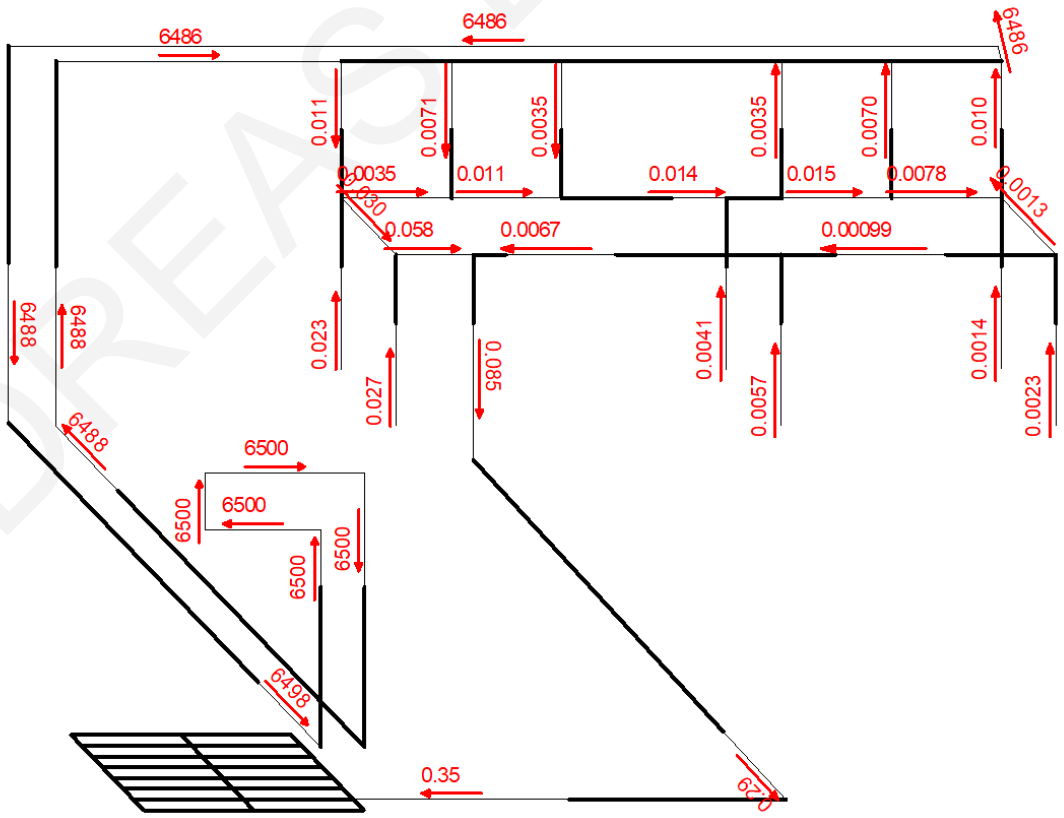

Figure 4-6: Calculated Current Flow in milliamps (mA) at the Origin of each Conductor Modelled

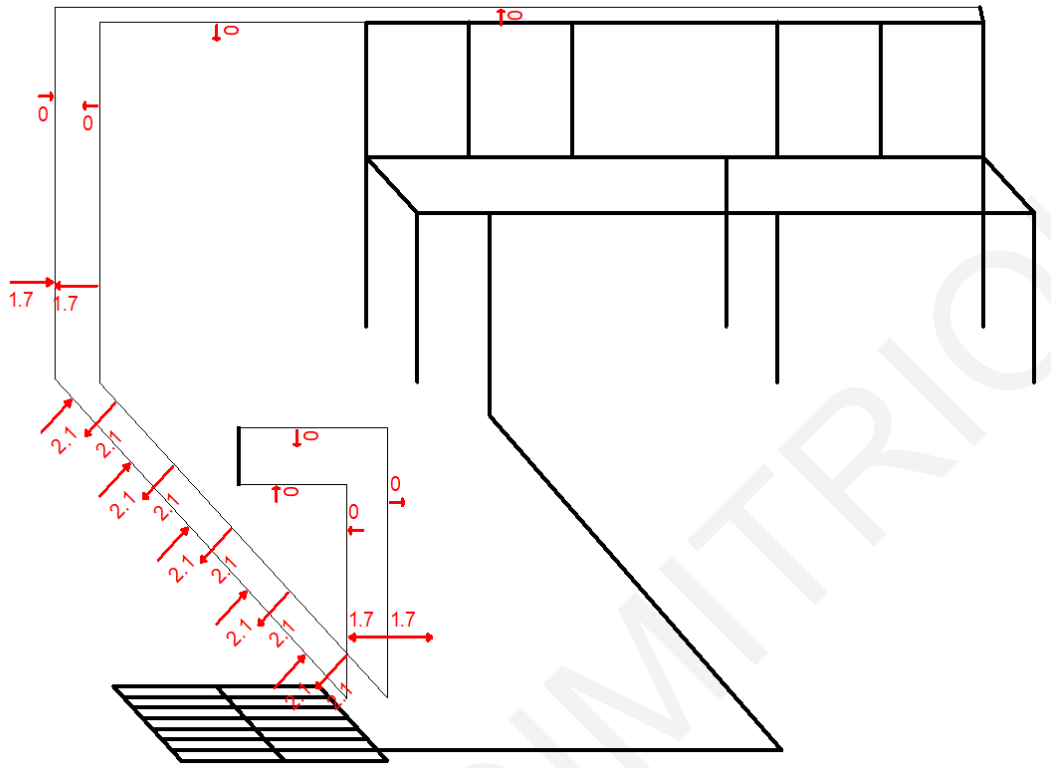

Figure 4-7: Calculated leakage current (mA/m^2) from PV cables

4.3 Case study of a utility-scale PV system and PV interference on nearby Gas Pipeline

The simulation principles and techniques described in Section 4.2 are applied to a more realistic case study that involves a large-scale 528 kWp floating isolated PV park that its operation interferes with a nearby pipeline system. The objective of this case study to model the PV interference on the pipeline system as well as to identify the factors that affect the interference level.

4.3.1 Description of Physical Model

A. Layout and electrical Specification

Figure 4-8 illustrates a topologically accurate top view of a floating PV system. It labels its actual dimensions as well as the most important features identified as crucial when it comes to assessing the stray current corrosion impact from a PV system operation. This physical model has been chosen as an example system that can be replicated in the simulation platform [79] by applying the developed simulation techniques described above.

In particular, the PV system considered has a nominal output power of 532.2 kWp and can be directly linked to the MV network. It is occupying an area of 7875.2 m^2 which hosts 12

similar structures (arrays) of fixed inclination. The PV modules are collectively wired in series strings, e.g., the positive lead wire of one module is connected to the negative lead wire of the next module. This results in a cumulative voltage output without altering the current. Thus, for example, two series strings imply two sets of wires, two positives, and two negatives. The output wires from multiple series strings (positive and negatives) are subsequently joined in strings-combiner boxes. From the strings-combiners, the wires are directed to a central-combiner and, from thereon, to a central inverter.

For clarity, Figure 4-8 illustrates only the cables (positive and negative) from each strings-combiner to the central combiner (*array-cables*) and the wires routed from the central combiner to the central inverter (*main-cables*).

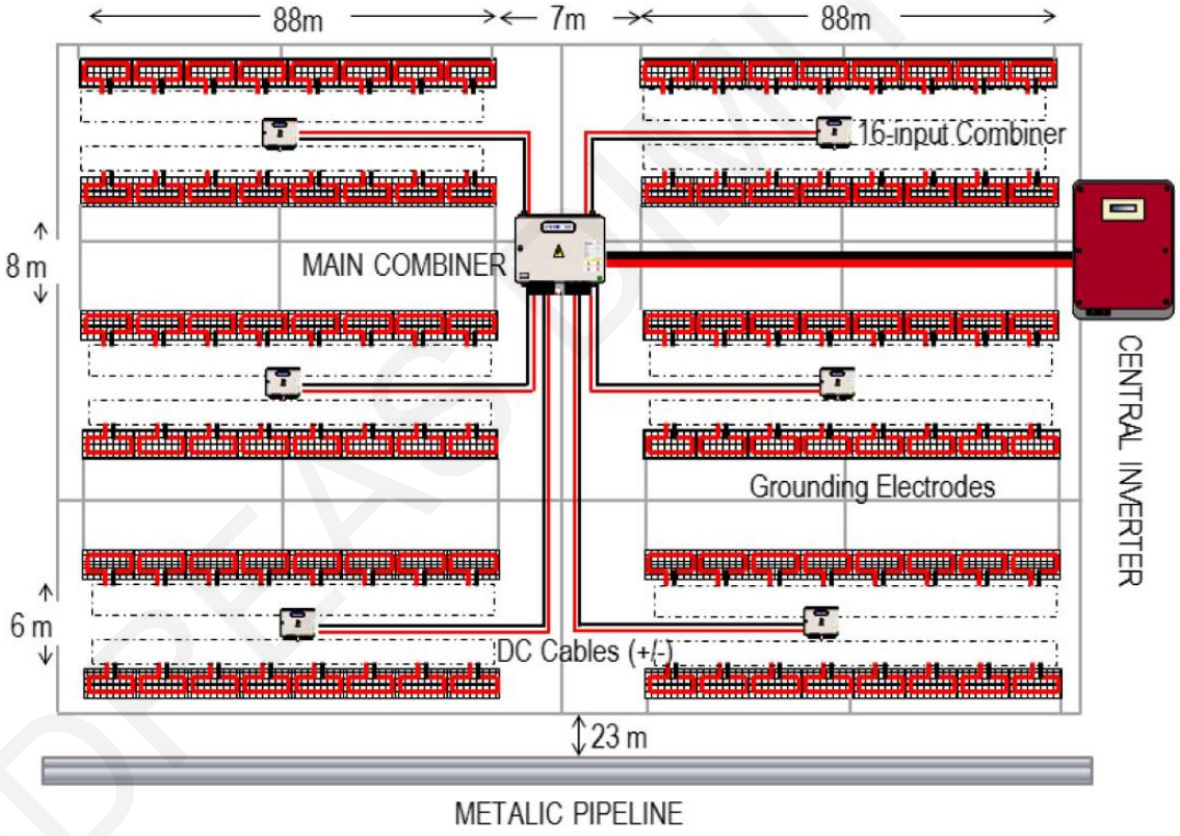

Figure 4-8: Top view of a realistic PV Park with actual dimensions labeling its elemental components

More explicitly, in the system considered, the PV modules (each 252 W) are configured in 22-module strings with 16 source circuits per strings-combiner box. At standard test conditions (1000 W/m^2), each 252 W module has an I_{mp} of 7 A, and hence, the I_{mp} of the PV output circuit per strings-combiner box is 112 A. The working voltages V_{mp} are 36 V for a 252-Wp module, and for each 22-module string, V_{mp} is 792 V.

B. DC Cable Specifications

The array cables, as well as the main cables, are installed underground. In PV systems, both the positive and negative cable conductors are current-carrying. Therefore, the size of the floating cable conductors (positive and negative) is based on their required ampacity value. The minimum required ampacity of these cables can be determined from the maximum short circuit current of the output PV circuit per combiner box. The current-carrying requirements and the insulation specifications should be complying with the relevant standards [8], [17], [42].

C. Grounding System Description

The central inverter housing is earthed by an earthing grid benefiting from 1Ω resistance. Besides, PV generators are earthed with the use of type *B* electrodes [31] (that ensure the equipotential bonding of all PV metal frameworks) which are installed in the perimeter of PV generators. For type-B grounding electrodes, the most common shape used is the strip conductor. To achieve an effective grounding system, the strip conductor is usually installed into the soil within a trench of about 0.5 m deep and 0.5 m wide, using some sort of fasteners while the metallic frames of PV generators are bonded directly through appropriate EGC conductors. Furthermore, the strip conductor is extended to inverter's earthing grid creating an interconnected global earthing system.

D. *Metallic Infrastructure Buried in Nearby Vicinity*

It is quite common for large PV plants installed in rural areas to be near metallic infrastructures, such as buried gas/oil pipelines or irrigation pipelines. Thus, a sufficiently sized buried metallic pipeline exists near the PV system as illustrated in Figure 4-8.

4.3.2 Simulation Model and Parameters

A simulation model is developed following an assessment of the infrastructure elements considered likely to be affected by leakage current originating from a) buried PV cables and b) from PV modules. The model allows currents to be injected and collected at various points in a network of conductors which are placed in a soil environment. Subject to users' intervention, the simulation platform is able to further compute the flow of these currents through each individual conductor within the modelled network. It thus allows computing a stray current and a voltage distribution along the actual length of the entire system of conductors considered. The computer model formulated to replicate the physical

configuration shown in Figure 4-8 is illustrated in perspective view in Figure 4-9. This model allows for the stray current performance of the PV plant's nearby infrastructure to be assessed in terms of their geometry, topological arrangement, and soil and physical characteristics.

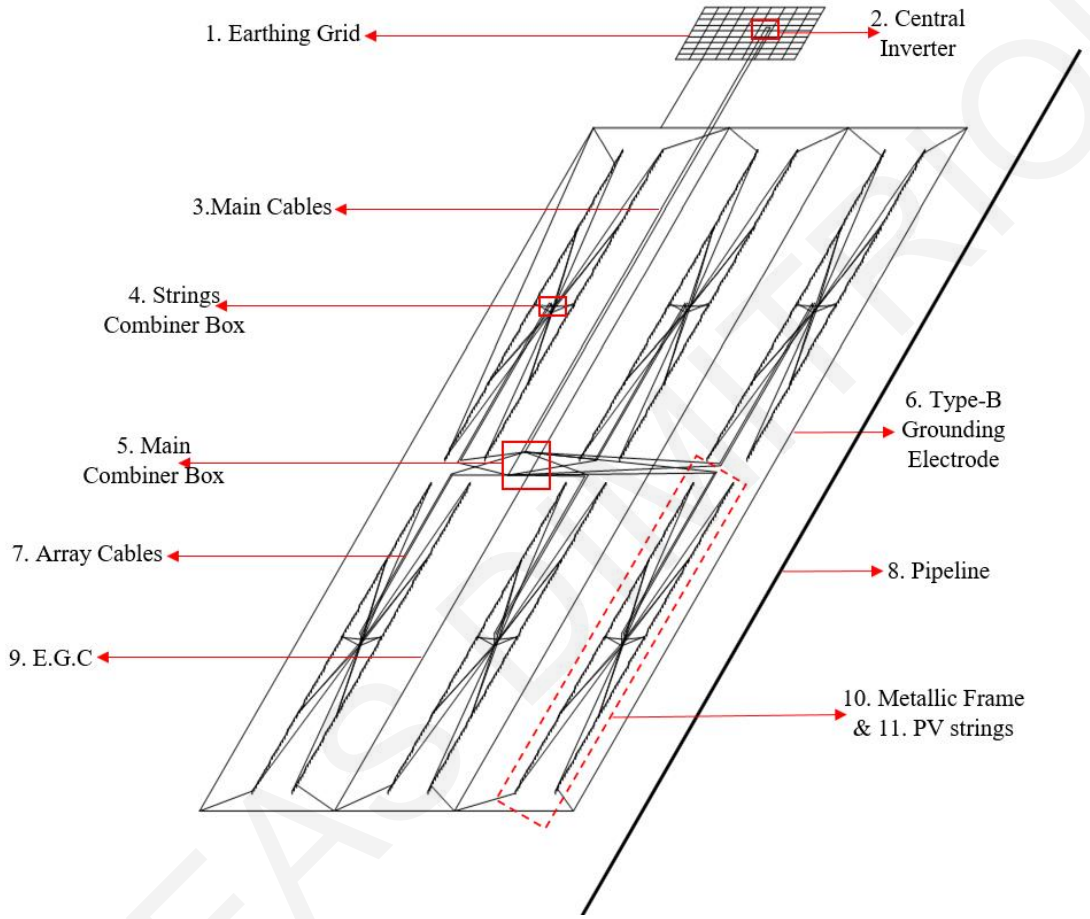

Figure 4-9: Perspective view of the arrangement of conductive elements in the PV system modelled

A. Description of Conductors' Sizing and Arrangement

With reference to Figure 4-9, the numbered items are described in more detail.

1) *Earthing Grid:* The earthing grid is modeled as a group of cylindrical conductors buried under the central inverter housing. The dimensions of the cylindrical conductors, as well as its buried depth, were chosen to provide an equivalent 1 Ω earthing resistance.
2) *Central Inverter:* Central inverter is modelled as an artificial current source that supplies the interconnected network with the desired production current.
3) *Main Cables:* The specifications of the main cables are shown in Table 4-3. The insulation resistance of the cables is given a rated value however this value will be

varied in the simulations to facilitate the intended sensitivity analysis. The conductors are buried into a soil model, 0.25 m below the earth's surface.

4) *Strings Combiner Box:* The output terminals of the wires from multiple series strings (positives and negatives) are combined at strings-combiner boxes.
5) *Central Combiner Box:* From the strings-combiner boxes, the array cables are directed to a central combiner and, from thereon, to a central inverter.
6) *Type-B Grounding Electrode:* Due to software constraints, the type-B grounding electrodes are modeled as cylindrical conductors, buried at some distance below the earth's surface. The cylindrical conductors are given a radius of 5.35 mm, to provide an equivalent per-unit length volume as that of a strip conductor with dimensions of 30 mm x 3 mm.
7) *Array Cables:* The specifications of array cables are shown in Table 4-3. The insulation resistance of the cables is given a rated value however this value will be varied in the simulations to facilitate the intended sensitivity analysis. The conductors are buried into a soil model, 0.25 m below the earth's surface.
8) *Metallic Pipeline:* Pipeline system is modelled as a hollow coated conductor, with suitable geometry that may be located at a range of distances from the PV system.
9) *EGC:* Equipment grounding conductor ensures the equipotential bonding of all PV metal frameworks as well as their connection to the earthing grid.
10) *Metallic Frames Driven to Soil:* These are galvanized steel conductors that are modeled to replicate the portions of the PV façade frameworks which are extended into the soil. These portions are interfaced to the grounding electrode system to ensure the equipotential bonding of all PV metal frameworks/ grounding electrodes.
11) *PV stings*: Based on the modelling technique described in Section 3.2, each PV string is modelled as a group of resistive loads (R_s) connected in series to substitute PV modules. Moreover, a group of resistances recreate the equivalent insulation resistance to earth (R_{ISO_m}) of each PV module.

Table 4-3: Specifications of Main and Array Cables

Specifications	Array Cables	Main Cables
Cross-sectional area of conductor (mm^2)	25	240
Current carrying capacity (A)	167	736
Thickness of insulation (mm)	0.9	1.7
Insulation resistance (MΩ.km)	340	200

B. Base Input Data and Assumptions

Table 4-4 tabulates the base input data and assumptions for particular items shown in Figure 4-9. These are employed in the simulation for assessing the stray current performance of the PV system model.

Table 4-4: Base Input Data and Assumptions

Element Description	Parameter Description
Earthing Grid	Grid Dimensions: (Width=15 m × Length= 15 m)
	Number of Horizontal Conductors: 10
	Number of Vertical Conductors: 10
	Depth of grid: 3 m
	Conductor Material: Copper
	Conductor CSA: 120 mm^2
Main Cables	Length of all Cables Modelled: 175m
	Buried Depth: 0.25m
	Conductor Material: Copper
	Conductor CSA:240 mm^2
	Coating thickness: 1.7 mm
	Coating resistivity: 6.46×10^{15} Ω.m
	Insulation resistance: 200 MΩ.km
Array Cables	Length of all Cables Modelled: 683.6m
	Buried Depth: 0.25m
	Conductor Material: Copper
	Conductor CSA:25 mm^2
	Coating thickness: 1 mm
	Coating resistivity: 6.03×10^{15} Ω.m
	Insulation resistance: 340 MΩ.km
PV strings	Total length of each PV String: 24.2 m
	Number of modules per PV string: 22 modules (modelled as conductors with series resistance R_s=5.142 Ω)
	Insulation resistance of module: R_{ISO_m} = 40 MΩ
Type B – Grounding Electrode	Total Length of Grounding Electrode: 864.4m
	Buried Depth: 0.5 m
	Conductor Material: Copper
	Conductor CSA: 89.9 mm^2
Metallic Pipeline	Total Length Modelled: 210 m
	Location: 23m away from the northern side of the PV Park (parallel routing)
	Pipeline Material: Heavy Duty Galvanized Steel
	Pipeline Size: Internal Radius 0.17m, External Radius:0.20m
	Pipeline Coating: XLPE coating with resistivity of 10^6 Ω.m and thickness of 1 mm
Metallic Frames Driven into the Soil	Length of each portion driven into the soil: 0.8m
	Number of elements modelled in the system: 528
	Material: Galvanized Steel
	Effective CSA of each portion: 141mm^2

C. Description of Soil Model

The simulation model shown in Figure 4-9 incorporates a uniform soil model that is embedded in the software platform used [79]. The resistivity assigned to the model can take a range of values depending on the soil type and moisture content (e.g., 10 Ω.m, 100 Ω.m, etc.). For the base model, the soil resistivity is defined as 100 Ω.m.

D. Description of Energization Principles

The model is singly energized at the inverter's level with a current source I_{inv}. The current flows via main cables to the central combiner box where it is distributed to string-combiners and from there on is directed to PV strings circuits. I_{inv} is adjusted at a maximum power of PV plant (732 A) providing an indirect snapshot of the DC circuitry's static power flow under rated energization conditions of the PV plant. As I_{inv} flows through series resistances R_s (which replicate PV modules) the rated voltage of PV inverter is established between positive and negative cabling.

4.3.3 PV interference on Buried Pipeline System

The developed model is simulated to evaluate the PV interference on the nearby pipeline system. Since the pipeline system is coated the evaluation is performed by monitoring the pipe to soil potential (*PSP*) along the length of the pipeline. As mentioned in Chapter 3, *PSP* is the voltage difference between the soil at the surface of the coating material and the pipeline's metallic wall. Positive values of *PSP* imply that in the presence of coating holiday the current inserted into the pipeline (cathodic interference) while negative values imply that current leaking out of the pipeline (anodic interference).

The examined PV interference of stray currents originated from the modelled floating PV plant is presented in Figure 4-10. This is a static interference situation since it provides a snapshot of the stray current activity for a certain energization level (under the rated current) of the PV plant. The simulated activity has also shown some localized high stray current activity at the area where the pipeline is neighboring with the PV plant. More explicitly, three discrete areas are exhibited along the length of the pipeline, a section with cathodic interference (positive values) and two sections with anodic interference (negative values). Stray current exhibits positive alteration of *PSP* at the section (X=-61 m to X=60 m) while at the sections (X=-61 m to X=-300 m) and (X=60 m to X=300 m) negative values have occurred. The symmetry presented in the graph is due to the uniformity of modelled components. The cumulative effect is attributed to the relative positioning between PV plant's energized components (which act as the source of stray currents) and the pipeline

system under assessment. This implies that some sections of the pipeline under study (near the source of stray/leakage current) will be more influenced.

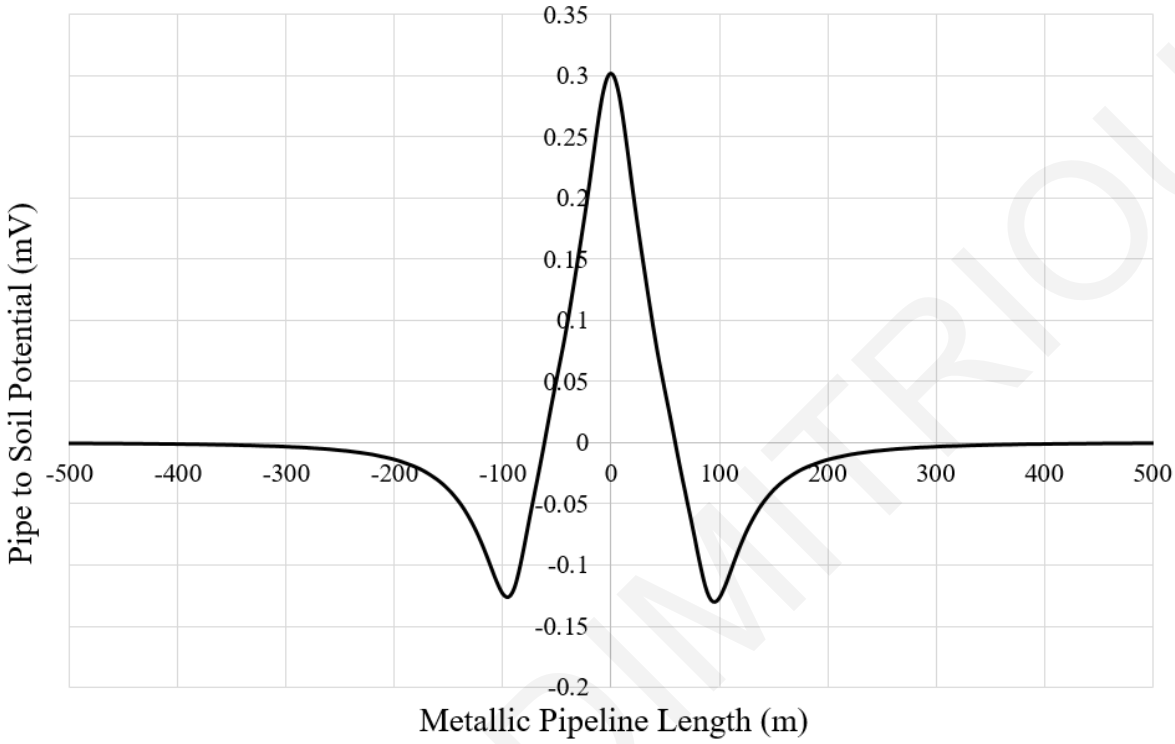

Figure 4-10: PV interference on the buried pipeline system

Nevertheless, the simulated PV interference (Fig. 4-10) evidently shows the ability of the developed model to examine localized stray current distributions on pipeline systems associated with the floating isolated PV Plant.

4.4 Sensitivity analysis of critical parameters that influence the stray current activity

As described in Chapter 2 the leakage activity in a PV plant is influenced by various factors associated with the technical characteristics of the electrical equipment as well as the prevailing weather conditions. To this extent, the objective of this section is to deliver some simulation studies that can provide an insight into the DC leakage activity with regard to floating isolated PV systems.

4.4.1 Sensitivity Analysis - Case Studies

The sensitivity simulations are re-executions of the original/reference case study by integrating some modifications depending on the purpose of each case study. The simulation results of five notable scenarios are presented below.

Case 1 - Modelling of the influence of PV Modules' Insulation:

The *GPR* of the PV modules drives the flow of leakage currents to earth through the insulation material (see Sec. 4.2). The electrical resistance of insulation materials may decrease permanently due to degradation factors [18], [19] [28] or temporarily due to the presence of moisture. Thus, this case study examines the leakage activity under a degraded insulation resistance of PV modules and the corresponding influence on the pipeline system. In particular, the reference simulation (where R_{ISO_m} =40 MΩ) is re-executed under 2 degraded insulation levels of PV modules with a value of R_{ISO_m} =20 MΩ and R_{ISO_m} =10 MΩ.

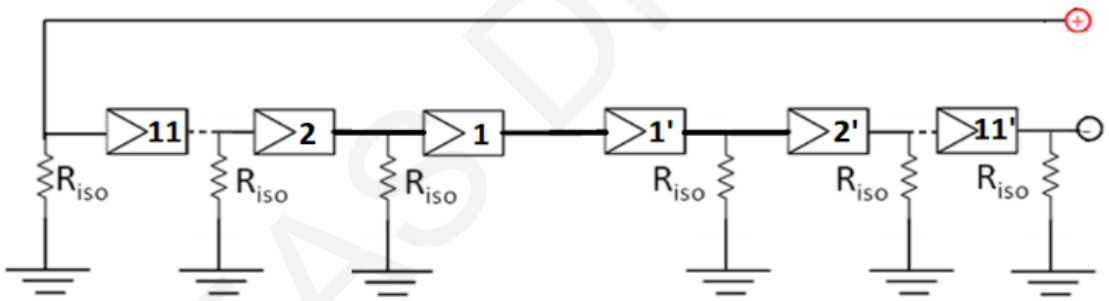

Figure 4-11: Schematic equivalent of modelled PV string

Indicatively, the chart of Figure 4-12 presents the calculated values of the leakage currents flowing from the PV modules of a single PV string - as numbered in Figure 4-11. Since the modelled PV strings have identical characteristics the calculated leakage activity is almost equal in all PV strings included in the modelled PV plant. It is worth mentioning that the simulated values of the leakage currents are in agreement with the theoretical values that can be calculated through Equation (4-1) and Equation (4-2). It is therefore verified that the simulated leakage activity of PV modules has an inversely proportional relation to the insulation resistance R_{iso}.

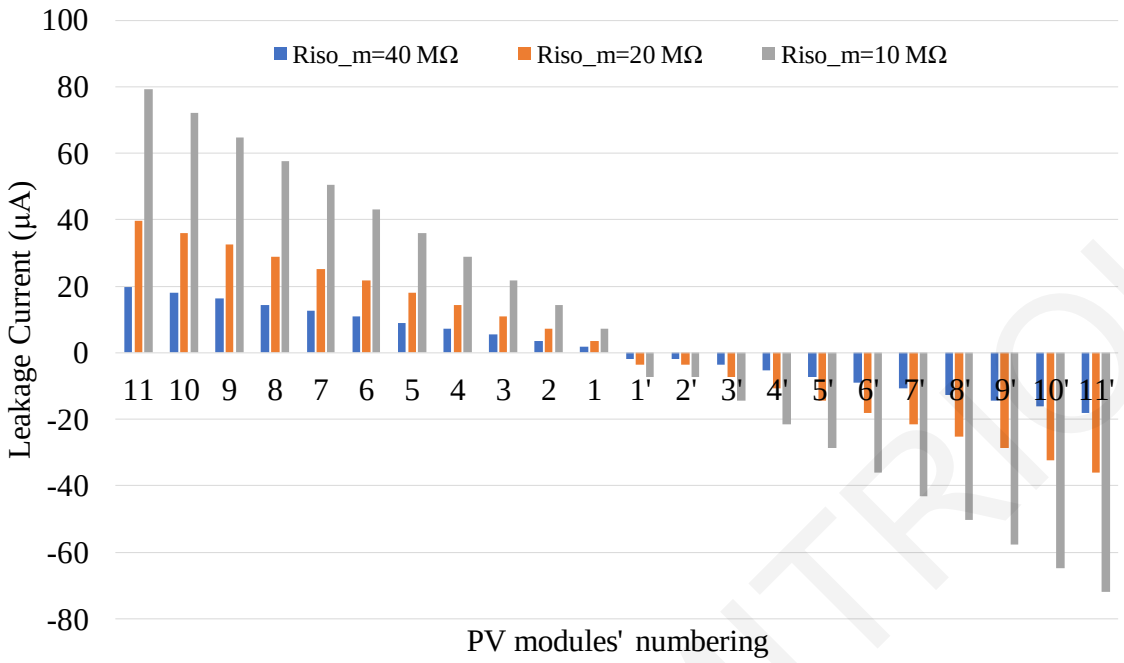

Figure 4-12: Leakage Currents of PV modules

Furthermore, Figure 4-13 presents the *PSP* variations along the length of the pipeline for the examined insulation levels of PV modules. As expected, the decrease in insulation resistance R_{ISO_m} results in an increase of stray current activity. This is because more leakage current is allowed to circulate via the PV strings. This increase of stray current activity is observed as alterations of the *PSP* along the pipeline section collocated near to the PV plant. The curves exhibit an identical trend (see Fig. 4-13) while the variation in *PSP* is calculated as equal to 170 % and 310 % for the cases R_{ISO_m}=20 MΩ and R_{ISO_m}=10 MΩ respectively, in comparison to the reference simulation results. In contrast to the leakage current from the modules, there is no purely linear relationship between (1/ R_{ISO_m}) and *PSP*, due to the dependence of the topology and the presence of other conductive elements (i.e. metallic poles, EGC) which influence the distribution of stray current interference.

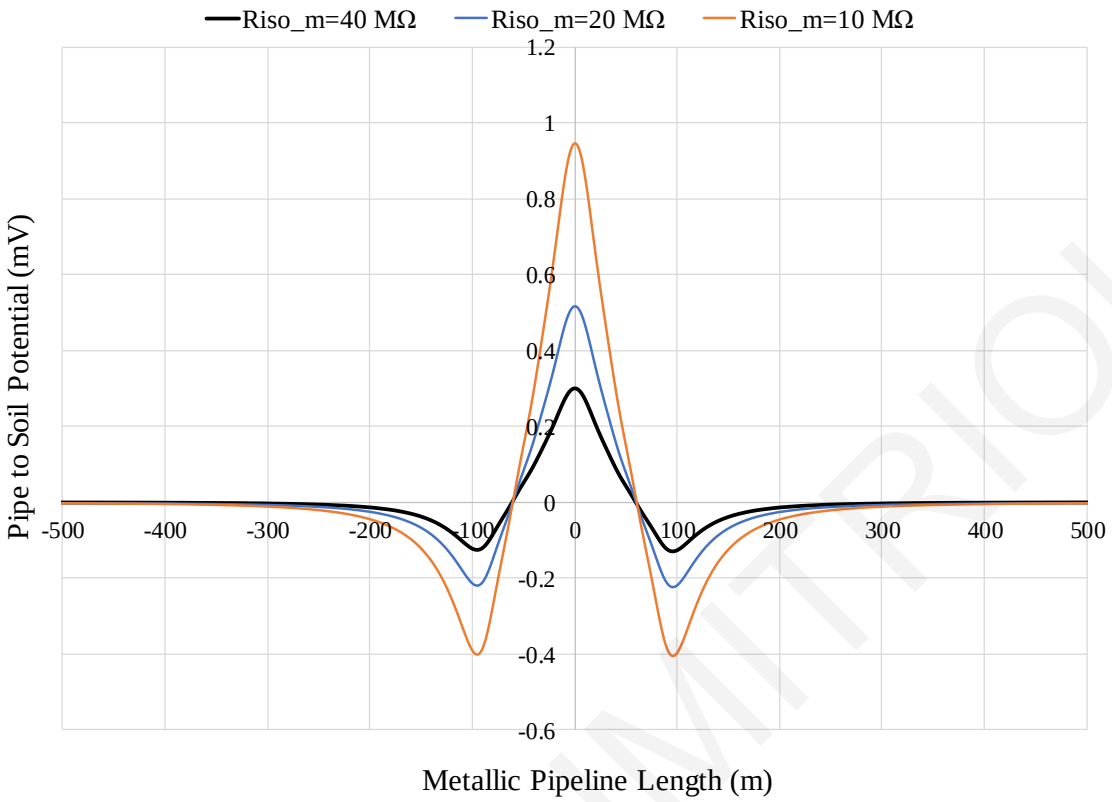

Figure 4-13: PV interference on buried pipeline system under different insulation levels of PV modules

Case 2 - Modelling of the influence Cables' Insulation:

The distinct potential difference between the positive and the negative current-carrying conductors creates *circulating currents* between the two (see Sec. 4.2). Thus, this case study will examine the leakage activity under several insulation resistances of the PV wiring cables, to identify the extent of these circulating currents and their influence on the pipeline system. In particular, the reference simulation is re-executed by reducing the insulation resistance of the array and main cables by 10 %, 1 % and 0.1 % of their rated values.

The cumulative calculated leakage current of the total modelled cabling (array and main cables) is presented in Table 4-5 for the examined simulation scenarios. Positive values imply that current is leaking out of the cables while negative values imply that current is leaking in (returns) the cables. The leakage current from PV cables is inversely proportional to the insulation resistance of the PV cables. However, the values of leakage currents are relatively low in comparison to the leakages of PV modules. Using Eq. (4-3) the calculated value of leakage current from a single PV string is 227 μA, which is higher even from the worst scenario where cables insulation had reduced by 1000 times.

Table 4-5: Leakage Current of PV Cabling

Scenario	Insulation Resistance	Positive Cabling Leakage (μA)	Negative Cabling Leakage (μA)
1	100 % of rated Value	0.26	-0.26
2	10 % of rated Value	2.6	-2.6
3	1 % of rated Value	26	-26
4	0.1 % of rated Value	261.2	-261.2

Furthermore, Figure 4-14 presents the variations of *PSP* along the length of the pipeline for the examined insulation levels of PV cables. Since the curves are overlapped, the stray current interference on the pipeline system is not affected by the insulation of the cables. This is because the leakage from the PV cables has a minor contribution to the overall stray current interference in comparison to the leakage of PV modules. Also, since the pair of the PV cables (positive & negative) are lying closely the stray current activity is limited locally, between the cables.

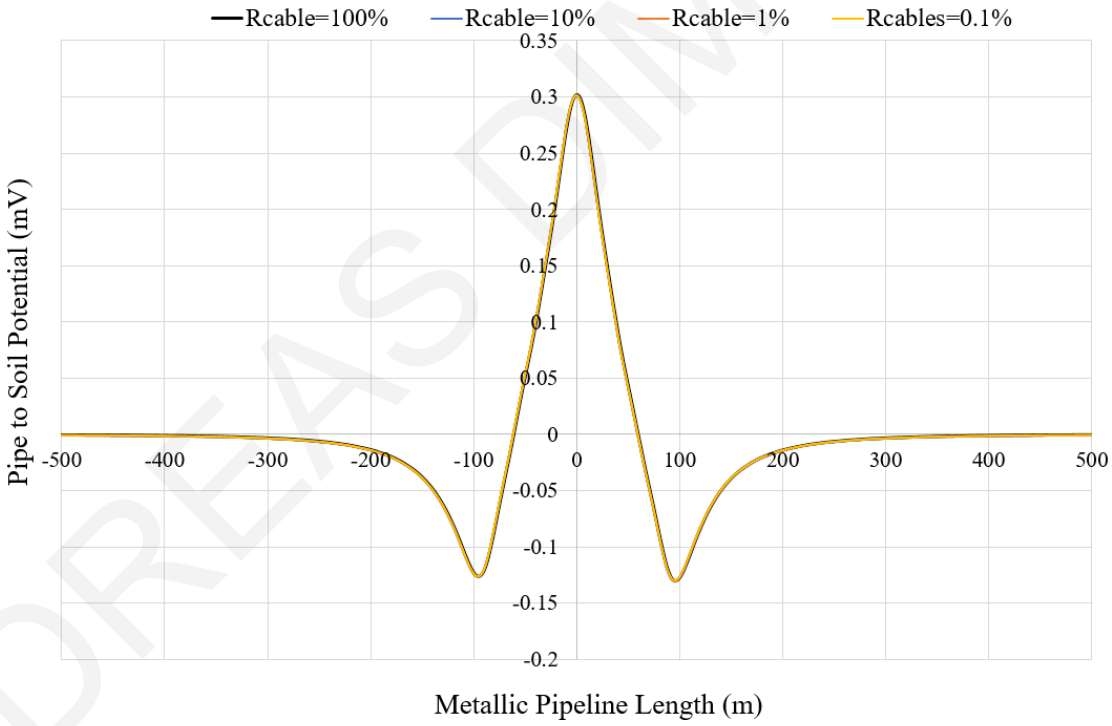

Figure 4-14: PV interference on buried pipeline system under different insulation levels of PV cables

Case 3 - Modelling of the influence of DC leakage activity under variable solar irradiation: During the course of a day, a PV plant operates under variable solar irradiation. The central inverter triggers the operation only if the incident solar irradiation is sufficiently high for power generation (i.e. 100 w/m^2). Below this value, the PV generators are open-circuited. While the irradiation increases the operating, the current increases proportionally, whilst the voltage exhibits slight variations depending on the maximum power point tracker's (MPPT)

operation. The MPPT is an embedded device in the central inverter that regulates the voltage and the current in such a way that the power generation is maximized [10]. By extension, the DC leakage activity can vary accordingly as this will be demonstrated. The reference model is executed under the operation levels of PV modules shown in Table 4-6. These simulation scenarios entail that the DC leakage activity correlates with environmental conditions such as the solar potential and its variation through a time cycle.

Table 4-6: Operation Level of PV Modules

Scenario	Irradiation Level (w/m^2)	Modules' Operation Voltage (V)	Modules' Operation Current (A)
1 (reference simulation)	1000	36	7
2	800	35	5.75
3	600	34	4.44
4	400	33	3.05

The PV interference on the pipeline system is presented in Figure 4-15. The stray current activity decreases as the irradiation level is reduced. However, because the MPPT adjusts the voltage level close to the nominal voltage of the inverter, the stray current activity is kept at relatively high levels. In conclusion, the operation voltage of the PV modules is the dominant factor for the leakage currents and consequently for stray current interference. However, since the operating voltage is maintained at high levels, the stray current interference does not vary significantly, even if the irradiation level exhibits noticeable variations.

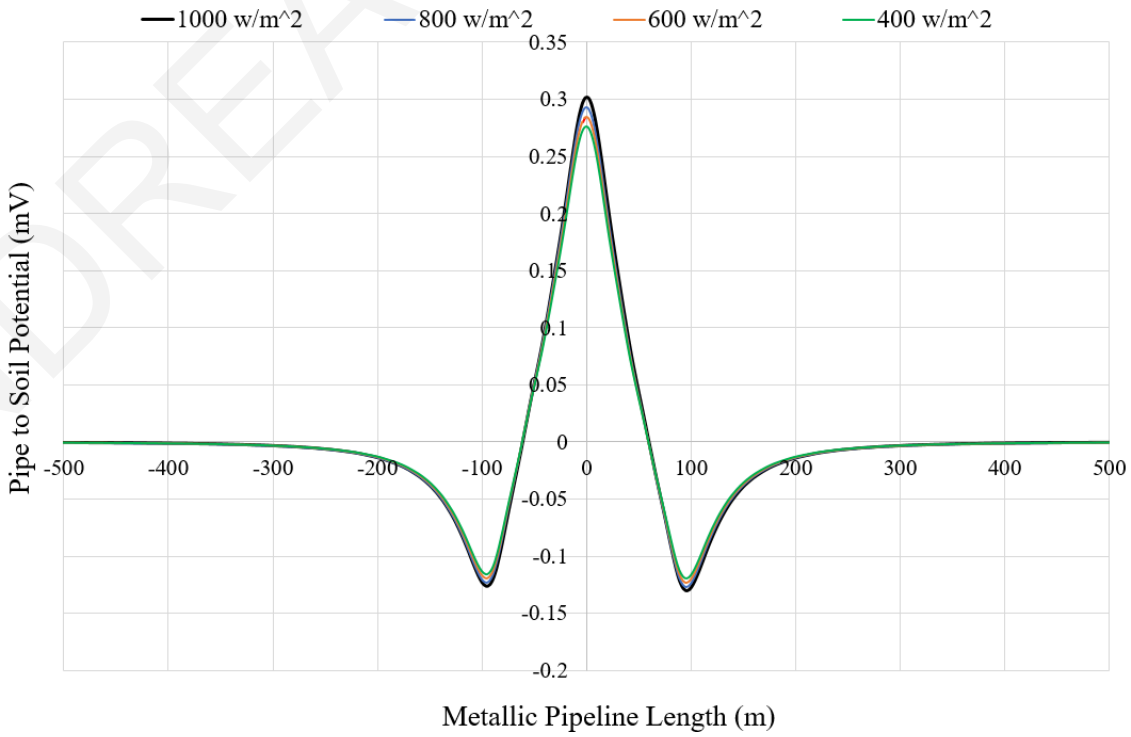

Figure 4-15: PV interference on buried pipeline system under different irradiation levels

Case 4 - Modelling of the influence of pipelines distance from PV plant:

This case study examines the area of influence of stray currents by calculating the *PSP* along the pipeline under different distances of the pipeline from the PV plant. In particular, the base simulation is executed by shifting the pipeline distance at 50 m and 100 m away from the PV plant.

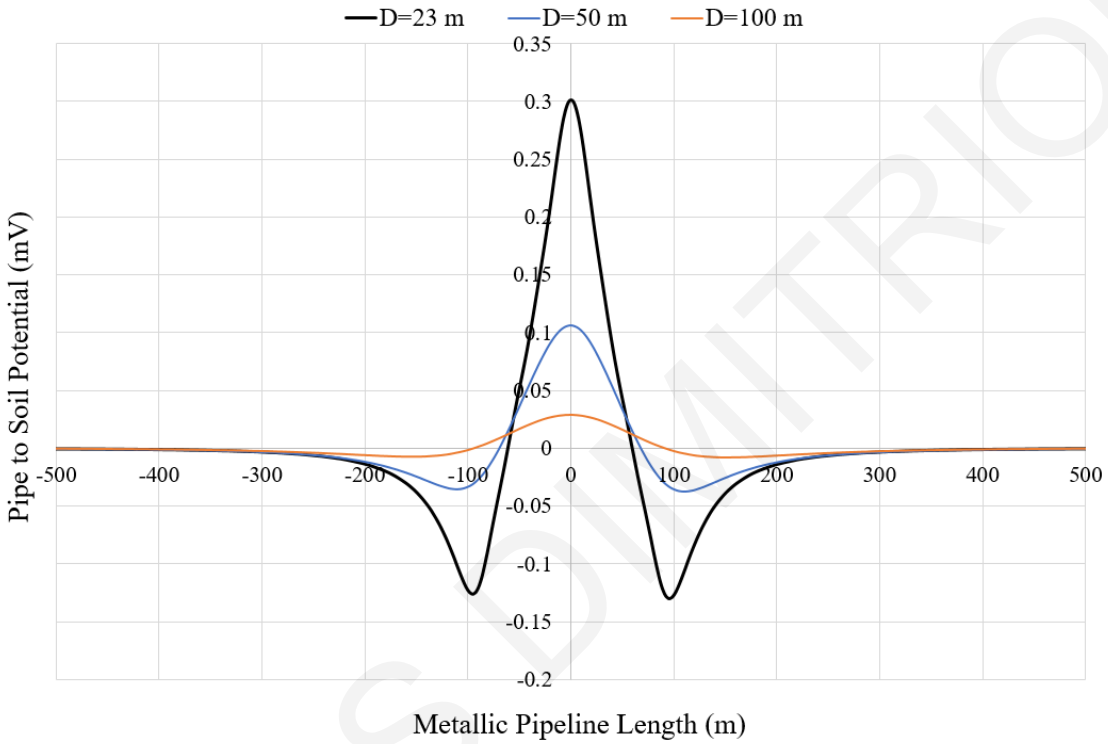

Figure 4-16: PV interference on buried pipeline system under different distance of the pipeline system

As the distance between the pipeline and PV plant increases the stray current interference is depreciated (see Fig. 4-16). For the specific case study, if the distance between the two systems is higher than 100 m the influence of stray current is insignificant.

Case 5 - Modelling of the soil resistivity influence:

Soil is an inhomogeneous medium with subcomponents that include: a) solid soil particles, b) ionic liquid and c) humid-air. Consequently, the soil resistivity depends on the mixture of solid, air and liquid elements. Depending on the type of soil the values of soil resistivity may vary significantly, indicative values are given in Table 4-7.

Moreover, seasonal variations have a considerable impact on the soil resistivity value. During the rainy seasons, the soil resistivity decreases abruptly due to moisture accumulation. In contrast, during the dry seasons, the soil resistivity increases especially at the upper layers due to moisture evaporation. To this extent, the level of the DC stray current

flowing through the soil is likely to be affected by the seasonal variations in soil resistivity over the course of the year.

To examine the influence of soil resistivity the simulation is re-executed under different soil resistivities. Two additional simulation scenarios were investigated with soil resistivity values of 10 Ω.m and 1000 Ω.m, replicating two extreme scenarios. With reference to Figure 4-17, the calculated magnitude of the *PSP* is altered at 182 % and 18% for the cases where soil resistivity is 1000 Ω.m and 10 Ω.m respectively. As the soil resistivity decreases, the stray current activity is enhanced because a larger amount of leakage current exploits the low resistance paths established in the soil for its return to the energy source. Although, the stray current injected into the soil is higher due to the lower soil resistivity the established earth potential rise is reduced. However, if we assume a coating holiday in a specific pipeline's section under anodic interference (i.e. negative values of *PSP*), the corrosion rate in the case where ρ_soil=10 Ω.m is more severe in comparison to the case where ρ_soil=100 Ω.m. This is because even if the *PSP* is reduced at 18% the coating holiday resistance (see Eq. 3) is also reduced at 10 %. To this extent, the holiday current rises to 180 % of its original value.

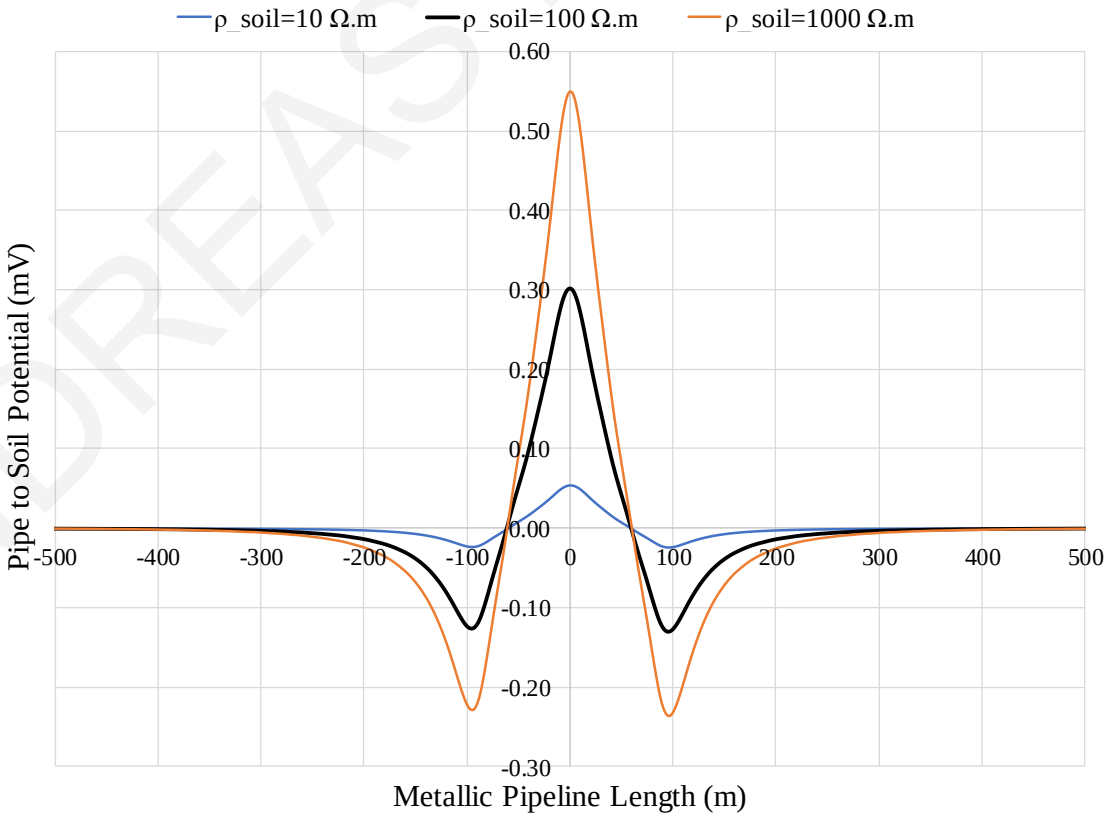

Figure 4-17: Stray current activity on buried pipeline system under different soil resistivities

Table 4-7:Indicative Values of Soil Resistivity

Type of Soil	Resistivity (Ω.m)
Garden soil	5-50
Clay	5-100
Sand & Gravel	40-250
Porous Chalk	30-100
Quartzite	300+
Rock	1000-10000

4.4.2 Concluding Remarks

The developed modelling techniques confirm the existence of the PV interference problem. The problem is affected by various factors as concluded via a series of sensitivity analysis simulations. It is demonstrated that the environmental conditions, the degradation of insulation materials as well as the distance of the pipeline system affect the level of interference. In particular, the insulation resistance of the PV modules poses probably the greater influence on the stray current activity, whereas the pipeline is not affected considerably by variations in the cabling insulation resistance. This is because the contribution of cabling in the cumulative leakage current is relatively low and also the leakage from the cables is circulating locally between cables. Changes that may result from seasonal variations, such as the value of soil resistivity allow more stray currents to reach the pipeline system. Furthermore, the irradiation level has an indirect effect on the PV interference since the variations of the operation voltage have an impact on leakage currents' flow and in extension to the interference level on third-party infrastructure.

In the light of the comments above, we can declare that the PV interference on the pipeline system which is located near the PV plant has a dynamic profile. The interference level can vary accordingly on a daily basis as well as on a seasonal basis. During the course of the day, the variable operation level, as well as any variations on the effective insulation resistance that may be due to the presence of moisture [18], [19] or on the dependence to the insulation materials with the temperature [45], [60], [82] affect the interference level. Moreover, PV interference is affected considerably due to the seasonal variation of soil resistivity. In addition, any natural or accidental degradation of the effective insulation of the energized components may affect the magnitude of the stray currents. Finally, the relative collocation of the PV system with the pipeline system is a critical parameter since in large distances the PV interference is reduced

In conclusion, the PV interference on pipeline systems has an identical trend in all simulated case studies. This is due to the specified fixed points where current injected and collected from the soil (i.e. metallic posts) as well as of the homogeneity in the changes applied on the examined case studies. To this extent, the areas with anodic and cathodic interference can be identified along the pipeline as well as the section which are more prone to corrosion (local maximums). Thus, modelling techniques are necessary for assessing the PV interference on pipeline systems in order to identify the areas which are more prone to corrosion.

Chapter 5

Identification of PV interference on pipeline systems

5.1 Introductory Remarks

The level of PV interference is influenced by various parameters that rely on the PV systems' operational characteristics as well as on weather and environmental conditions. Consequently, the magnitude of PV interference may vary considerably within the course of the day. To this extent, the need for dynamic simulation arises for the true visualization of PV interference. However, the understanding of PV interference's specific profile can facilitate its identification in existing installations by incorporating measuring procedures.

Within this chapter, a methodology is provided for the dynamic simulation of PV interference on pipeline systems (Section 5.2). The execution of dynamic simulations unveils the unique characteristics of PV interference (Section 5.3). The specific profile of PV interference is highlighted and is compared with the most common types of DC interference systems. Finally, based on the important conclusions and useful insights, guidelines for the identification and measurement of PV interference on pipeline systems are provided (Section 5.4).

5.2 Dynamic Simulation of PV interference

The modelling techniques developed in Chapters 3 & 4 are only able to examine the static nature of PV interference on pipeline systems. This is expressed in terms of spatial pipe-to-soil potential. However, since the coupling mechanism between the external DC stray current source (i.e. the PV Plant) and a pipeline system is purely conductive, there is very limited iterative dependence on the interference mechanism. Therefore, the dynamic PV interference can be examined by a series of discrete simulations, which reflect on a timestamp of the operating conditions of the PV plant [12].

To illustrate the process, a set of explicit steps is defined to enable the dynamic (i.e. time-varying) PV interference on pipeline systems. The process is shown in Figure 5-1. Each step is described in more detail below:

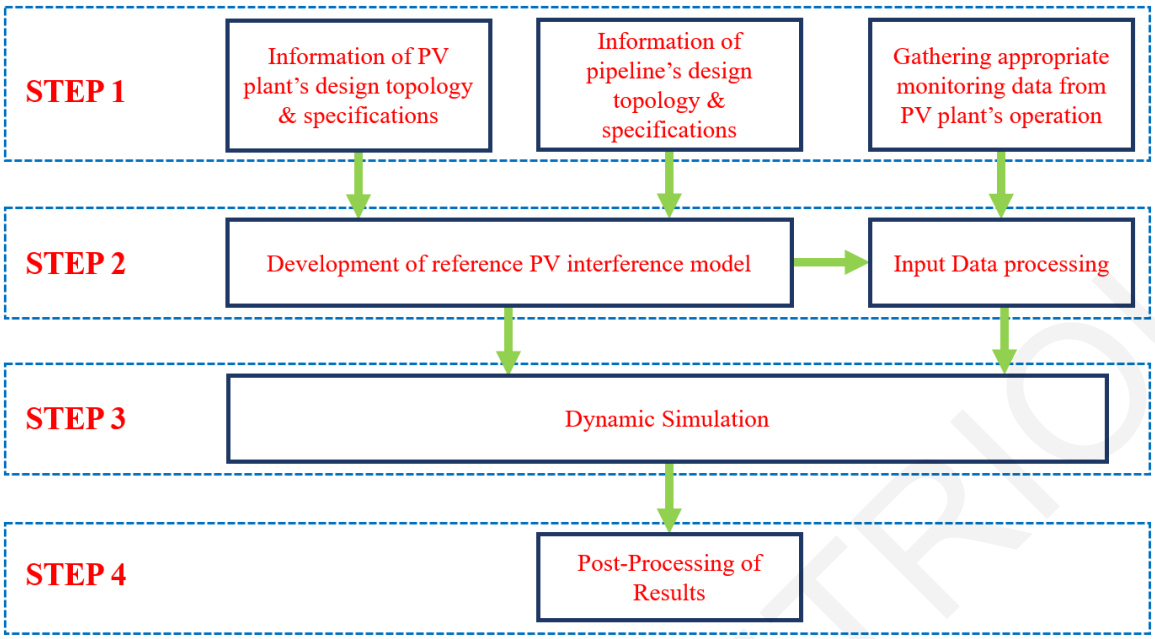

Figure 5-1: Examination of Dynamic PV interference- Proposed Procedure

- **Step 1:** The first step involves: a) the collection of relevant data that pertain to the PV plant and to the pipeline design topology and specifications and b) the collection of appropriate monitoring data associated with the operation of the PV plant. Table 5-1 details the required information/data that are needed in this step.

- **Step 2:** The second step involves: a) the development of a reference PV interference model and b) the processing of the input data that will allow the dynamic simulation of the reference model.

  In particular, the reference simulation model depends on the earthing configuration of the PV system. The modelling principles for each type of system (earthed/floating) are provided in chapters 3 and 4.

  The second sub-step embraces the sampling of the monitoring data. The selected sampling interval should capture the critical time-variations of the monitoring data (i.e. insulation resistance, operational voltage and current of PV array) collected during Step 1. Through this procedure, three sets of samples are exported which correspond to the current, voltage and insulation resistance of each PV array. Depending on the adopted modelling principles, the data processing aims at reproducing the time-varying current and voltage of the modelled energized-electrical components as well as their varying insulation resistance.

- **Step 3:** This step includes the sequential simulations of the reference model as per the input data obtained/prepared in step 2. This is necessary to examine the dynamic nature of PV interference on a pipeline system as per the varying operating conditions of the PV system.

- **Step 4:** The results of the sequential simulations are appropriately processed to construct the time-dependent PV interference on the pipeline system.

Table 5-1: Required Data/ Information to Perform Dynamic Simulation

Information on PV plant's design topology & specifications	
1	Computer-Aided Designs (CAD) that accurately indicate the topological arrangement of PV modules' supporting frames (façades) within the park.
2	Computer-Aided Designs (CAD) that accurately indicate the topological arrangement of the buried earthing electrodes as well as their connection points to the PV supporting frames.
3	Information on number, size, grounding configurations and location of Inverters.
4	Information on the use and location of DC cables (e.g. routing, type of cables, insulation properties, and cable manufacturers' specifications).
5	Information on PV modules' technology.
6	Information on PV stings' sizing.
7	Information on the location of combiner boxes and connection of PV strings
8	Information on size, design, earthing and material characteristics of PV modules' supporting frames (façades)
9	Soil Resistivity Reports about measurements carried out near or within the PV park.
Information on pipeline's design topology & specifications	
1	Pipeline route and position in relation to the PV Plant.
2	Pipeline wall resistivity and permeability.
3	Pipeline coating resistivity and thickness.
4	Pipeline size and thickness, depth and backfill conditions.
5	Description of cathodic protection units and DC injection levels.
6	Pipeline route and position in relation to the PV Plant.
7	Pipeline wall resistivity and permeability.
8	Pipeline coating resistivity and thickness.
9	Pipeline size and thickness, depth and backfill conditions.
10	Description of cathodic protection units and DC injection levels.
Collection of appropriate monitoring data from PV plant's operation	
Effective Insulation resistance (i.e. Riso) and Operational Current and Voltage of PV arrays for a specific period (i.e day) with an appropriate time resolution. (* Note: Modern PV plants are benefited with devices which automatically monitor and record these values)	

5.3 Case studies for dynamic PV interference examination on a nearby Pipeline System

By means of an example, the simulation model developed in Chapter 3 (see Sec. 3.3) of an earthed PV system is selected as a reference model to perform dynamic simulations of PV interference on a nearby pipeline system. Moreover, the recorded monitoring PV data available in [18] have been exploited to reproduce a set of realistic input data for the dynamic simulation of the developed reference model. Two case studies have been examined referring to a winter day and a spring day.

5.3.1 Analysis and processing of Monitoring Data

The recorded monitoring data of a 68 kWp PV plant available in [18] are used as a reference to generate an equivalent set of realistic input data for the subsequent dynamic simulations. In the following paragraphs (A-B), the processing steps of the monitoring data are provided.

A. Analysis of monitoring Data

As noted earlier, the available monitoring PV data were obtained during a test program of an operational 68 kWp PV plant. Data measurements include the continuous logging of:

1) the insulation resistance of the PV array (R_{iso}),
2) the irradiance level (G),
3) the relative humidity (RH),
4) the modules' temperature (T_{mod}),
5) the atmospheric pressure (AP) and
6) the leakage capacitance (C_{lek}).

There are two sets of data measurements regarding a sunny winter day (see Fig. 5-2) and a cloudy rainy day in spring (see Fig. 5.3). Readings were captured over a 24-hours period with 5 seconds resolution. The available data are treated, in order to be fine-tuned and be compatible with the developed simulation models to facilitate the dynamic simulations.

Based on the analysis performed by Hernandez et al. [18], on the winter day during the nighttime hours the value of R_{iso} is relatively low since the level of RH is high and the T_{mod} is low. A sharp reduction in R_{iso} is evident between 8:30-9:30 because the solar irradiance liquefies the frost on the back surface of the modules. The liquefied frost reduces the value of R_{iso} as the moisture penetrates the insulation material. During the course of the day, the value of R_{iso} increases gradually as the PV plant starts its operation and the moisture of the

PV modules progressively evaporates due to the increase of T_{mod}. Between 12:00-16:30 the value of R_{iso} is set at the highest level because the modules are fairly hot and the moisture has been completely evaporated. In the evening, between 16:30-18:30, as the irradiation level decreases (sunset), the R_{iso} decreases, since the T_{mod} is reduced while RH increases. At night hours the value of R_{iso} does not exhibit significant variations because RH and T_{mod} are not fluctuating considerably.

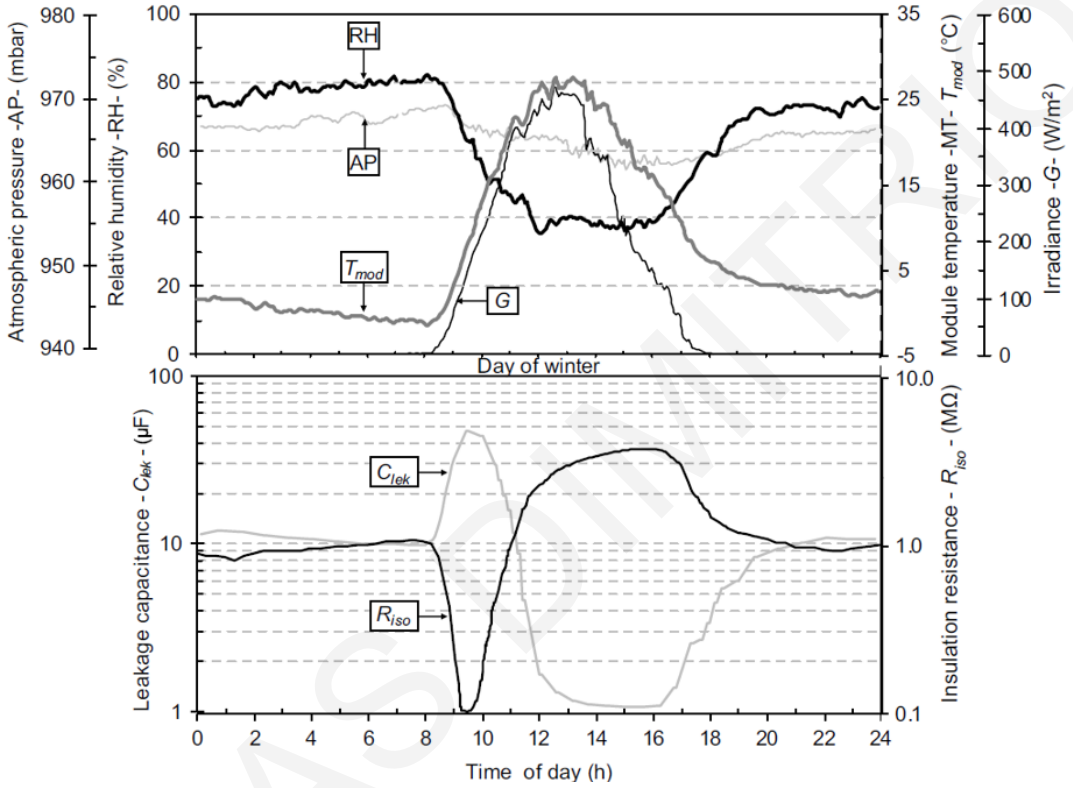

Figure 5-2: Semi-logarithmic graph of the daily variation of PV array insulation data and meteorological variations in the 68-kWp PV plant on a typical winter day [18]

Regarding the spring day, there are sudden rises in the RH caused by sharp drops in the daytime ambient temperature. This occurred after drizzles (9:20, 0:55, 2:20, 3:25, 17:05) or rainstorms (5:20, 7:00, 21:25). In extension, the value of R_{iso} exhibits sharp troughs. Even if the RH is comparatively higher at night hours (00:00-1:00) during the day there exist greater reductions in R_{iso} due to the temporary rainstorms, which diminish the effective insulation resistance of the PV modules (due to the presence of rainwater).

The seasonal variation indicated that the lowest R_{iso} value occurred on the sunny winter day. Therefore, moisture absorption by the PV insulation through the back of the module at the dawn after a cold winter night was greater than through the top cover glass when it rained in spring. As concluded, neither the wind speed nor the atmospheric pressure had a direct influence on the insulation resistance, albeit the wind speed's indirect influence through accelerating the evaporation of the moisture.

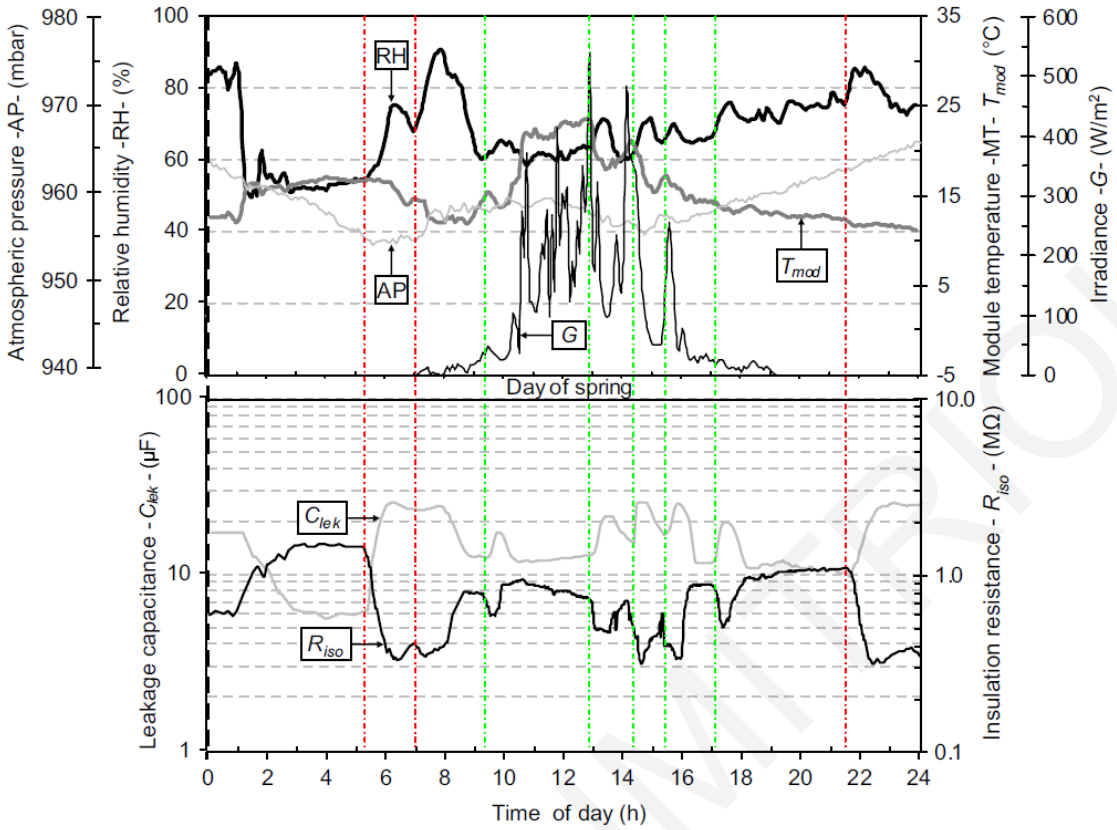

Figure 5-3: Semi-logarithmic graph of the daily variation of PV array insulation data and meteorological variations in the 68-kWp PV plant on a typical spring day [18]

B. Data processing procedure

The recorded data have been processed to generate an equivalent set of realistic input data for the developed simulation model. Subsequently, the constructed data are loaded sequentially on the reference CDEGS simulation model in order to examine the time-varying PV interference. The data processing procedure that followed is shown in the diagram below (see Fig. 5-4):

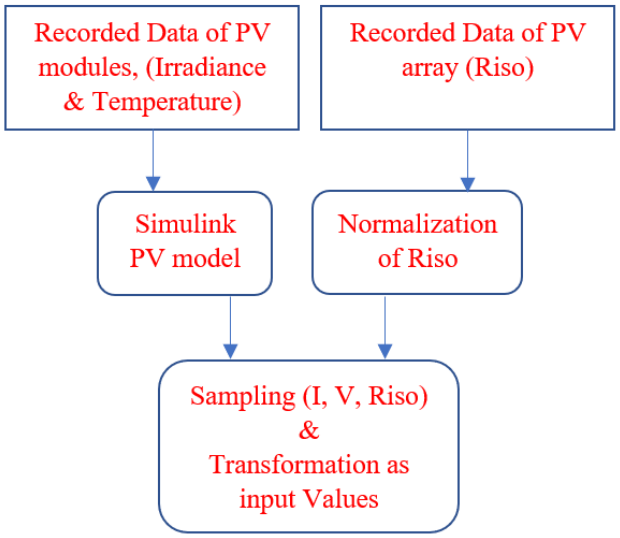

Figure 5-4: Data processing

An application tool in Simulink (see Appendix B) reproduces the expected operational current (I_m) and voltage (V_m) of the specific PV modules incorporated in the simulation model. In particular, the Simulink model calculates the PV module's current and voltage by considering the recorded values of the irradiance and the module's temperature. The values are obtained by taking into account the IV characteristics of commercially available PV modules which are incorporated in simulation models.

The next step is the normalization of the PV array's insulation resistance value. Since the recorded values represent the effective insulation resistance of a whole PV array of 68 kWp PV plant, the values are modified in order to correspond to the insulation resistance (R_{iso_m}) of a single PV module considered in the modelled PV plant. In particular, the values of the recorded data are normalized, considering as a maximum value the rated insulation resistance of modelled PV modules (i.e. 40 $M\Omega/m^2$).

The constructed data of current (I_m) voltage (V_m) and insulation resistance (R_{iso_m}) for PV modules are sampled. Sampling is performed with appropriate time intervals to include the time variations of PV generation. The sampling period is 3 samples per hour for the winter day and 20 samples per hour for the spring day. The number of samples is not the same because during the spring day there are variations of critical measures in shorter time-periods. Finally, an algorithm transforms the samples in desired input values in order to reproduce the energization and insulation characteristics of the involved components. It should be noted that the sampling has been performed only during the operational hours of the PV plant.

5.3.2 Dynamic Interference of an Earthed PV system under Blind Spot Fault

The developed CDEGS simulation model of an earthed PV system (see Fig. 5-5), which is demonstrated in Section 3.3, has been dynamically simulated to examine the PV interference on a pipeline system. It should be kept in mind that a blind spot fault is integrated into the model. With reference to Figure 5-5, the developed model is repeatedly simulated using the input data constructed through the procedure described in the diagram shown in Figure 5-4, for the winter and the spring day, respectively.

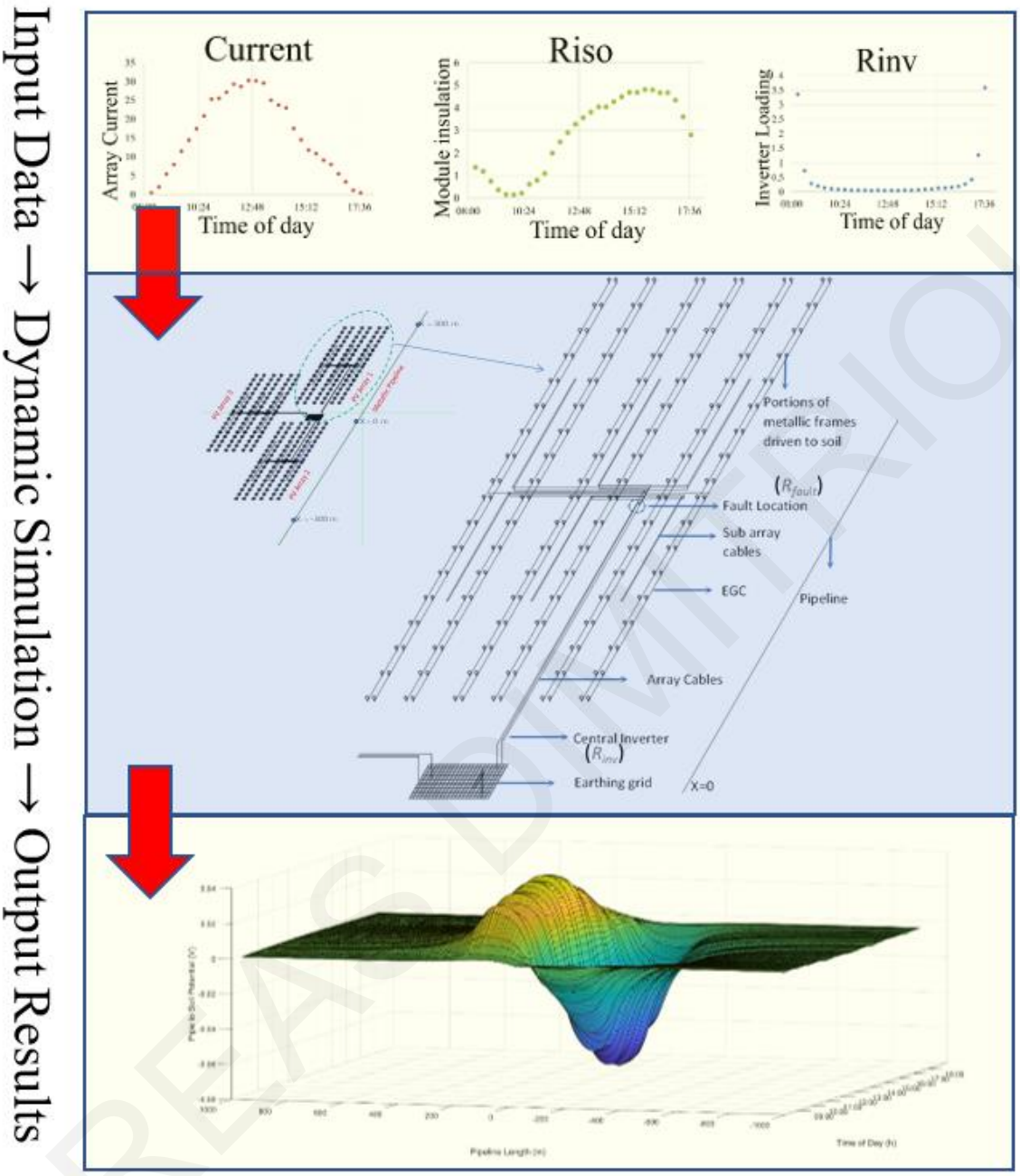

Figure 5-5: Dynamic Simulation of a PV interference model

A. Winter Day

Using the model developed in Simulink (see Appendix B), the operational current and voltage of PV modules are extracted. The calculated current and voltage of a single PV module during the winter day are shown in Figure 5-6. It should be mentioned that identical operational conditions had been assumed for all PV modules embraced in the simulation model. With reference to Figure 5-2, the calculated current of the PV modules is proportional to the irradiation level while the calculated voltage has a relatively stable magnitude.

Moreover, the extracted insulation resistance R_{iso_m} of each PV module considered in the simulation process is presented in Figure 5-7.

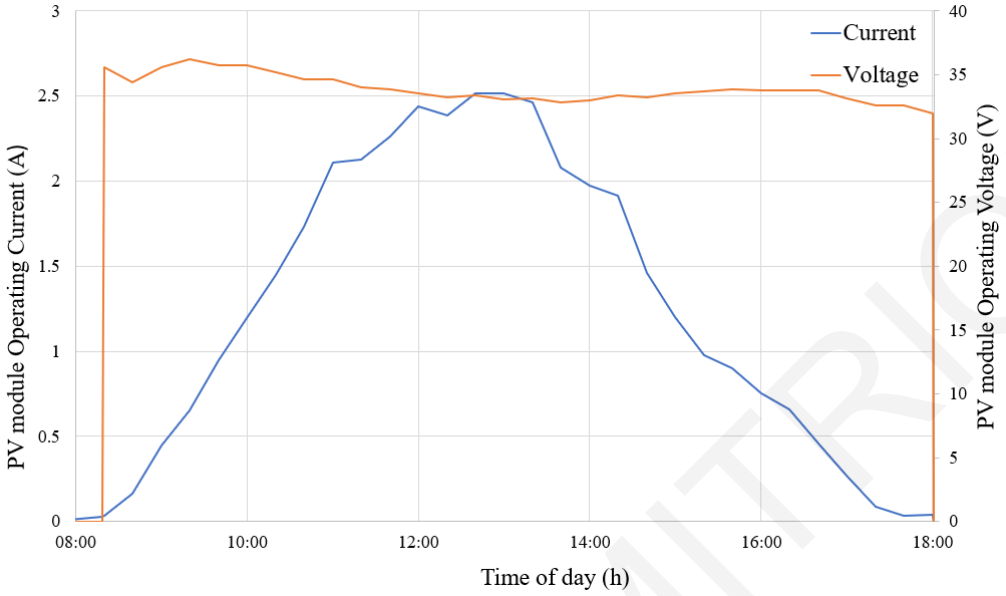

Figure 5-6: Operational Current and Voltage of a PV module during a winter day

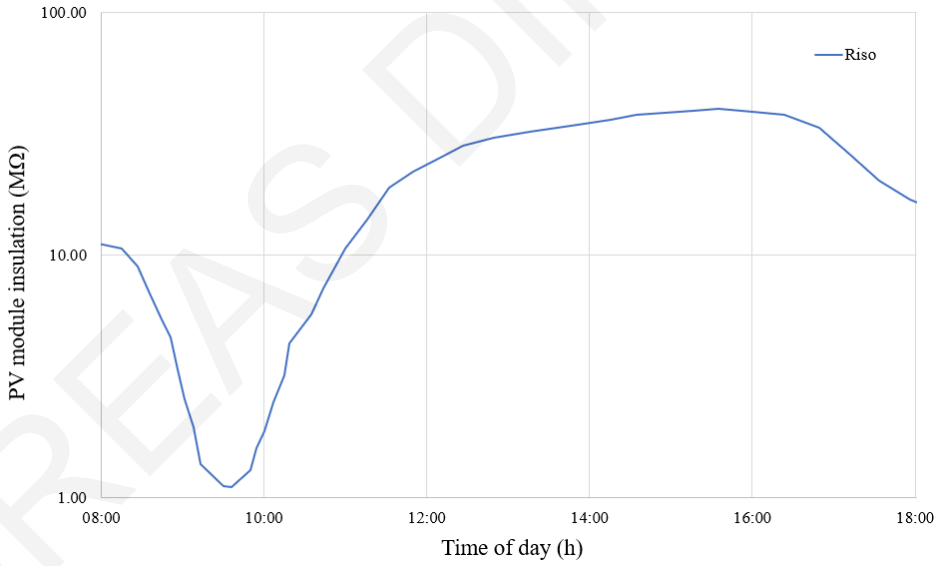

Figure 5-7: Insulation resistance of a PV module R_{iso_m} during a winter day

Thus, a series of simulations are executed regarding the operational hours (8:20 to 18:00) of the PV plant. The 3D-plot in Figure 5-8 presents the dynamic PV interference along the length of the pipeline system in terms of pipe-to-soil potential (PSP) during the examined period. It is clearly exhibited that there is a time-variation of PV interference in the course of the day. The simulation results reveal that there is a strong correlation between the operational current and PV interference when the PV plant exhibits a blind spot fault. This is because the fault loop develops a parallel route that delivers a portion of the PV current. To this extent, the variations of the PV current are reflected in PV interference.

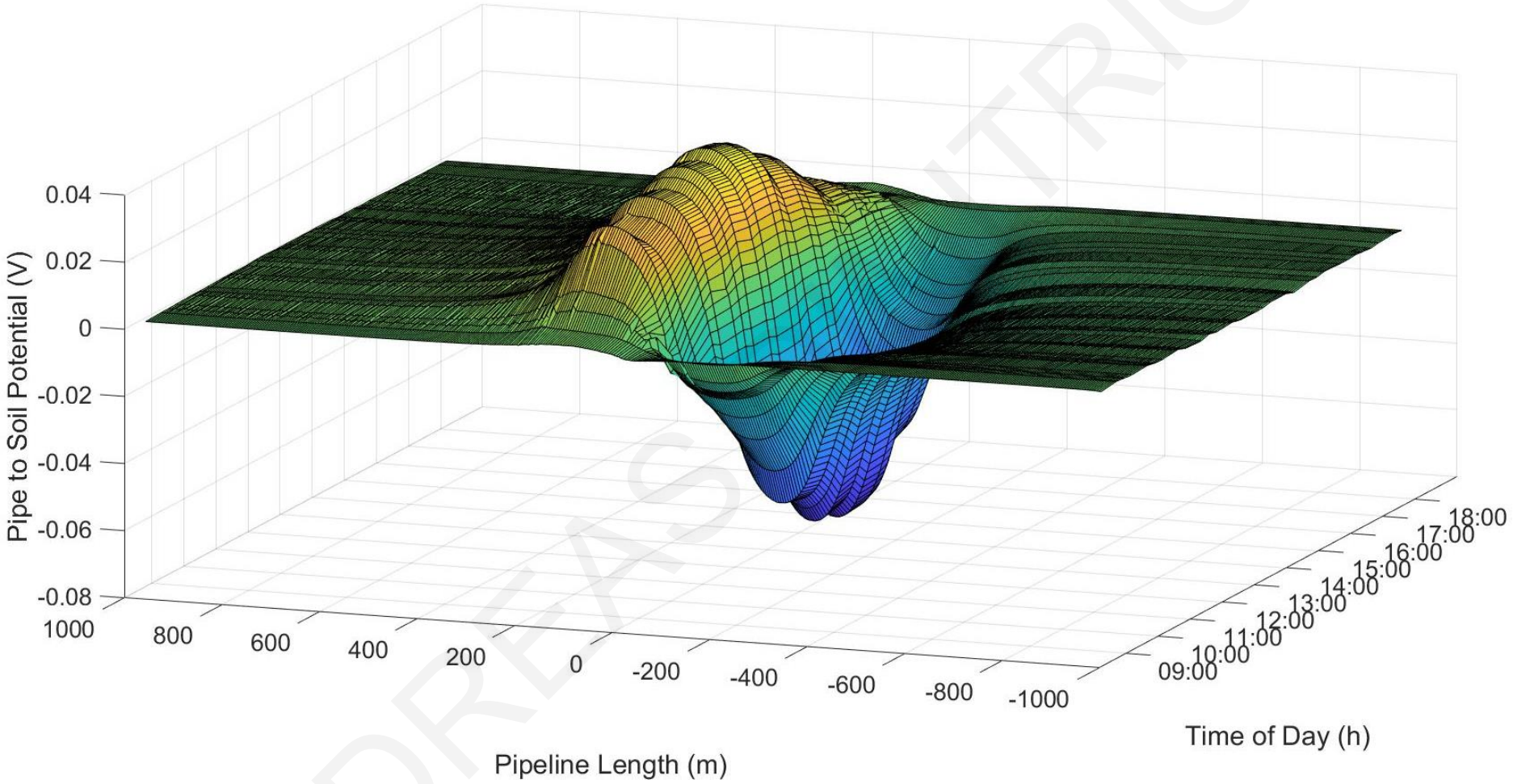

Figure 5-8: Dynamic PV interference on Pipeline System during a winter day

Indicatively, Figure 5-9 exhibits the captured PV interference values along the length of the pipeline for specific time snapshots, beginning at 8:40, followed by 9:00 and then every 1-hour interval.

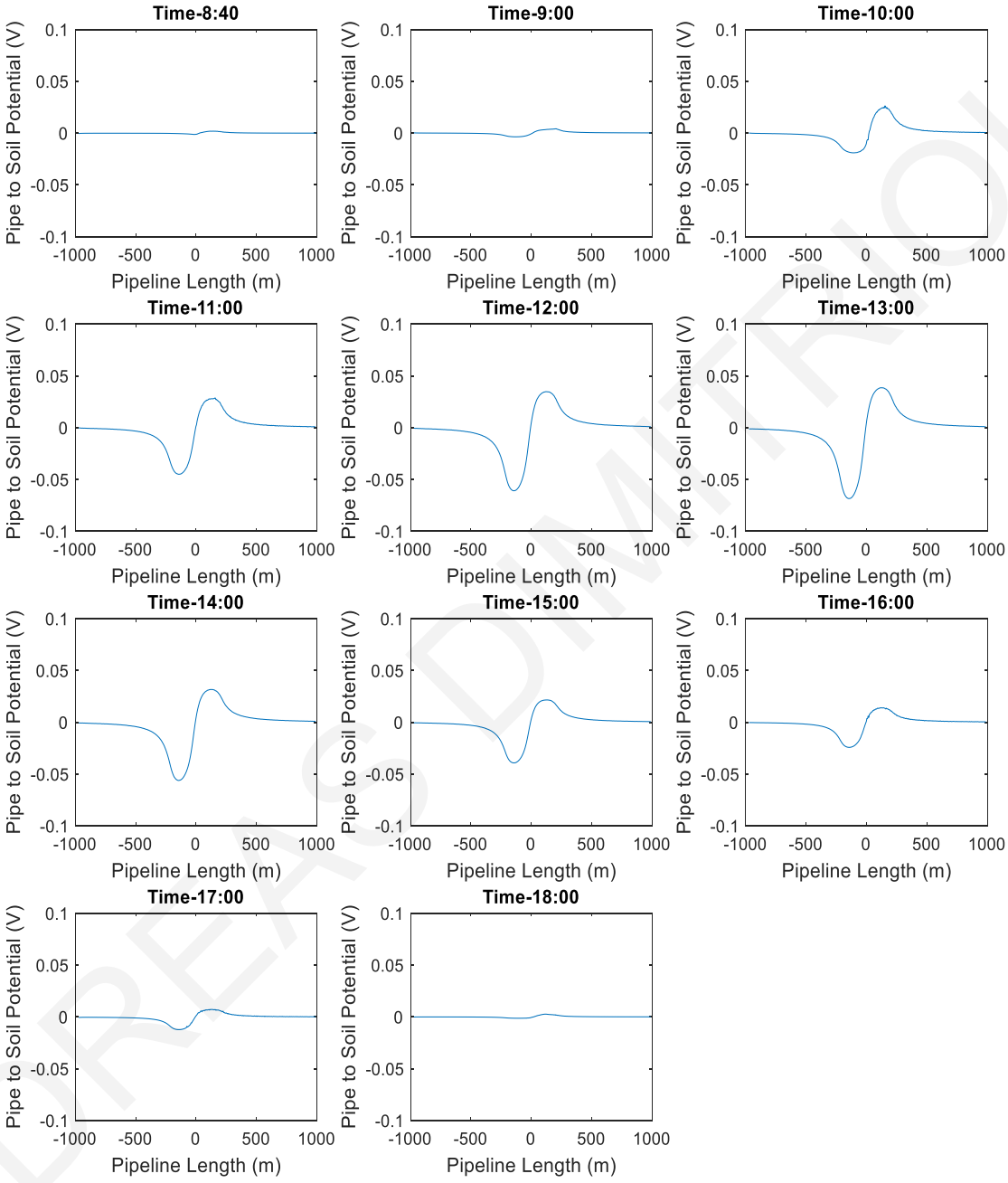

Figure 5-9: PV interference along the length of the pipeline at specific time snapshots during a winter day

The maximum PV interference values during the course of the day are captured at 13:00, where the power production of the PV plant is maximized. The values of interference range between -68,5 mV to 38,5 mV. The most negative value (-68,5 mV) captured at the section of pipeline X= -143 m while the most positive value (38,5 mV) captured at the section X=123 m.

With reference to Figure 5-10, the time variation of PSP at sections X=-143 m and X=123 m of the pipeline is presented in Figures 5-11 and 5-12 respectively. In both sections, the interference level is correlated to the production current. However, the R_{iso_m} value has a slight impact on the interference level especially during the morning hours 8:20 to 12:00 where R_{iso_m} value exhibits great variations. This is because the decrease of R_{iso_m} value results in an increase of leakage current of the PV modules. In particular, the leakage currents from the PV modules which are adjusted predominantly from R_{iso} value (since the voltage is relatively stable) are injected in multiple points (i.e frames' metallic post) into the soil returning to the grounded conductor (negative current currying conductor) via the inverter's earthing grid.

Since the current flow in the inverter's earthing grid has an opposite direction in comparison to the fault current, the leakage currents from the PV modules tend to reduce the interference level. The impact of the leakage currents originated from PV modules is reflected in the cumulative leakage current which returns via the grounded point of the negative current currying conductor (see Fig. 5-13).

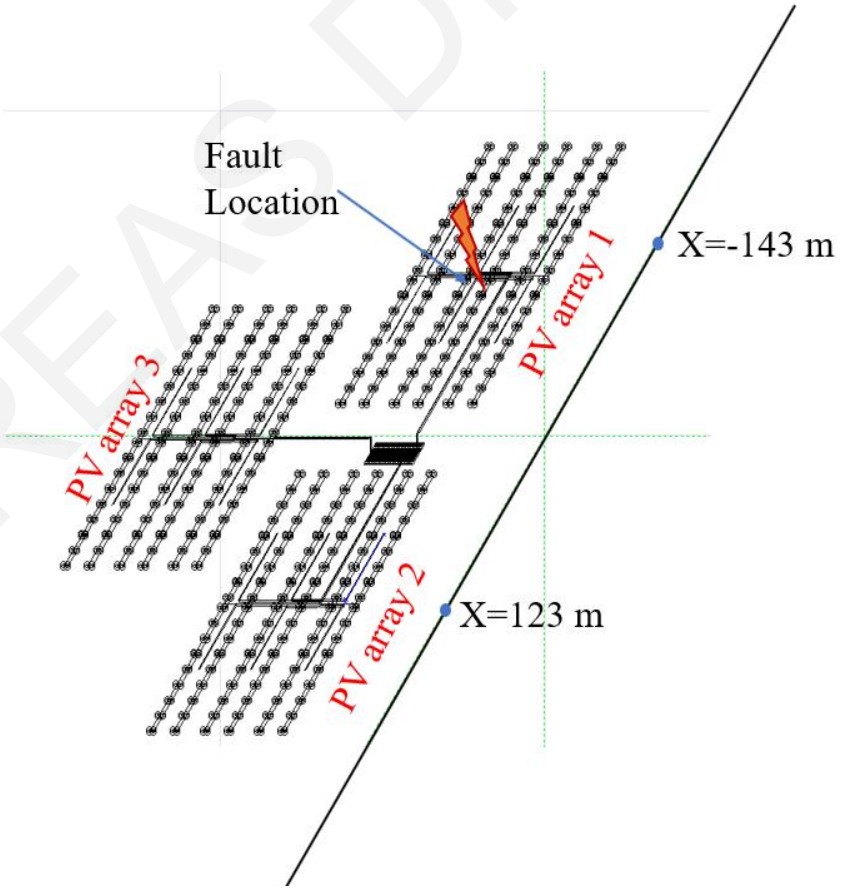

Figure 5-10: Illustration of the pipeline's section with maximum captured PV interference during a winter day

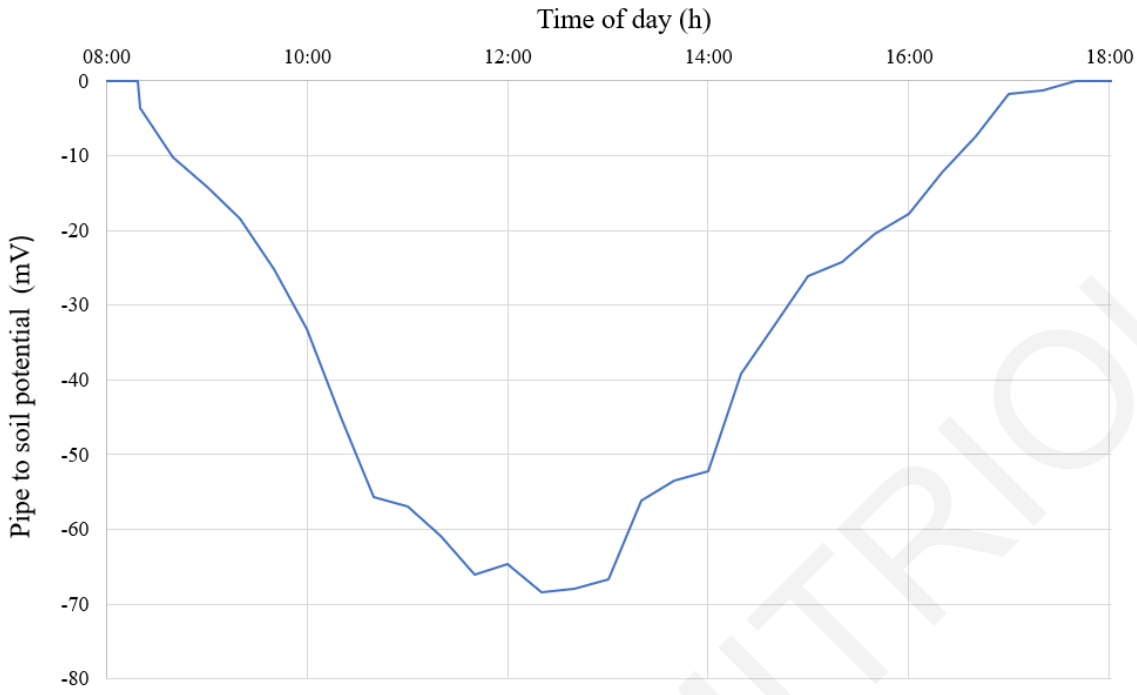

Figure 5-11: Dynamic Interference at Section X= -143 m of the pipeline system during a winter day

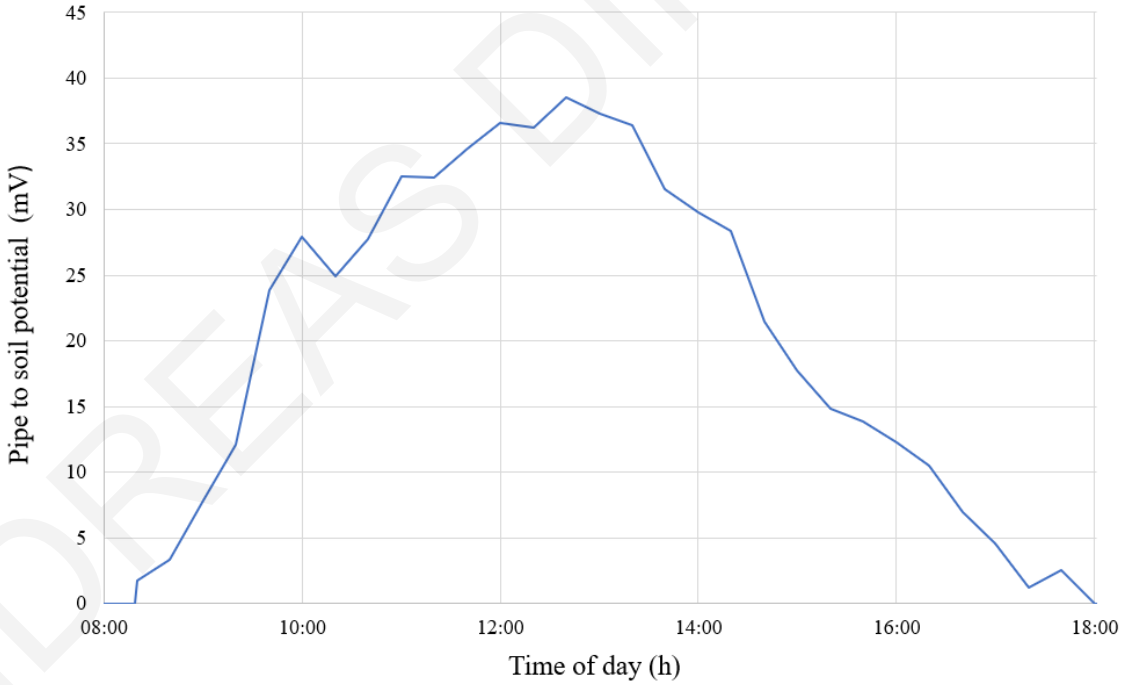

Figure 5-12: Dynamic Interference at Section X= 123 m of the pipeline system during a winter day

The leakage currents I_R returning to the grounded point of the negative conductor for the three PV arrays included in the simulation model (see Fig. 5-13) are provided in Figure 5-14. As explained in chapter 3, a portion of the cumulative leakage current is captured by the equipment grounding conductor while the remaining current returns via the soil to the grounding point. For the healthy arrays 2 & 3 the return current I_R is almost identical in both

arrays since it is exclusively originated from the leakage of PV modules. The return current in arrays 2 & 3 has an inversely proportional relation to the R_{iso_m} value since the voltage of PV modules is relatively stable (see Eq. 3-1). Positive values indicate that the current I_R flows into the grounded conductor via the earthing point.

On the contrary, in the faulted array 1 (which exhibits a blind-spot fault), the return current differs considerably because it is superimposed with the current streaming from the faulted point. As shown in Figur 5-14 there are periods where the polarity of the current flowing through the grounded conductor of a faulted array is inversed. Positive values indicate that the leakage current flows into the grounded conductor, while negative values indicate that the leakage current flows out of the grounded conductor (towards the earthing grid). The current originated from the PV modules flows towards the grounded point, while the current originated from the blind spot fault flows in the opposite direction. The overall current presented in Figure 5-14 has positive values when the leakage originated from PV modules prevails the fault current. On the contrary, if the fault current prevails the leakage current from the modules, then the current values are negative.

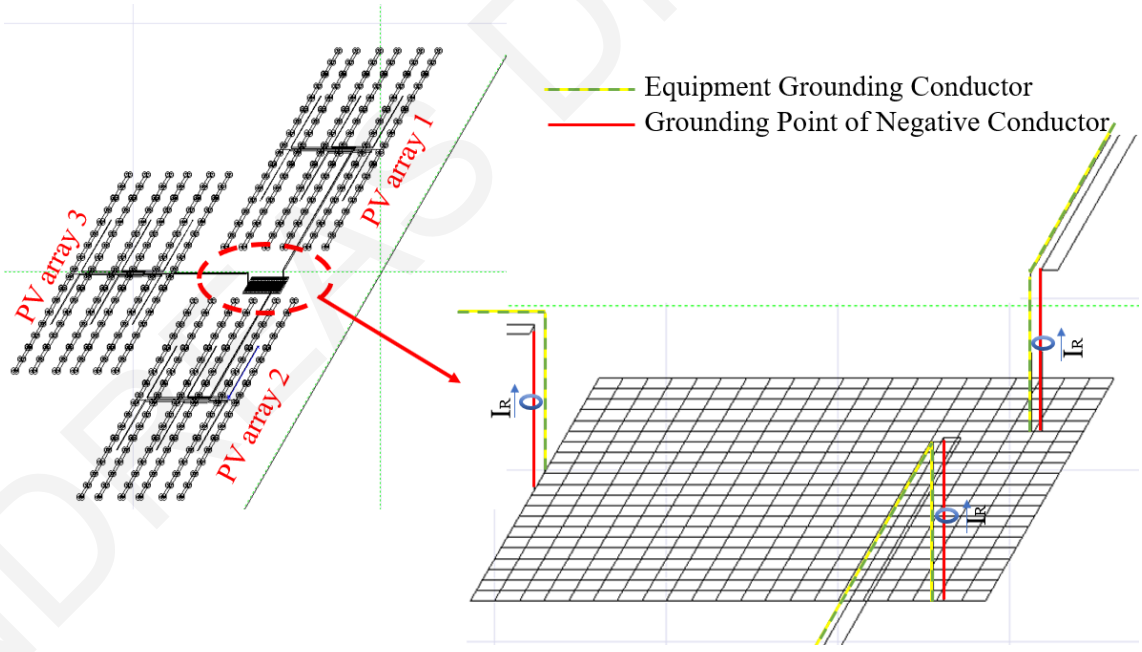

Figure 5-13: Illustration of grounding return points of leakage current

At this point it should be noted that the cancellation effect, from the leakage current originated from the PV modules against the current originated from the fault point has as an impact in the decrease of the PV interference magnitude as well as a slight distortion of the PV interference waveshape along the length of the pipeline. To this end, Figure 5-15 shows the PV interference at times: a) 9:40 where the leakage from the PV modules is maximized

and b) 13:00 where the leakage from the PV modules is negligible while the fault current magnitude is maximized. By comparing the two graphs, it is obvious that the leakage current from the PV modules alters the wave-shape of the PV interference curve. In addition, the local maximum/minimums are slightly shifted.

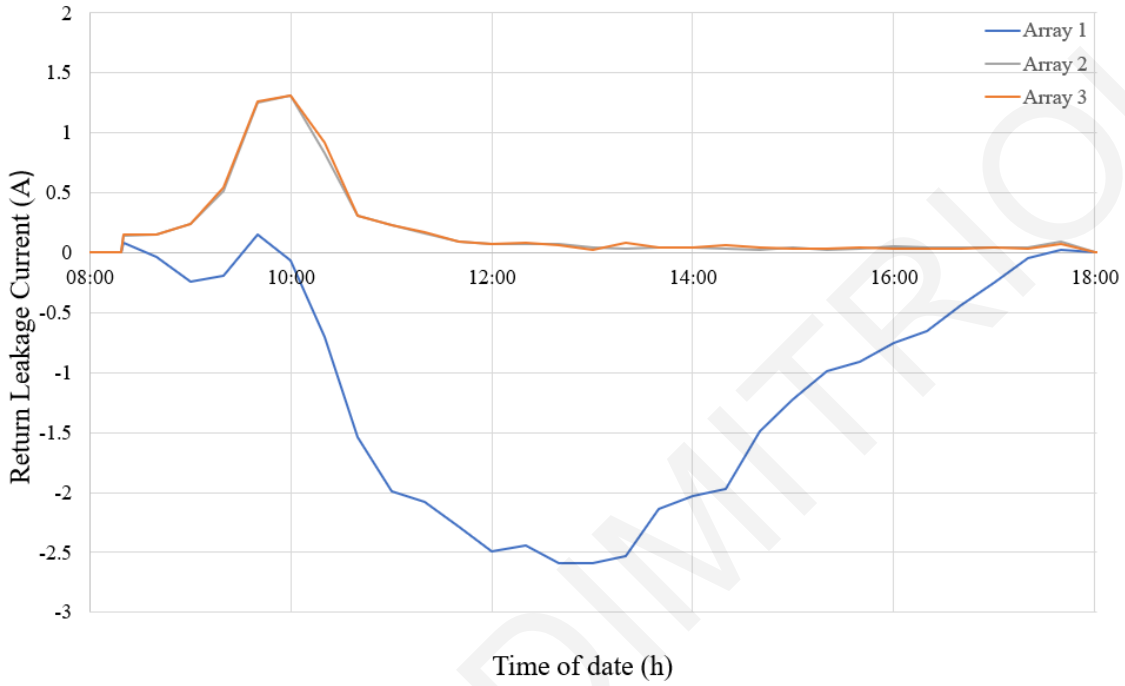

Figure 5-14: Return Leakage Current to the grounded point during a winter day

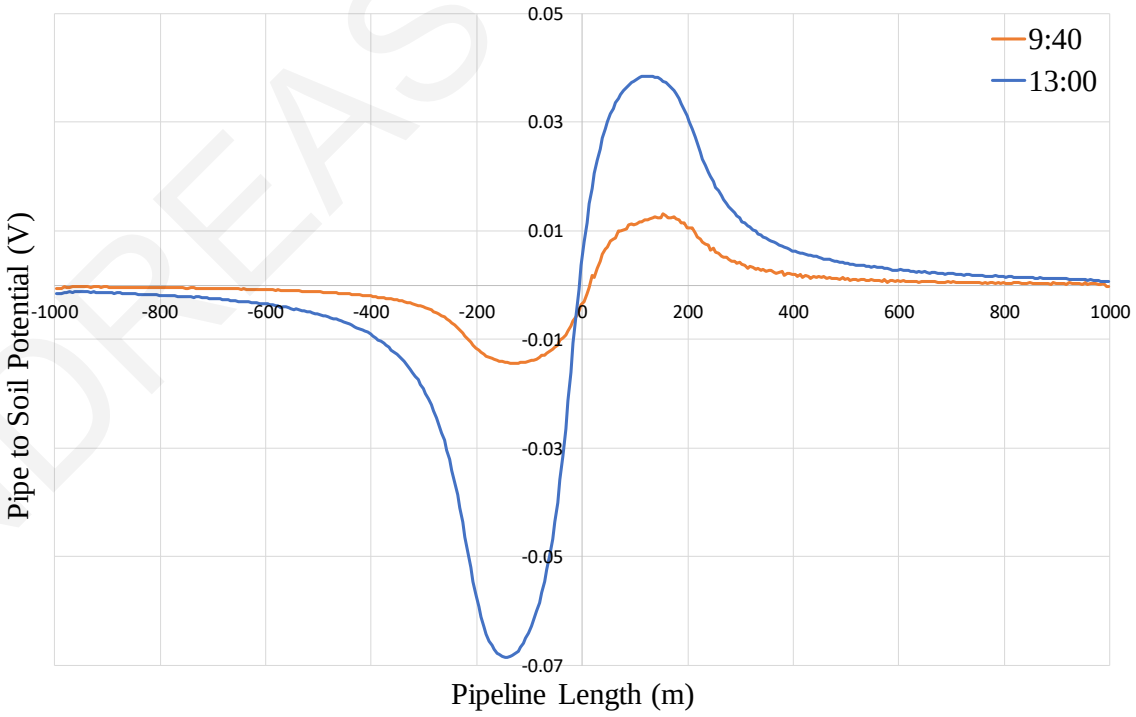

Figure 5-15: PV interference along the length of the pipeline at specific times during a winter day

B. Spring Day

The operational current and voltage characteristics of the PV modules during the spring day are reproduced using the Simulink model (see Fig. 5-16). As expected, the calculated current of the PV modules is proportional to the irradiation level (see Fig. 5-3). The calculated voltage has a relatively stable magnitude around 33 Volts, except the morning period (till 9:30) where the voltage is slightly higher. This comes as a result of the lower PV modules' operational temperature. Moreover, the insulation resistance R_{iso_m} of each PV module that is considered in the simulation process is presented in Figure 5-17.

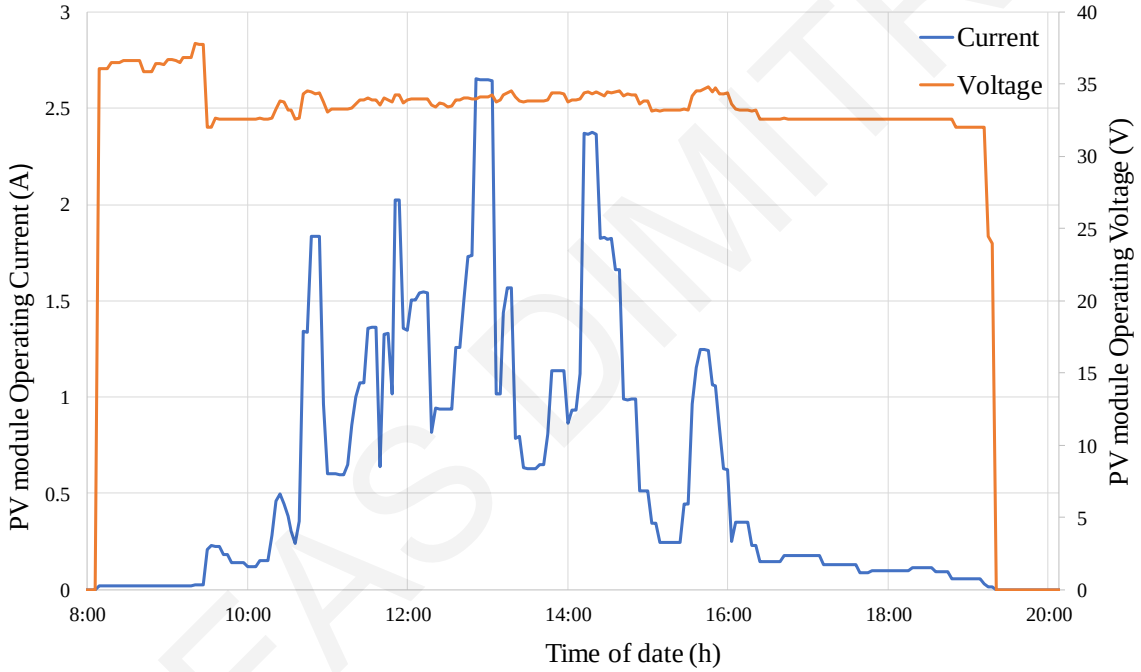

Figure 5-16: Operational Current and Voltage of PV module during a spring day

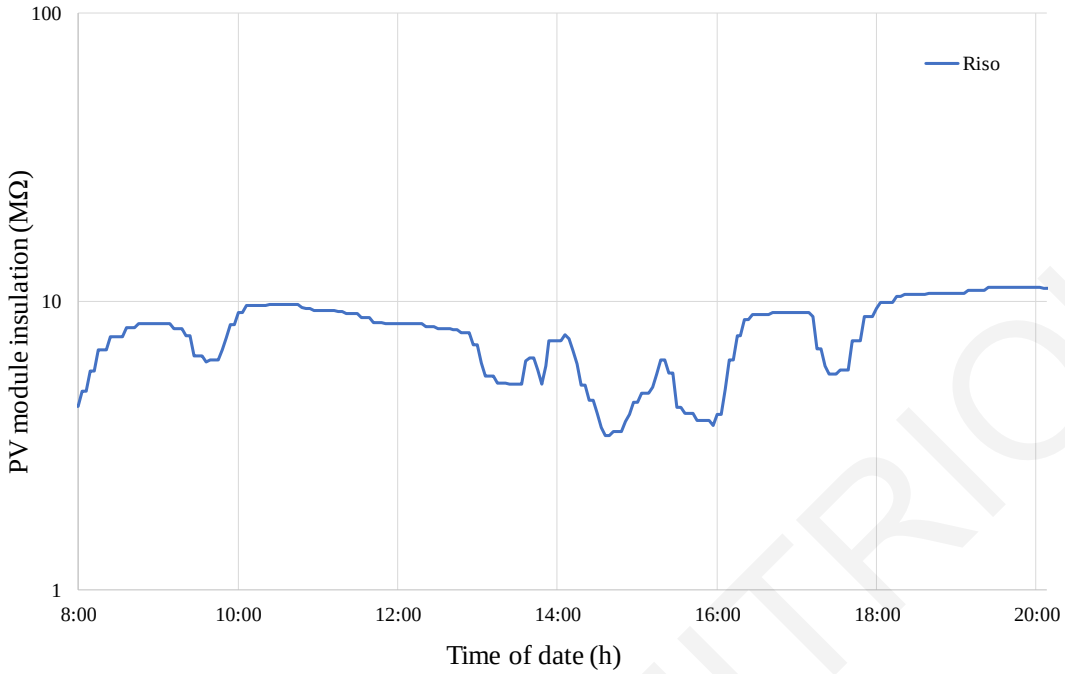

Figure 5-17: Insulation resistance R_{iso_m} of PV modules during a spring day

A series of simulations are executed regarding the operational hours (8:06 to 19:18) of the PV plant. The 3D-plot in Figure 5-18 presents the dynamic PV interference along the length of the pipeline system in terms of the pipe-to-soil potential (PSP) during the examined period. As in the case study of the winter day, the PV interference is correlated to the operational current. Therefore, in this case study several peaks propagate along the time axis as a consequence of the multiple fluctuations of the operational current. Indicatively, Figure 5-19 exhibits the captured PV interference values along the length of the pipeline for specific time snapshots, beginning at 8:09, followed by 9:00 and then every 1-hour interval.

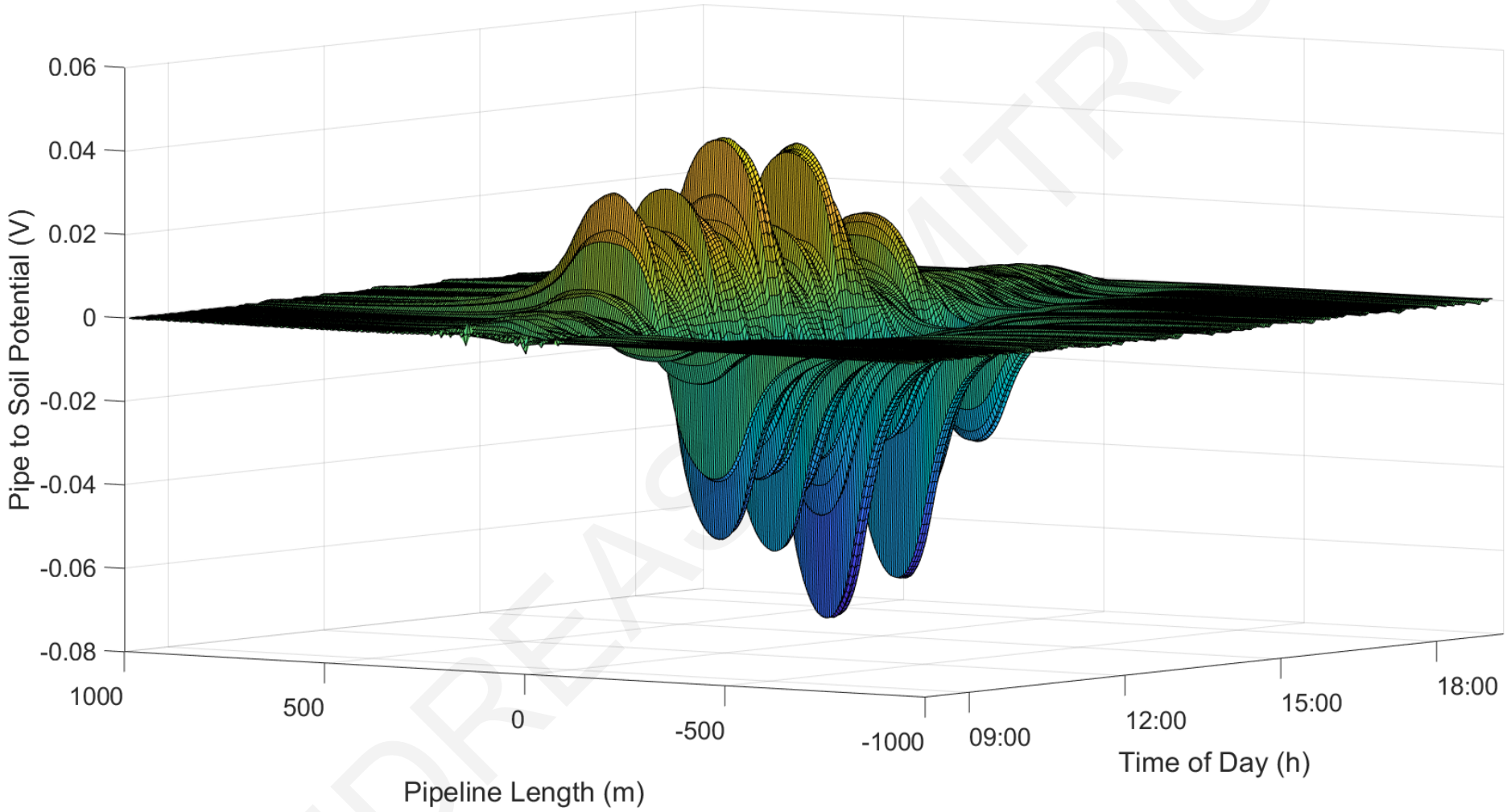

Figure 5-18: Dynamic PV interference on Pipeline System during a spring day

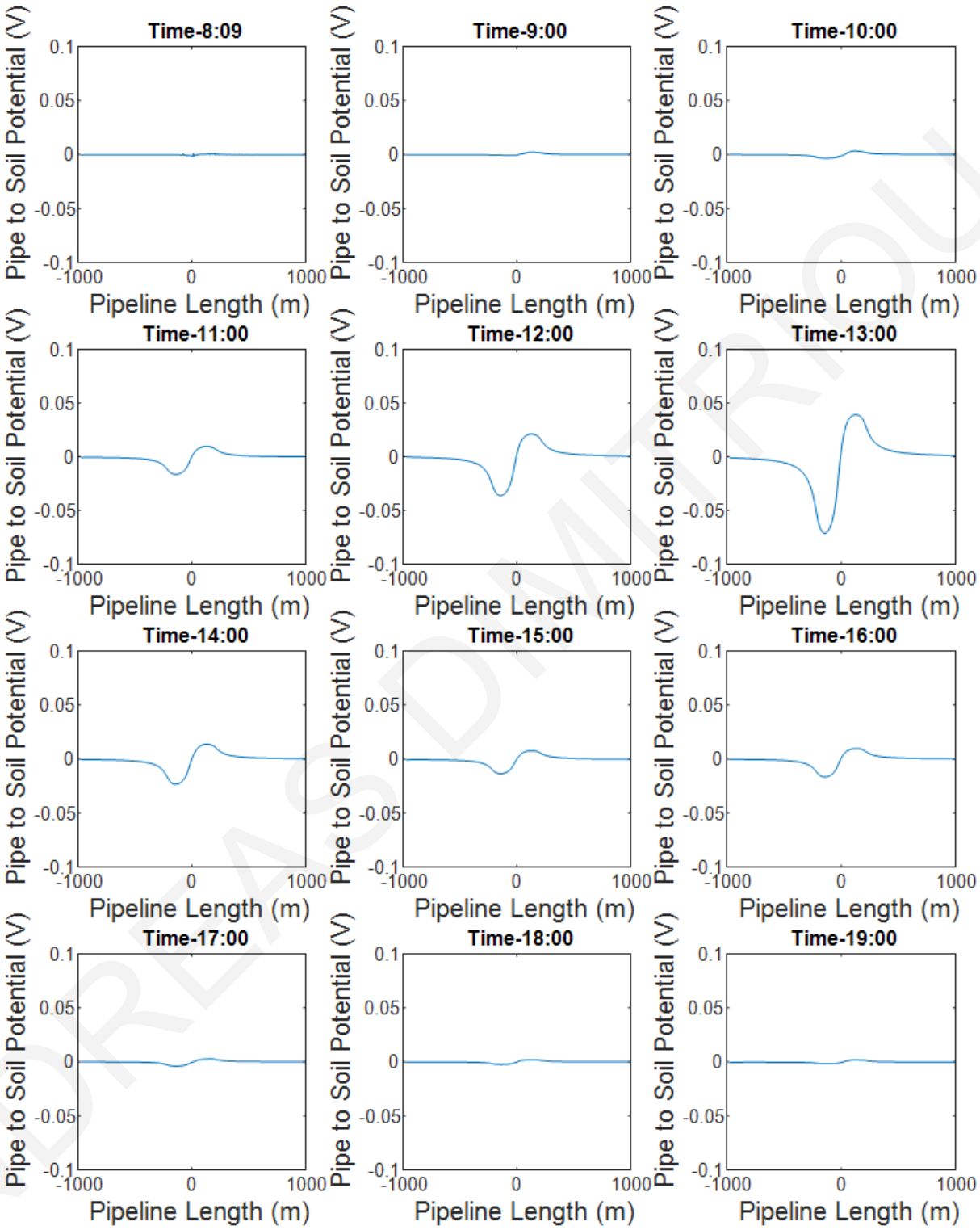

Figure 5-19: PV interference along the length of the pipeline at specific time snapshots during a spring day

The maximum PV interference values are captured at 12:57 where the PV plant operated at its maximum performance. The values of interference range between -72 mV to 41,5 mV. The most negative value (-72 mV) captured at the section of pipeline X=-144 m while the most positive value (41,5 mV) captured section X=123 m (see Fig. 5-20). It is worth mentioning that the position of local maximum and minimum remains almost in the same place as in the case of the winter day (see Fig. 5-10).

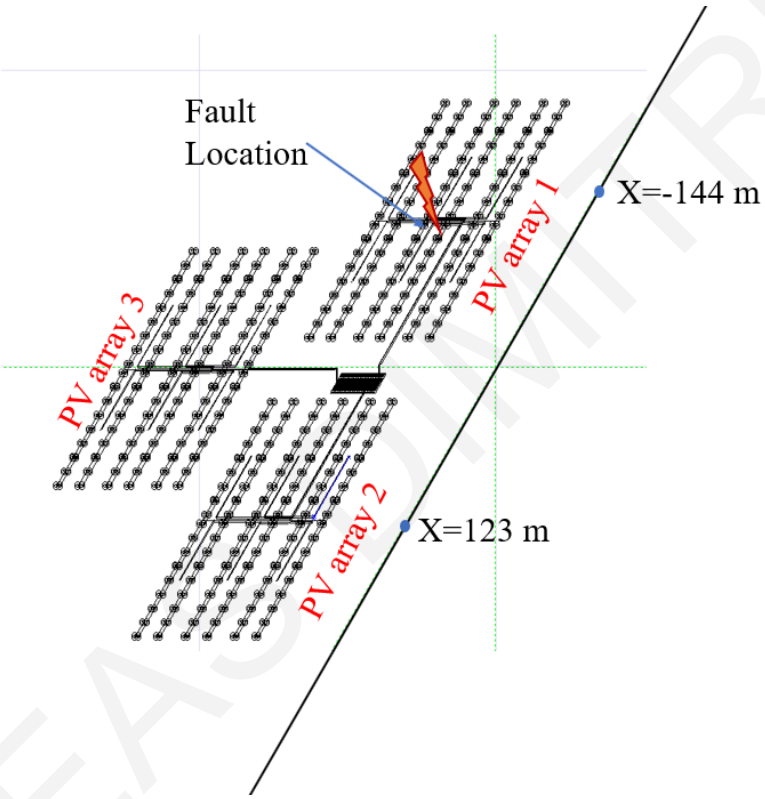

Figure 5-20: Illustration of the pipeline's section with maximum captured PV interference during a spring day

With reference to Figure 5-20, the time variation of PSP at sections X= -144 m and X=123 m of the pipeline is presented in Figures 5-21 and 5-22 respectively. The profile of the PV interference depends on the magnitude of the leakage current originated from PV modules and the leakage current at the faulted point. At the period between 9:30 and 16:30, the PV interference level is more influenced by the fault current as illustrated in both sections (X=-144 m and X=123). This is because the operational current is relatively high. Since the fault current magnitude is proportional to the operational current, the captured PV interference profile follows the operational current profile.

During the periods 8:06-9:30 and 16:30-19:18, where the operational current is very low, the PV interference is dominated by the leakage current originated from the PV modules. Especially at times 8:21, 8:39, 8:54 and 9:24, the polarity of the PV interference is inversed. This is because the fault current magnitude is almost zero and the PV interference is dominated by the leakage currents of PV modules.

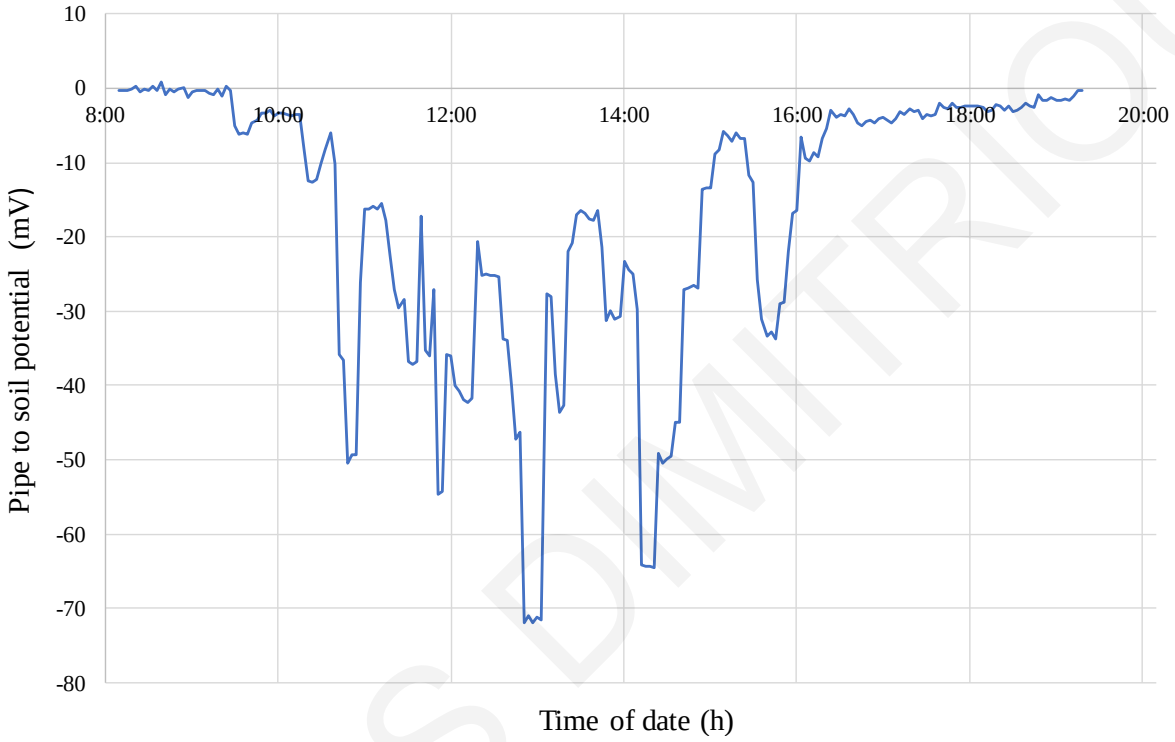

Figure 5-21: Dynamic Interference at Section X= -144 m of the pipeline system during a spring day

With reference to Figure 5-13, the cumulative leakage current I_R which returns via the grounded point of the negative current currying conductor for the modelled arrays is illustrated in Figure 5-23. At the healthy arrays (2 & 3), the cumulative leakage current I_R has a positive polarity since the current is flowing into the grounded conductor. This leakage is exclusively originated from the PV modules and has a low magnitude, ranging between 20-120 mA.

The I_R for array 1 has positive polarity at the period (8:06-9:30) because during this period, the leakage current of PV modules is higher than the leakage current of the faulted point. After 9:30 as the operating current increases, the leakage current from faulted point increases proportionally, resulting in a negative polarity of I_R. In extension, the I_R follows the time-variations of operational current.

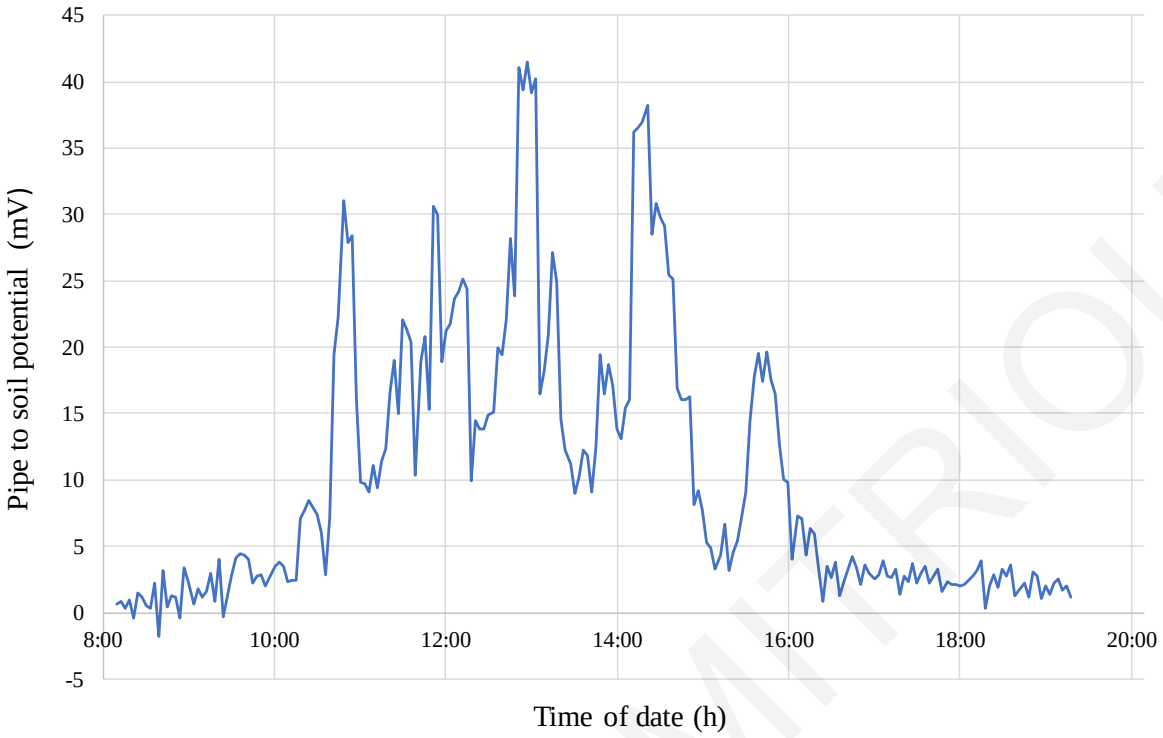

Figure 5-22: Dynamic Interference at Section X=123 m of the pipeline system during a spring day

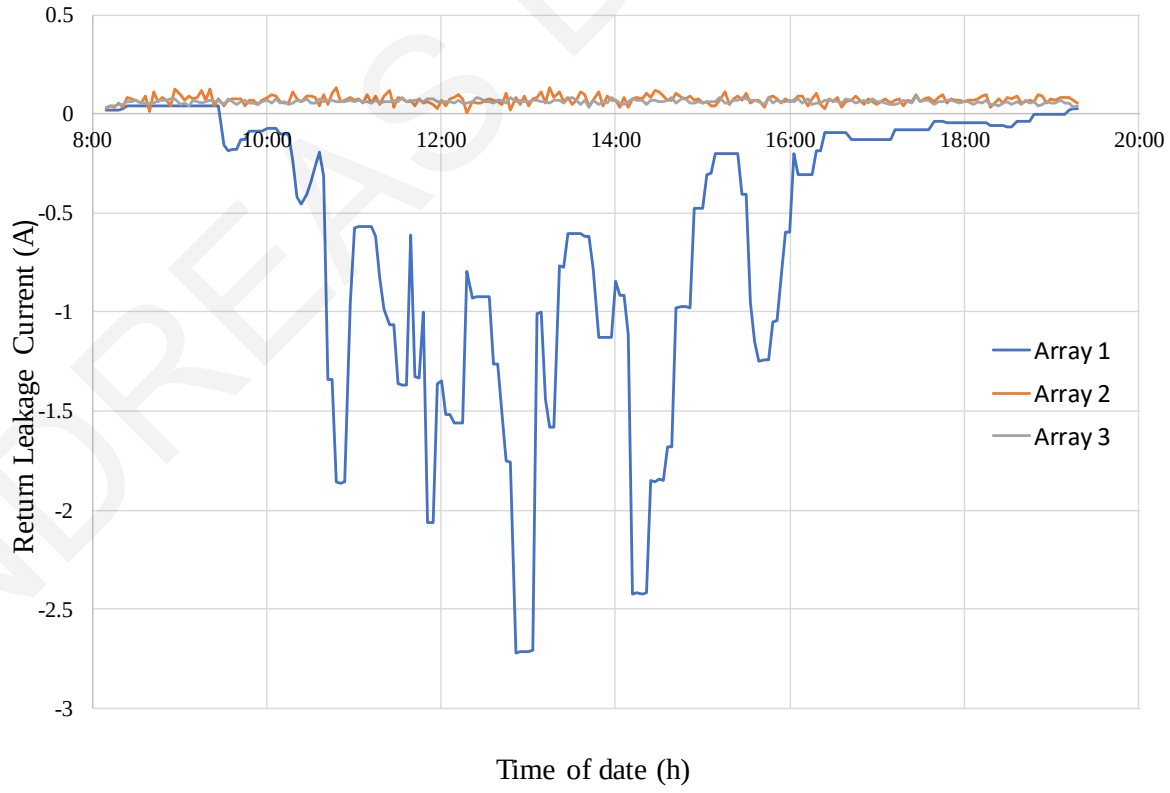

Figure 5-23: Return Leakage Current to the grounded point during a spring day

The cumulative leakage activity is adjusted by the leakage current of the PV modules and the fault current. However, the PV interference depends on the leakage current magnitude

as well as on the points where the current is leaking into the earth. More explicitly, the PV interference is determined by the location of the leakage currents which are transformed in stray currents and circulating through the grounded conductor. The above conclusion is verified through the captured PV interference presented at 9:24 and 12:54 (see Fig. 5-24). At 9:24, the PV interference is more influenced by the leakage currents of the PV modules, while at 12:54 PV interference is more influenced by the current leaking at the fault. This is reflected by the difference in their magnitude and profile (Fig. 5-24).

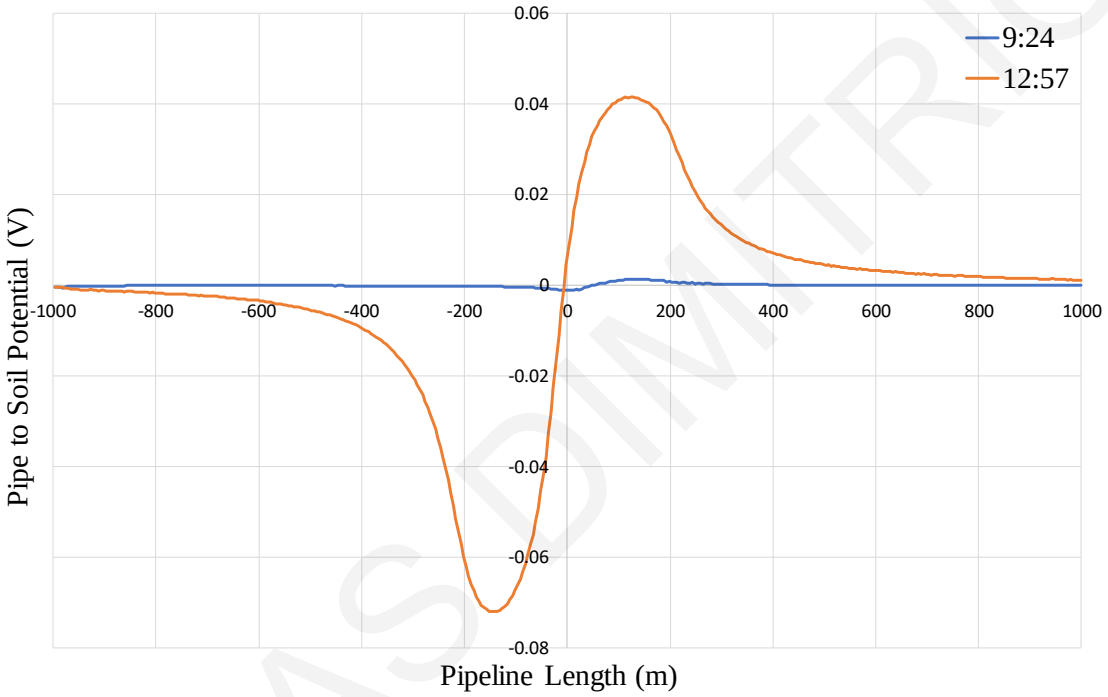

Figure 5-24: PV interference along the length of the pipeline at specific times during a spring day

5.4 Identification and measurement of PV stray current interference on pipeline systems

The dynamic simulations described above have provided very important conclusions as well as useful insights that can be appropriately used in the identification and measurement procedures that regard PV interference on pipeline systems. In particular, dynamic modelling has revealed the local/static nature of PV interference. This characteristic entails difficulties in identifying PV interference when solely relying on the measurement procedures - currently prescribed in International Standards for stray current corrosion assessments [7], [11].More specifically, DC traction systems are the most common type of power system which induce DC stray current. To this extent, the developed measuring procedures [1], [2], [7] of DC interference on third-party infrastructures are more applicable to this type of power system.

In the following paragraphs, is highlighted the need for measuring the DC interference on the pipeline systems using current probes. The profile of PV interference is compared with the profile DC interference originated from traction systems and its explicit characteristics are highlighted. PV interference exhibits a special timestamp which is correlated with the static nature of the PV leakage current activity. Moreover, based on the explicit characteristics of PV interference, guidelines are provided for the measurement of PV interference on buried pipelines located in the vicinity of PV systems.

5.4.1 Identifying DC stray current interference on pipeline systems

In general, if a buried infrastructure is extended in an area where there is DC stray current activity, then standardized measurements are performed in order to identify the interference level and to evaluate the corrosion risk. The measurements are based on the current, or on the voltage potential variations that occur within the soil and the interfered structure due to the presence of stray currents. More specifically, the standard EN 50162 [7] specifies four principal ways to identify stray current interference by performing one or more of the following measurements:

1. Structure to electrolyte potential fluctuations
2. Deviations from normal structure to electrolyte potentials
3. Voltage gradients in the electrolyte
4. Line currents in pipeline probes

In essence, the above specialized techniques have been introduced for the measurement of DC interference on buried pipeline systems [7], [11]. However, since modern buried pipeline systems benefit from both high insulation coatings and cathodic protection - to control corrosion [10], [11], [80], the majority of these techniques can be deemed ineffective [24], [80]. To this extent, the predominant technique for identifying the DC stray current interference is through the use of current probes which are connected to the structure under investigation. In particular, current probes can simulate the corrosion activity of coating holidays [7], [24].

Coating holidays allow the bare metallic surface to electrochemically react with the soil (i.e. electrolyte). In the absence of any external DC sources, the corrosion rate is relatively low because is limited by natural corrosion reactions [9], [10]. On the contrary, in the presence of external DC sources, stray currents may cause acceleration of the corrosion rate. Although the holiday surface is extremely small, any anodic current can cause severe damage to the

pipeline because the metal loss is restricted locally. This type of corrosion in which small volumes of metal are removed by corrosion is called "pitting" corrosion [10], due to the pits created on the surface of the pipeline's metallic wall at coating holidays spots. Consequently, pitting is considered as one of the most aggressive types of corrosion because even a small amount of metal is corroded, perforations can lead to costly repair of expensive equipment. In all cases, the perforation of the metallic wall is unacceptable because it will be followed by leakage of the transmitted elements (e.g. oil, gas).

At this point, it is worth mentioning that, a new ISO standard [24] recommends the use of probes and specifies their requirements for the measurement of DC interference. However, the existing testing-methodology [7] has been largely developed to assess DC interference resulting from traction systems. Moreover, the simulation results of Section 5.3 unveil the unique characteristics of PV interference's profile along the length of a nearby buried pipeline system which exhibits significant differences in comparison to the DC interference due to the operation of traction systems. Bearing in mind these unique characteristics, a testing-methodology for the measurement of PV interference in field-conditions is drawn in the following subsection.

5.4.2 PV Interference Vs DC Traction Interference

The main differences between DC traction systems and PV plants regarding the emitted DC interference on pipeline systems are summarized in Table 5-2.

Table 5-2: Differences of DC Interference from DC Traction Systems and PV Plants

DC interference profile	DC Traction Systems	PV Plants
Stray Current Source	Mobile	Static
Area of interference	Multiple locations along railway's parallel routing	Certain locations near PV plant
Time variations	Rapid fluctuations	Smooth alterations
Distribution along pipeline parallel segments	Uniformity of measured DC interference	Diversity of measured DC interference with local maximums and minimums.

In the case of DC traction systems, the interference source (i.e. train) moves along the metallic running rails (see Fig. 5-25). Also, the rails are used as the return current path. Since the rails are not perfectly insulated from the earth, part of the current leaks into the soil. A nearby pipeline can establish a convenient corridor for the return current, picking up leakage current and drives it back to the substation. To this extent, DC interference issues can occur

in multiple locations along railway's parallel routing. Furthermore, there is uniformity on the measured interference on pipeline segments that are located in parallel to the traction railway while rapid fluctuations characterize the magnitude of interference [12], [83]. With reference to Figure 5-25, the interference on a pipeline segment located in parallel to a rail system is almost identical along the entire length of the segment. For example, the measured interference of M1 would be identical to M2 with a time delay caused by the movement of the interference source. This behaviour simplifies the measuring procedure because the DC interference can be examined by measuring a single point of the parallel pipeline segment under investigation.

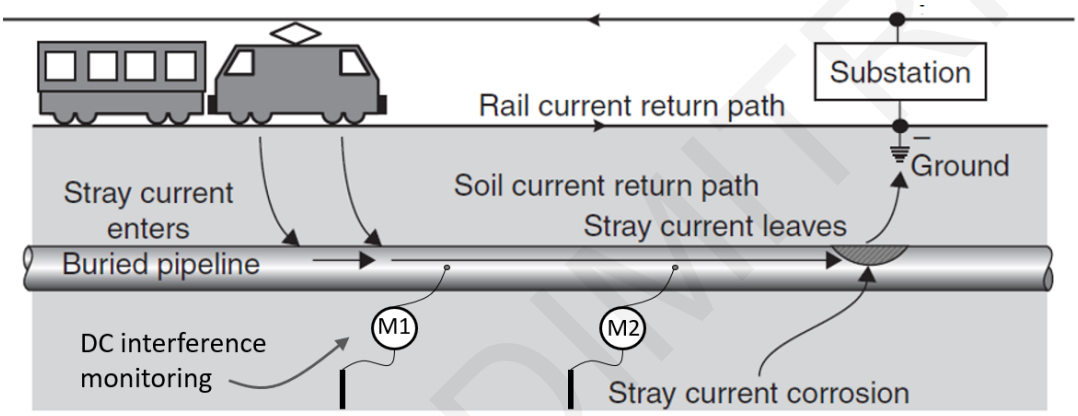

Figure 5-25: Stray current interference on pipeline system due to DC operated railways [10]

In contrast, when considering PV plants, the interference on a pipeline system is restricted to very narrow sections near the PV plant. For example, at measuring points M1 & M2 (see Fig. 5-26) which are located in close proximity to the PV plant, a higher interference level is expected in comparison to the measuring point M3. Since M3 is relatively away from the PV plant, the interference level will be attenuated dramatically.

However, the most significant characteristic of the PV interference is the diversity that is exhibited along the length of the pipeline's segment located in proximity to the PV plant. Although the interference level of M1 and M2 would be relatively high, their profiles may exhibit opposite signs. As illustrated in the case studies of an earthed PV system operated under blind spot fault (see Sec. 5.3), the PV interference may exhibit local maximums and minimums along the length of the interfered segment. Moreover, the PV interference exhibits smoother time-variations which are correlated with the operational levels as well as environmental factors. However, in the time-domain, the measured PV interference at different points of the pipeline follows a similar timestamp which is correlated with the leakage current activity.

Taking into account the unique characteristics of the PV interference it is recommended that the measurement of the PV interference should take place at multiple points along the pipeline's segment - located in proximity to PV plant - in order to definitely identify it.

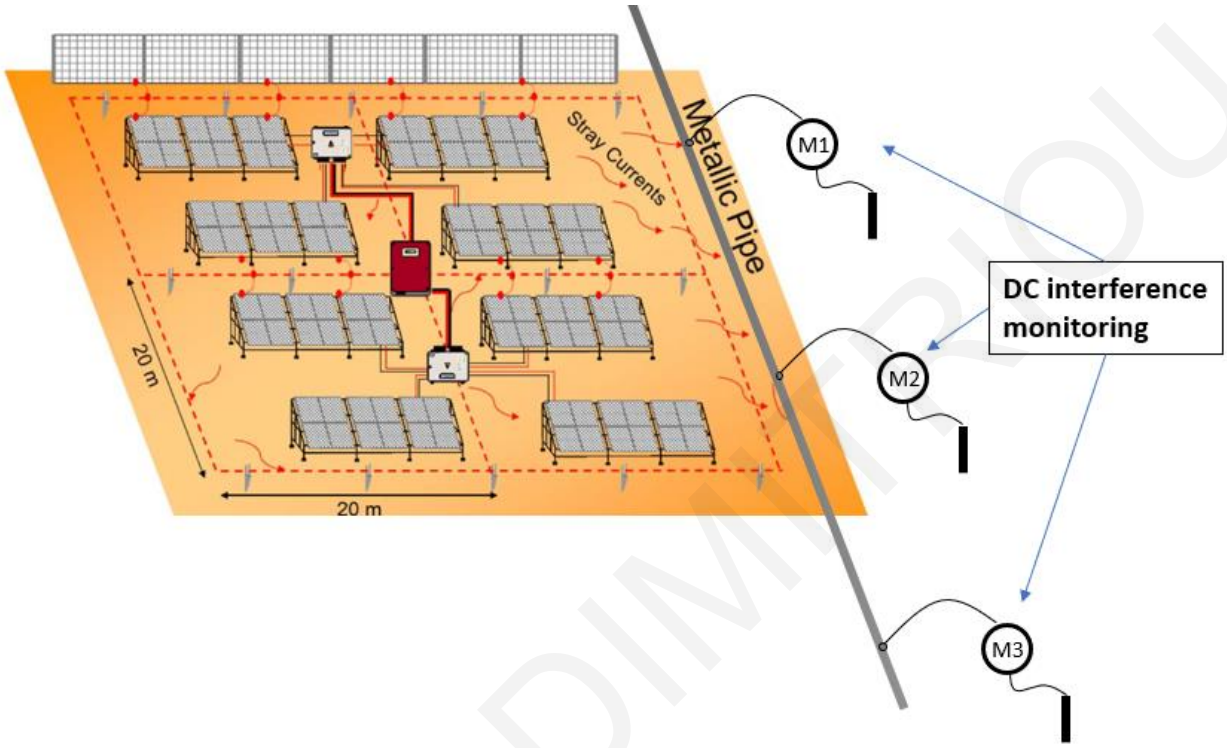

Figure 5-26: Stray current interference on pipeline system due to PV plant operation

5.4.3 Guidelines for PV Interference measurement on a nearby pipeline system

The diversity associated with PV interference necessitates the installation of testing probes on multiple points along the length of an interfered pipeline segment. By applying testing probes on the pipeline system, the expected current flow through potential coating holidays/defects can be measured. At this point, it should be recalled that, although the pipeline is well coated, any anodic current flow through coating holidays results in acceleration of corrosion rate.

The testing set-up is illustrated in Figure 5-27. An insulated probe with a bare pointed edge is pushed into the soil at the depth of the pipeline. As the probe is electrically connected with the pipeline's metallic wall, the bare end of the probe acts as a coating defect where the stray current can be inserted/exerted to the pipeline. An amperemeter records the magnitude and direction of the current for the examined time interval.

As highlighted from the simulations results of Section 5.3, the PV interference has a dynamic profile. In such cases, where the interference level exhibits time-variations, the standard

practice [7] suggests the monitoring of the interference level for an interval where maximum and minimum levels are expected. Consequently, the measuring time interval should include the period where the PV plant is in-operation and the period where the interference source is out-of-operation, in order to define the reference level. Especially if the pipeline benefits by a cathodic protection system, the cathodic current will be captured as a stable DC component which is superimposed on the measured value [7], [24]. To this extent, the magnitude of the DC component can be specified when the PV plant is out-of-operation.

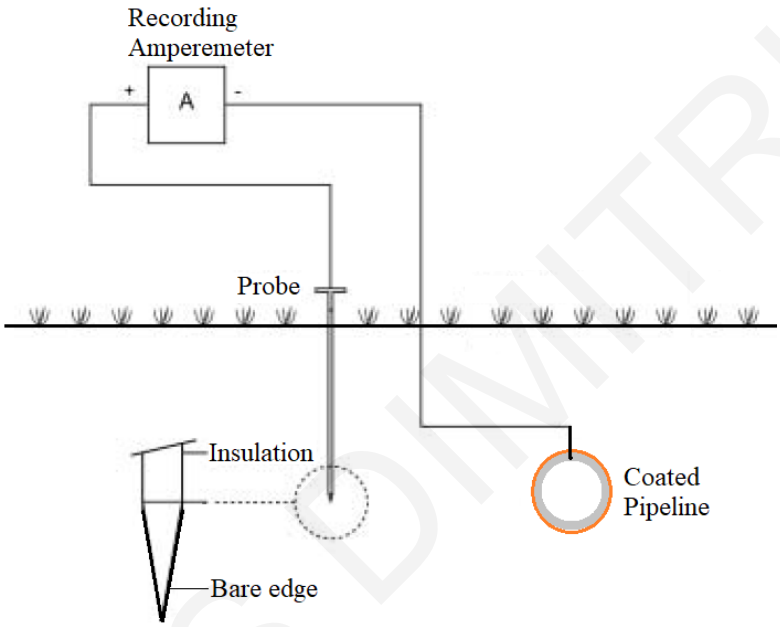

Figure 5-27: Measuring method for DC stray interference

A correlation between the operational level of PV plant and the recorded data can reveal whether the measured interference on a pipeline system is originated from a PV plant. Depending on the recorded data, the corrosion risk is evaluated. Annex D of [7] provides a general procedure for evaluation of time-varying stray current interference using current probes. However, the evaluation procedure is mostly applicable to interference due to DC traction systems since is based on a long-term practical experience extracted from the DC traction area. Therefore, there is an emerging need for a dedicated procedure to evaluate corrosion risk due to PV interference. A preliminary step would be a qualitative corrosion risk evaluation by applying Faraday's electrolytic law.

5.4.4 Corrosion Risk evaluation of PV Interference

By applying Faraday's electrolytic law, it is possible to calculate the metal loss that can be consumed in an anodic reaction should the anodic current is known [9], [10]. To this extent, the current density of coating defects is one of the key parameters used to evaluate the corrosion rate in coated pipeline systems.

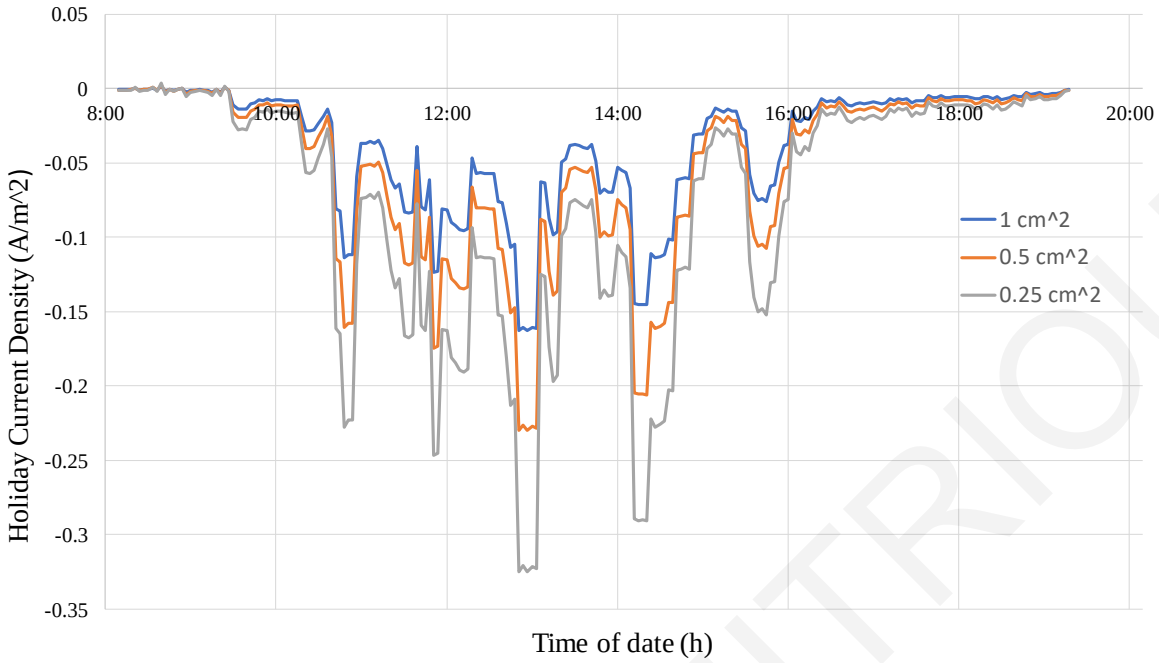

Figure 5-28: Current density through coating holidays

By means of an example, the expected current density of a holiday is calculated regarding the case study of a spring day considered in Section 5.3. The holiday current density can be calculated as the ratio between the pipe to soil potential with the product of the holiday resistance by the holiday base area (see Eq. 3-3). Figure 5-28 presents the expected holiday current density of the section X=135 m based on the simulated pipe to soil potential variations (see Fig. 5-22) under different holiday sizes. As shown in the figure, the current density increases as the holiday size decreases. It should be mentioned that this methodology actually reproduces the equivalent current that would have been recorded using current probes equal to that of the coating holidays surface.

By integrating the current density for the examined period (Time 8:06-19:18) and applying Faraday's electrolytic law the thickness of corroded metal is calculated. The thickness of corroded metal for the 3 sizes of coating holidays considered above are presented in Table 5-3.

According to [3], the corrosion rate should be lower than 10 μm per year. Corrosion rate below this value is considered sufficiently low, thus ensuring that during the design lifetime of the infrastructure, no significant damage will occur. Since the corresponding daily threshold is 27 nm the values presented in Tab. 5-3 can certainly arise corrosion issues. In such a case, the installation of cathodic protection systems is recommended to avoid any detrimental corrosion issues. The cathodic protection system supplies the coating holidays

with a cathodic current (which has an opposite direction to anodic current) in order to suppress the corrosion activity.

In conclusion, the above procedure can be used in combination with the recommended measuring tests (see Sec. 5.4.3) for the evaluation of corrosion risk on pipeline systems located in proximity to PV plants. Based on the evaluation, the design of an appropriate cathodic protection system may be required.

Table 5-3: Thickness of Corroded Metal Vs Holiday Size

Coating Holiday Size (cm^2)	**Coating Holiday Resistance* (kΩ)**	**Thickness of corroded metal (nm/day)**	**Allowable Threshold (nm/day) [3]**
1	4,43	61	27
0,5	6,26	86,3	27
0,25	8,86	122	27
*Coating Holiday Resistance= ρ/4r [7] where, ρ : soil resistivity value (100 Ω.m for the specific case study) r : is the radius of coating holiday			

Chapter 6

Conclusion

6.1 General Remarks

Stakeholders across the world undertake significant research efforts to investigate the effects of DC stray currents from various power systems. This thesis is posing an unexplored source of DC interference originated from PV systems. The findings of this research work could be considered by critical infrastructure's operators and the Photovoltaic (PV) installation industry since PV interference may undermine the integrity of these installations. From a management's point of view, the corrosiveness due to PV interference can cause undesirable situations related to financial losses, disruption of services, environmental contamination and hazards to human life. To this extent, the targeted approach of PV interference issue described in this thesis aims to preserve the integrity of critical infrastructures located in proximity to PV plants for a long-term and harmonious coexistence.

6.2 Review of the Work Described

The research activities included in this thesis expose the issue of potential corrosion problems on critical infrastructures due to the interference induced by the PV plants' operation. A targeted examination to address the problem of PV interference is provided, by analyzing the electrical mechanism that triggers the interference, followed by the modelling and simulation of the problem and finally proposing a tailored methodology for PV interference's field-measurement.

In Chapter 2, the PV interference mechanism on third-party infrastructures has been conceptually illustrated, by providing explicit insights of DC leakage current activity under normal/fault conditions. The PV interference patterns have been demonstrated, regarding the applicable PV earthing configurations. Furthermore, the PV interference has been electrically elucidated as a result of the formation of DC stray currents by considering the topology of the PV system's components in a spatial arrangement. The hidden aspects which generate the corrosive stray currents have been revealed through an extended examination of:

a) the operational conditions of electrical equipment incorporated in PV systems,
b) the PV earthing configurations and
c) the fault detection schemes.

Leakage currents from PV systems cannot be avoided since it is an inevitable consequence of their operation principles and the finite insulation properties of their energized components. As presented, the magnitude of PV leakage currents may vary considerably

within a day/seasonal period. To this extent, the fault detection mechanisms are adjusted in relatively high threshold-levels in order to avoid the unwanted trips of PV inverters under high leakage activity. At this point, it should be mentioned that the magnitude of the maximum allowable leakage currents based on criteria related to fire and personnel safety issues. However, this practice may lead to the presence of undetected ground faults and by extension, in an increase of the leakage current activity. This comes as a result of the weakness of currently adopted fault detection schemes, which supervise the dynamic PV leakage current with a fix threshold-level.

The in-take of products that include more sensitive ground fault detection mechanisms with an adjustable-smart threshold level based on the environmental and the operational conditions of PV plants can eliminate this weakness. The threshold levels of fault detection devices can be revised, considering the indicated corrosion issues. Moreover, specialized audits at regular intervals can be performed for the detection and the treatment of the undetected ground faults. In cases where the level of stray current cannot be controlled to acceptable levels, measurement and monitoring of the third-party assets may be required, with mitigation applied to the affected structure if required.

In Chapters 3 and 4 the formulation of appropriate simulation models to further elaborate on the theory that describes the prevailing electrical characteristics of PV systems' under normal and faulty operation, that lead to interference and corrosion concerns on underground critical infrastructure have been discussed. Chapter 3 focused on Earthed PV systems while Chapter 4 focused on Floating isolated PV systems. The modelling techniques that have been developed have reproduced the expected stray currents in a commercially available software platform. Using this software, the electrical circuit behaviour of the PV systems with respect to the DC leakage current (under normal and fault conditions) was transferred in an object-based graphical environment that is able to examine the PV interference of pipeline systems in a topologically accurate representation. By applying these techniques on realistic case studies, the PV interference on buried pipeline systems was expressed in terms of spatial pipe-to-soil potential. Moreover, an in-depth understanding of the PV interference has been facilitated through the execution of multiple simulation models, comprising different design principles. The critical parameters which affect the problem of PV interference have been disclosed. The magnitude of the stray current is affected by the insulation level of PV array's components (i.e. PV modules, cables) and their operational current and voltage. The formation of PV stray currents within the soil strongly depends on the earthing configuration,

the soil resistivity value and the presence of metallic elements extended into the soil (i.e. PV modules supporting infrastructure, earthing grids, etc.). As a consequence of the PV stray current activity, the PV interference occurring on third party infrastructure is affected by its relative position respect to the PV plant. It was also proved that in the occurrence of undetected ground faults (in earthed PV systems) the PV interference level is increased by several orders of magnitude.

To this end, the modelling endeavours are an essential step towards assessing the impact of accelerated DC corrosion on critical infrastructures, such as natural gas pipelines that are operated near large-scale PV plants. The proper coordination between a PV plant and an interfered system (i.e. pipeline system) is critical for the harmonic and long-term coexistence of both systems. The involved entities (i.e. owners, operators) are encouraged to cooperate by exchange information regarding the operational principles (i.e. effective insulation level, permanent leakage activity, etc.) of their systems, cathodic protection system, buried metallic infrastructure and other critical data that may affect the PV interference [7]. The developed modelling techniques can be utilized during the design stage for the erection of a new pipeline system near PV plants or vice versa for the calculation of a minimum separation distance and the evaluation of mitigation measures for the reduction of PV interference's effects. By performing a set of simulations scenarios under steady-state and fault conditions, the PV interference can be evaluated as per its corrosiveness. Depending on the results, it may be appropriate to apply mitigation measures and modifications on both interfering and interfered source. After the commissioning of the system, field measurements can be performed to evaluate the effectiveness of mitigation measures and also complimentary periodic measurements during the design lifetime of the system.

However, the PV interference profile exhibits unique characteristics which entail difficulties in identifying PV interference when solely relying on the field measurement procedures - currently prescribed in International Standards for stray current corrosion assessments. Since the magnitude of PV interference is influenced by various parameters that rely on the PV systems' operational characteristics as well as on weather and environmental conditions, dynamic simulations are presented in Chapter 5 in an attempt to fully visualize the time-dependent PV interference on pipeline systems. The unique characteristics of the PV interference are highlighted and are compared with the most common types of DC interference systems having as an ultimate objective the composition of an appropriate methodology for measuring PV interference in field conditions. To this end, guidelines for

the identification and measurement of the PV interference on pipeline systems are provided. The proposed dynamic simulation techniques of PV interference can be used complementary to the measuring procedures for:

1. The calculation of PV interference at pipeline sections where field-test measurements can not be executed. Since the installation of test posts in close intervals along the pipeline is not practically feasible, the examination of PV interference at sections which they are not benefitted with test-post can be examined using a simulation model.

2. The execution of sensitivity analysis scenarios regarding the critical parameters affecting PV interference. Soil resistivity, PV array's insulation resistance, operational current and voltage of PV modules are the most critical parameters which affect the level of PV interference. However, these parameters can vary on a daily or seasonal basis. To this extent, the utilization of simulation models can be used to examine PV interference under variable conditions avoiding the costly field-test measurements.

3. To evaluate the PV interference due to the occurrence of undetected ground faults or degradation of the PV system's insulation resistance. The natural degradation of insulation materials or the occurrence of undetected ground faults can increase the magnitude of leakage currents and by extension the interference level. These conditions can be integrated in simulation models to examine the associated interference level.

6.3 Message to the relevant stakeholder

The DC stray current interference from DC power systems (i.e. DC traction systems, HVDC systems) can generate corrosion issues on third-party infrastructures. Corrosion may cause, reduction of the expected service-life of infrastructure, equipment failures, costly interruptions, environmental pollution as well as life hazards. The recognition of the impact of DC stray current corrosion has forced stakeholders across the world to consider a variety of design specifications, codes of practice and international standards to ensure DC stray current interference is minimised. Such codes and standards are intended to provide designers and utility companies with a corrosion management strategy that defines a level of corrosion risk which is acceptable across infrastructures. Moreover, the legal framework of several countries has strict restrictions on the erection of a new large-scale infrastructure

that may endanger interference problems which can cause malfunctions, safety issues, or undermine the integrity of other infrastructures located in proximity. To this extent, compliance with the adopted code of practice and standards should be fulfilled in order to avoid catastrophic situations.

To this extent, the development of documentation or services for corrosion management assessment and mitigation practices will very soon become obvious for critical infrastructure operators and the Photovoltaic (PV) installation industry. One should note that a typical useful life-cycle of commercial PV systems is around 25 years. Thus, system designers and contractors should ensure a similar life-cycle for the grounding and supporting infrastructure of PV systems and at the same provide evidence that reasonable efforts are made to prevent damage to third-party utility services in areas near the PV plants.

We argue that the consequences of PV interference should promote the revision of existing standards related to the topics presented in Table 6-1.

Table 6-1: Revision of Existing Standards

Revised Topics	Relevant Standard
Protection against corrosion by stray currents from DC systems: PV systems should be included as a potential source of DC interference	ISO 21857 [25] EN 50162 [7]
DC stray current interference measurement: The proposed methodology (see Sec. 5.4) can be adopted for the measurement of PV interference.	EN 13509 [11] ISO 22426 [24]
Fault Detection Devices of PV Plants: The threshold levels of fault detection devices should be updated considering the interfering corrosion issues.	EN 62109-2 [4] UL 1741 [21] IEC 62548 [17]
Cathodic Protection of buried metallic structures: The unique characteristics of PV interference should be considered in the design of an efficient cathodic protection system.	EN 12954 [3] ISO 15589-1 [84]

Finally, part of the research described in this thesis has been normatively and informatively included in the new ISO 21857 [25] standard "*Petroleum, petrochemical and natural gas industries — Prevention of corrosion on pipeline systems influenced by stray currents*". This poses a major achievement of the research efforts described in this thesis. It should be noted that it is the first time that the impact of PV interference on pipeline systems is addressed in technical standards.

6.4 Future Work

This thesis has described the research efforts performed to highlight the corrosive stray current interference due to the operation of PV plants. Having explored and discussed the core research aspects in this thesis, it is suggested that future work can have a significant benefit on the following topics. These points are summarized below:

- **Step 1: Examination of PV interference on Energy Efficient Buildings**
  Examination of PV interference should be carried out on energy-efficient buildings that benefit from Building-Applied Photovoltaic Systems (BAPVs) and Building-Integrated Photovoltaic systems (BIPVs). The impact of accelerated DC corrosion on the envelope and reinforcement should be studied since it may undermine the integrity of structural buildings.
- **Step 2: Development of Modelling Techniques to address PV Interference from Floating Non-Isolated PV Systems**
  Modelling techniques regarding Floating non-isolated PV systems are subject of a future work which presupposes the modelling of the interaction between AC and DC side as controlled by PV inverters. The operation of the transformerless inverter under the presence of leakage currents has a wide field of research due to several circuit topologies, electronic components, and modulation techniques. Since most of the PV systems integrated into energy-efficient buildings use transformerless inverters (i.e. Floating non-isolated systems), this task comes as complementary to the work of step 1.
- **Step 4: Mitigation measures of PV interference**
  Mitigation measures to address the impact of PV interference should be proposed in order to avoid potential corrosion issues. The reduction of PV interference can be firstly achieved by taking measures at PV plant's installations. The measures should aim to reduce the magnitude of the PV leakage currents which are subsequently evolved in stray currents. Moreover, practical techniques can be applied aiming to control the PV leakage current flow in an intended path (i.e. installing of return conductors). Besides, the PV interference can be moderated by applying measures suitable for the disintegration of conductive paths which generate circulating stray currents.

  As a second line of defense, if the stray current interference cannot be limited to an acceptable level, protection measures should also apply on the interfered structure,

taking into account the unique characteristics of PV interference. Generally, these measures may require the installation of cathodic protection devices, bonding of interfering and interfered structure, modifications on electrical continuity of interfered structure and increases the separation between interfering and interfered structure.

Appendix A-Electrochemical Corrosion and Faraday's electrolytic law

A.1 Electrochemical Corrosion

Generally, metallic corrosion is a destructive phenomenon that appears on metallic elements having, as a result, the degradation of metal's properties. It is frequently observed as a rush on the metals external surface. The driving force that causes metals to corrode is a natural consequence of their temporary existence in metallic form. To reach this metallic state from their occurrence in nature in the form of various chemical compounds (ores), it is necessary for them to absorb and store up for later return by corrosion, the energy required to release the metals from their original compounds [10]. To this extent, metals are tending to revert back to their original state as they were in nature through corrosion. This process is basically a chemical reaction that involves the development of corrosion products with an energy release. The mechanism of corrosion is very complicated depending on various aspects relative to the environmental conditions where the metal is placed [9], [10]. Within this section, a synoptic explanation of electrochemical corrosion will be done in order to facilitate the reader understanding of DC stray current corrosion.

Metals which are submerged within an electrolyte, they are almost always corroded through an electrochemical process. Electrochemical corrosion is a type of a chemical reaction that is characterized by the transfer of electrons. The reaction involves the release of ions to the environment and the movement of electrons within the metal. This type of corrosion comprises two interdependent procedures, an oxidation anodic corrosive procedure in combination with a cathodic reduction procedure [10].

Generally, the anodic reaction is described by Equation (A-1). In the anodic area, the reaction of metal M results in oxidation of the metal to an ion with valance charge of $n+$ and release of n electrons. The value of n depends on the nature of the metal element. Simultaneously, the generated electrons are consumed in the cathodic area. These electrons can serve to neutralize positive ions such as the hydrogen ions (H+), or create negative ions. The anodic and cathodic reactions are effectuated at the same time and at equivalent rates.

$$General\ anodic\ reaction\ equation: M \rightarrow M^{n+} + ne^{-} \qquad \text{(A-1)}$$

For example, the net reaction of an iron (Fe) element within an aqueous solution (see. Fig. A-1) involves two sub-reactions as described by the equations (A-2) and (A-3) respectively.

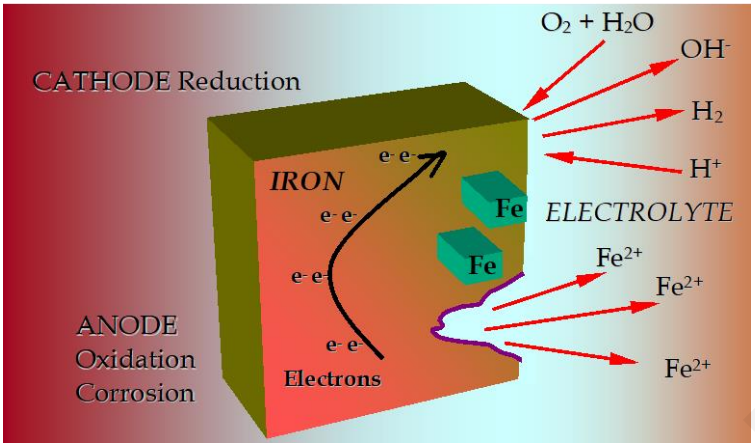

Figure A-1: Electrochemical reactions occurring during the Corrosion of Iron (Fe)

$$Anodic\ reaction: Fe \rightarrow Fe^{2+} + 2e^{-} \quad \text{(A-2)}$$

$$Cathodic\ reaction: 2H^{+} + 2e^{-} \rightarrow H_2 \quad \text{(A-3)}$$

At some point on the surface, iron element is transformed into iron ions (Fe^{2+}), according to Equation (A-2). The electrons ($2e^{-}$) released by this reaction are pass through the solid conducting metal to other sites of the metallic surface where hydrogen ions ($2H^{2+}$), are reduced to hydrogen gas (H_2) according to Equation (A-3). The combination of anodic and cathodic activity is basically the establishment of a galvanic cell that derives electrical energy. The electrons generated at the anode are consumed via the simultaneous reaction at the cathode surface. This migration of electrons through the metal is actually producing an electric current. Since the conventional current flow is opposite to the direction of electrons, the generated current flows from the cathodic area to the anodic area.

A.2 Faraday's electrolytic Law

By applying Faraday's electrolytic law, it can be feasible to calculate the metal loss that is consumed in an anodic reaction (see Eq. (A-1)) if the anodic current is known [9], [10]. Faraday's law correlates the current of an electrochemical reaction with the number of moles of the element being reacted and the number of moles of electrons which are participated in the reaction process.

In general, an anodic oxidation reaction that occurred on a metallic element produces metal oxides and releases electrons as shown in equation (A-1). According to Faraday's law, 1 mol of a specific metallic element would require m number of mol of electrons, or m times Avogardo's number of electrons ($m \times 6.022 \times 10^{23}$). The total charge included in 1 mol of electrons is known as 1 Faraday (F). Since the charge of an electron is 1.6×10^{-19} coulombs (C), the total electric charge in coulombs of a Faraday unit (F) equals to 96485 C/(mol of

electrons). Equation (A-4) originated from the combination of Faraday's principles with the specific electrochemical reaction of known stoichiometry. This equation correlates the electric charge Q with chemical descriptors *N* and *n*, where:

N: is the number of moles and ΔN the change in that amount and

n: is the number of electrons per molecule of the species being reacted.

$$Q = F * \Delta N * n \qquad \text{(A-4)}$$

With reference to equation (A-5), the value of total charge resulting from time integral of current *I* (in amperes) flowing in the duration *t* (in seconds) of the electrochemical process.

$$Q = \int_0^t I.dt \quad \text{(A-5)}$$

Using Faraday's law, the corrosion rate can be expressed in other useful quantities such as thickness and mass of corroded metal (see Table B-1) in the period of a year. These quantities are frequently used in industry as an index for assessing the risk of corrosion.

Table A-1
Faraday's Law Application Formulas

Description	Equation
Mass m of corroded metal per year	$m = (Q * M)/(n * F)$ (A-6)
Thickness t_m of corroded metal per year	$t_m = (Q * M)/(n * d * F * A)$ (A-7)
t_m: thickness of corroded metal per year in (m/y) *Q*: total charge in (C) *M*: atomic mass in (g/mol) *n*: number of electrons per molecule of the species being reacted *d*: mass density volume in (g/m^3) *F*: Faraday Unit=96485 C/(mol of electrons) *A*: Surface area of metal reacted (m^2) *m*: mass of corroded metal in (g)	

A.3 Application of Faraday's Law

Metallic pipelines are protected against corrosion using protective coating layers. However, the presence of coating holidays is inevitable. These coating holidays are occurred either during installation process either due to natural degradation of coating material. This case study provides the calculation process for the estimation of corrosion rate that can be occurred at pipeline's metallic wall due to the presence of a coating holidays if holiday current is known.

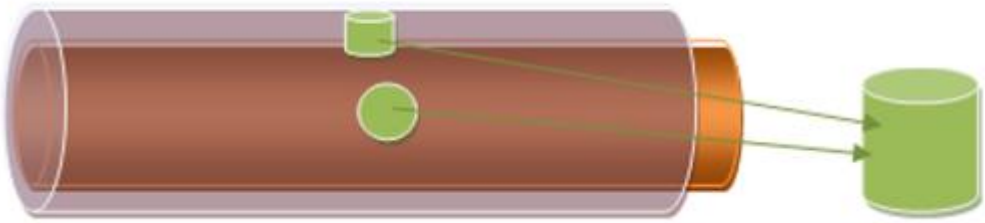

Figure A-2: Visualization of Coating Holiday

An underground steel pipeline that is buried in soil has a coating holiday with 1cm^2 surface (see Fig. A-2). If we assume that the average anodic holiday current is 45 μA, then using equations (A-6) & (A-7) the corrosion rate can be estimated in terms of metal mass loss and thickness of corroded metal. The calculations for year period are shown in table (B-2) below.

TABLE A-2
Calculation Results for Corrosion Rate

Variable	Symbol	Unit	Value	Comments
Average Anodic Current	I	A	4.51e-6	Current injected through holiday
Surface area of metal reacted	A	m^2	0.0001	Surface of coating holiday
Current Duration (for a year)	t	s	31536000	Period of a year
Total Charge	$Q = I * t$	C	1424104.577	Eq (B-2)
Atomic mass	M	g/mol	55.85	Atomic mass of steel
Mass density volume	d	g/m^3	7880000	Mass density of steel
Number of electrons per molecule reacted	n	-	2	Number of electrons released per molecule of steel
Faraday Unit	F	C/(mol of electrons)	96485	Constant
Mass of corroded metal (for a year)	m	g/year	0.0412	Eq (2-8)
Thickness of corroded metal (for a year)	t_m	m/year	5.23e-5	Eq (2-7)

Appendix B -Simulink PV model

An equivalent electric system (see Fig. B-1) to the PV system examined in Chapter 3 has been developed using the block diagram environment of the Simulink® software. In particular, the developed Simulink model reproduces the operation of a 288kWp PV plant connected in to the utility grid.

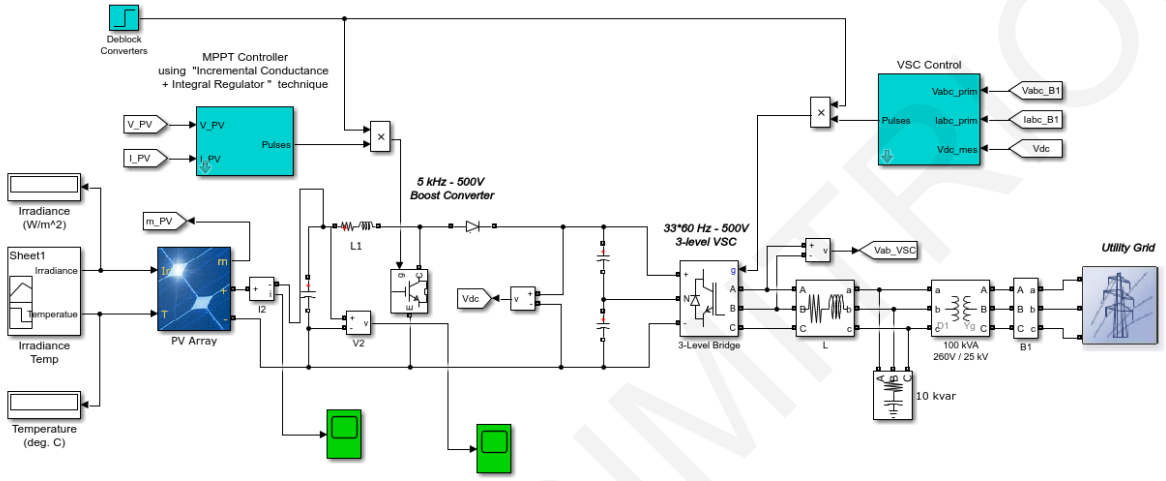

Figure B-1: Simulink PV model

The Simulink model is used to simulate the current and the voltage of PV modules considered in the system. By incorporating the PV array block, the recorded values of temperature and irradiance can be imported to reproduce the operation of PV modules (i.e. current, voltage). It should be noted that the PV array block takes into account the performance data of commercially available PV modules as given by National Renewable Energy Laboratory (NREL) providing accuracy and traceability to the simulation. Moreover, the PV Array block is a five parameter model using a current source IL (light-generated current), a diode (I0 and nI parameters), a series resistance Rs, and a shunt resistance Rsh to represent the irradiance- and temperature-dependent I-V characteristics of the modules (see Fig. B-2).

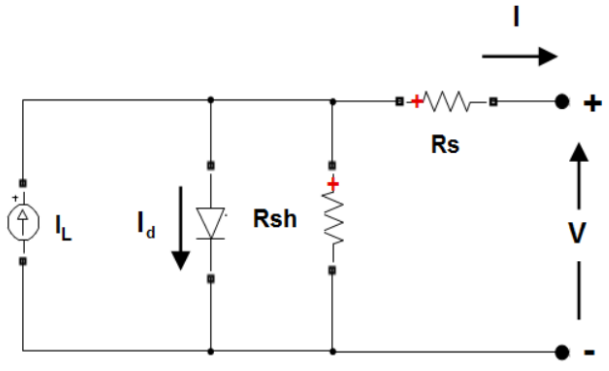

Figure B-2: PV module five-parameter model

The I-V characteristics of a single PV module are defined by the equations (B-1) and (B-2).

$$I_d = I_0[\exp\left(\frac{V_d}{V_t}\right) - 1] \qquad \text{(B-1)}$$

$$V_T = \frac{kT}{q} \times nI \times Ncell \qquad \text{(B-2)}$$

where:

- I_d - diode current (A)
- V_d - diode voltage (V)
- I_0 - diode saturation current (A)
- nI - diode ideality factor, a number close to 1.0
- k - Boltzman constant = 1.3806e-23 J.K-1
- q - electron charge = 1.6022e-19 C
- T - cell temperature (K)
- $Ncell$ - number of cells connected in series in a module

It should be mentioned that the maximum power point tracker adjusts the current and the voltage of the PV modules in order to operate under their maximum performance Pm (see Fig. B-3) depending on temperature and irradiance.

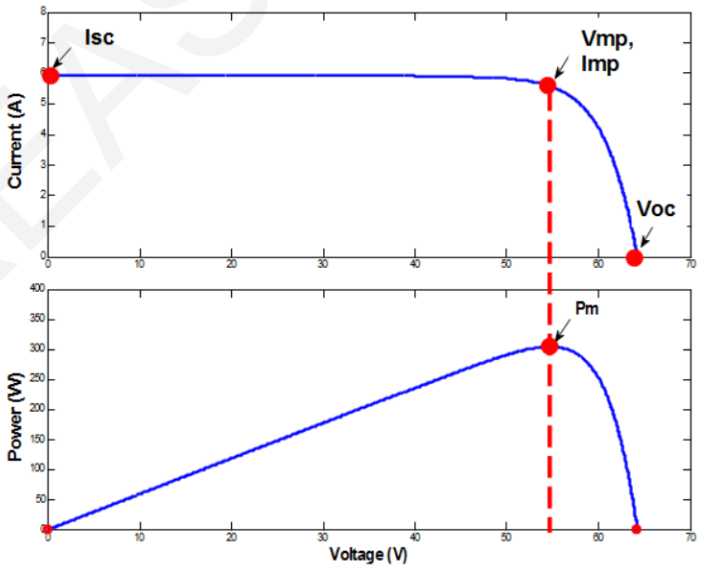

Figure B-3: PV module maximum power performance

Appendix C- Fundamentals of CDEGS Computational Methods

CDEGS (Current Distribution, Electromagnetic Fields, Grounding and Soil Structure Analysis) [79] is a powerful engineering tool designed to accurately analyse problems involving grounding/earthing, electromagnetic fields, electromagnetic interference including AC/DC interference mitigation studies and cathodic protection design. The software is produced by Safe Engineering Services & Technologies (SES), Montreal, Canada. The CDEGS software package consists of several independent modules designed to solve different problems.

The research efforts of this thesis involved the development of simulation models using the MALZ module of CDEGS to enable the DC interference on a nearby pipeline system, due to the operation of a PV plant. In the case of DC-conductive interference, when buried energised cables and grounding system leak currents into the earth, the soil potential is altered within the adjacent area. In extension, if a section of a buried pipeline running in proximity then the ground potential rise of pipeline's metallic wall, as well as the coating stress voltage of the protective coating are expected to be affected. The magnitude of the conductive interference decreases with increasing distance away from the faulted structure, while the rate of decrease of conductive interference is strongly soil structure-dependent.

The use of MALZ enables the development of networks of buried conductors which reproduce the desire energized cables, grounding systems and every other conductive element that influence DC interference. Since the current in the energised cables and grounding system does not distribute uniformly over all the conductors, when using MALZ/CDEGS it is necessary to subdivide each conductor (of energized cables and grounding system) into a number of smaller conductor segments, in order to achieve an accurate computation of the distribution of the conductor earth leakage current. In particular, CDEGS computation module uses a hybrid method for calculating responses from buried conductors, namely, a quasi-static approximation of Maxwell equations dealing with ground conductor segments leakage currents coupled with a circuit model that links the longitudinal current flow between segments based on Kirchhoff's laws. The computational methods used by the software module are included in the technical papers [85]–[92] provided by Dawalibi which is also the founder of SES company.

Since the DC interference is a result of the variations in earth potential due to the leakage of buried conductors, it is essential to describe the basic equations used for calculation of DC interference regarding earth's scalar potential and conductors' leakage current. These are described in the following paragraphs, as in [93].

Scalar Potential of earth and leakage current of buried conductors.

In the case where a DC current I_{dc} injected into a uniform soil though a point electrode perpendicular to the surface of the earth the current flows radially from the surface of the electrode into the soil. If it is assumed that the return point of the injected current is sufficiently remote, its earth potential variation can be neglected. If we consider a hemispherical surface with its center being the electrode and radius *s*. The area of this hemispherical surface is $2\pi s^2$ and the radial current density in the earth at the distance *s* is then $J = I_{dc}/2\pi s^2$. In extension the electric intensity in the earth in the radial direction at the distance *s* is (see Eq. (C-1)):

$$E(s) = \frac{I_{dc}*\rho}{2\pi s^2} \quad \text{(C-1)}$$

where ρ is the value of soil resistivity.

Moreover, the scalar potential of the earth at distance *s* from the electrode is the integral of the electric intensity between *s* and an infinitely remote point (see Eq. (C-2)).

$$U = \int_s^{\infty} E(s)ds = \frac{I_{dc}*\rho}{2\pi s} \quad \text{(C-2)}$$

The ratio potential to current, or the mutual resistance of the electrode and the point under consideration is then,

$$Q(s) = \frac{\rho}{2\pi s} \quad \text{(C-3)}$$

If we assume a two-point electrodes on the earth's surface (see Fig. C-1) where the current is injected into the earth via electrode 1 and returns back to the source via electrode 2. The mutual resistance at the point 3 in the ground or on the surface can be calculated through (C-4),

$$Q_{(1-2)3} = \frac{\rho}{2\pi}\left(\frac{1}{S_{13}} - \frac{1}{S_{23}}\right) \quad \text{(C-4)}$$

Where S_{13} and S_{23} are the distances between points 1 and 3 and points 2 and 3 respectively.

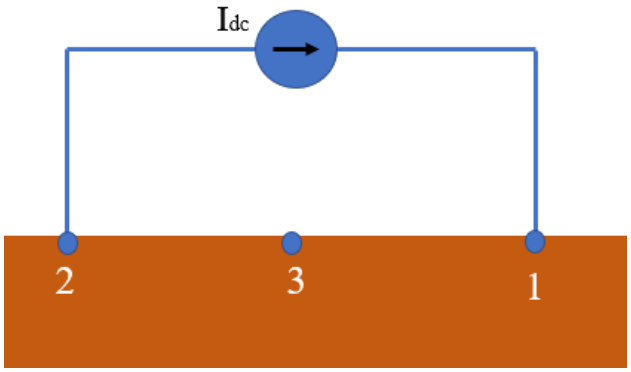

Figure C-1: Mutual resistance of electrodes 1 and 2 with 3

By adding an additional point 4, in the ground or on the surface the mutual resistance of the circuit between 1 and 2 with a circuit between 3 and 4 (see Fig. C-2) is:

$$Q_{(1-2)(3-4)} = Q_{(13)} - Q_{(23)} - Q_{(14)} - Q_{(24)} = \frac{\rho}{2\pi}\left(\frac{1}{S_{13}} - \frac{1}{S_{23}} - \frac{1}{S_{14}} + \frac{1}{S_{24}}\right) \quad \text{(C-5)}$$

Where S_{13} and S_{23} are the distances between points 1 and 3 and points 2 and 3 respectively.

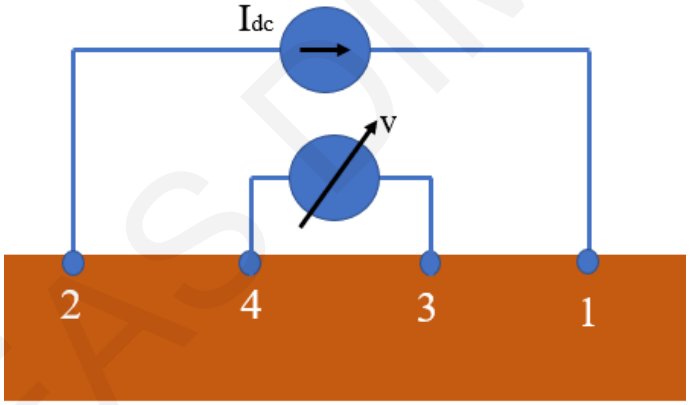

Figure C-2: Mutual resistance of the circuit between 1 and 2 with a circuit between 3 and 4

The above formulas are specifically applicable on point electrodes, however in most cases, the earthing electrodes are long cylindrical conductors or wires installed underground (i.e. earthing systems). In the case of horizontal or cylindrical conductors buried near the surface of the earth their resistance and scalar potential of earth can be obtained as follow.

Assumed that a buried conductor extends along *x*-axis between $x = -l/2$ and $x = l/2$, and the current I_{dc} is injected in the mid-point (see Fig. C-3). The conductor current at distance $x = u$ is $I(u)$. The reduction of current flowing along the conductor's segments quals to the current leaking out of the conductor. Consequently, the potential at a point x, y of the surrounding medium due to current leaving a conductor element du at $x = u$ is then,

$$dV(x,y) = \frac{dI(u)}{du}\frac{\rho}{4\pi}[(x-u)^2 + y^2]^{-1/2}\, du \quad \text{(C-6)}$$

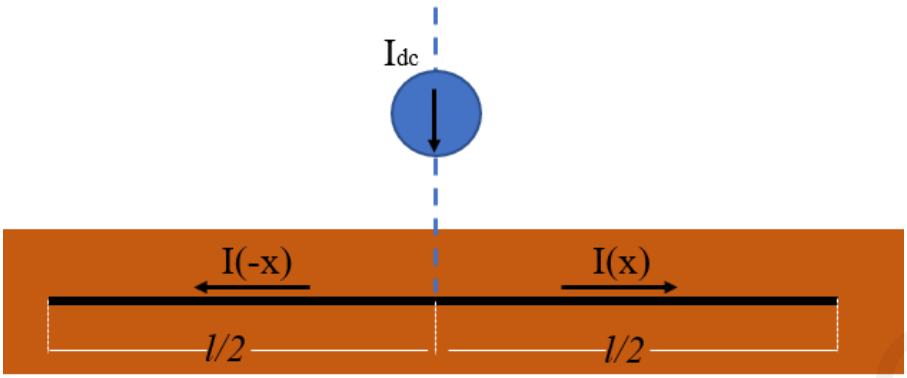

Figure C-3 Enegiazation of buried conductors

Where the term $\frac{dI(u)}{du}\,du$ is the mutual resistance between the two points in a soil medium with an infinite extent as described above. In this expression, the potential due to the current leaving a conductor element is the same as for a point source at the axis of the conductor. This assumption is permissible in dealing with long conductors. The expected scalar potential at a point x, y of the surrounding medium due to the leakage current along the entire conductor's elements is then,

$$V(x,y) = \frac{\rho}{4\pi}\int_{-l/2}^{l/2}[(x-u)^2 + y^2]^{-1/2}\,\frac{dI(u)}{du}\,du \quad \text{(C-7)}$$

Since the resistance of the conductor is relatively low (i.e. copper conductor) the voltage drop along the length of the conductor can be disregarded because is negligible. In this case in order to be satisfied the boundary conditions at the surface of the conductor $y = a$ is that $dV(x,a)/dx = 0$. In extension, the current distribution along the conductor should satisfy the following equation,

$$0 = \frac{d}{dx}\int_{-l/2}^{l/2}[(x-u)^2 + a^2]^{-1/2}\,\frac{dI(u)}{du}\,du \quad \text{(C-8)}$$

The distribution of the leakage current $dI(u)/du$ along the conductor can be given through successive approximations for the solution of equation (C-8). However, as a long conductor is energized in shunt (see Fig. C-3) the attenuation of the current and potential is to a first approximation exponential except at large distances from the energization point. To this extent the current $I(x)$ the potential to remote ground $V(x)$ and the leakage current $I'(x)$ can be expressed through the following basic equations:

$$\text{Current: } I(x) = I_{dc}\,e^{-\Gamma x} \quad \text{(C-9)}$$

$$\text{Voltage: } V(x) = I_{dc}\,K e^{-\Gamma x} \quad \text{(C-10)}$$

$$\text{Leakage: } I'(x) = -\Gamma\,I_{dc}\,e^{-\Gamma x} \quad \text{(C-11)}$$

Where the propagation constant Γ and the characteristic resistance K are related to the unit length longitudinal resistance R and the unit length leakage conductance of conductor to earth G. The leakage conductance G depends on the conductor's insulation and coating [91].

Numerical Methods for Analysis of DC Interference:

CDEGS uses various numerical computation methods or approaches to compute the earth leakage current distribution in the conductor segments. Depending on the parameters of the specific case study CDEGS incorporates a set of computational methods and approaches. Specific details for the numerical methods are included in [81], [85]–[92].

Numerical methods have been applied in several case studies for the analysis of corrosion problems resulting from DC stray current interference. The majority of these case studies examine the impact of DC stray currents on metallic pipelines buried into the soil [94]–[101]. The source of DC interference can be an external DC source (i.e. an impressed current cathodic protection system of a second pipeline) or may be due to the galvanic coupling [95] with a third-party metallic infrastructure. Besides, in some case studies, the under-examination system (i.e. Ship Hull) may be submerged in seawater [101], [102].

The analysis of the DC interference problem consists of 3 main stages:

***Stage-1*:** Involves the formulation of the mathematical model that reproduces the problem through a set of mathematical equations. More specifically, interrelated equations describe the current density and the electric field [94], [96]–[99], [102], [103] within the electrolytic medium (i.e. soil, seawater) and the buried metallic infrastructure (i.e. pipeline). Most of the equations are represented in the form of partial differential equations. Also, boundaries conditions are defined between the involved elements (i.e. metallic infrastructure and soil) based on the specific assumptions considered in the modelling procedure. However, these equations cannot be solved analytically, due to the high complexity of the problem. To this extent, the application of a numerical method is required.

***Stage-2*:** Involves the integration of boundary conditions and the equations formulating in Stage-1 in an appropriate solver to calculate the response of the system (due to the impact of DC stray currents). Several commercially available software simulators calculate the DC interference by incorporate several numerical methods for the solution of the equations which describe the problem [79], [104]–[106]. Advanced, user-friendly software allowing the reproduction of the under-examination system in an object-based graphical environment.

The most commonly applied numerical methods [94][107] are, the finite-element method (FEM), the boundary-element method (BEM), and the finite-difference method (FDM).

FEM is a common powerful numerical method used in engineering applications for the solution of partial differential equations in two or three space variables. The solution of the problem is achieved by the subdivision of the examined system into smaller, simpler to handle parts that are called finite elements. In particular, space discretisation is performed by the construction of a mesh of the system which has a finite number of points. The FEM formulation of a boundary value problem finally results in a system of algebraic equations. The unknown function is approximated by linear combinations of basic functions which are derived from the fundamental partial differential equations for each mesh point. Finally, FEM approximates a solution with the use of variational methods [107] in order to minimise the computational error.

BEM is an alternative numerical method used to solve partial differential equations which can form integral equations. The BEM based on the formation of boundary conditions at elements which are derived through discretisation of the boundaries of the main problem. Also, a system of algebraic equations is developed to solve for the unknown boundary values. Finally, the integral equation is used in the post-processing stage to calculate the response at any boundary element.

FDM can solve partial differential equations by transforming them into a system of algebraic equations. The main difference of this method is that the differential equations are solved by approximating them with difference equations [107]. Also, the approximation of derivatives by finite differences is performed for the solution of the differential equations.

***Stage-3*:** Performs the evaluation of the calculated values in terms of corrosion. The calculated current density and potential on the surface of the under-examination system are examined since these values are directly related to the corrosive activity. As a post-processing procedure [94], [101], the corrosion mass loss is calculated based on the electrochemical behavior of the system. Moreover, for the identification of the factors that influence the problem the repetition of stages 1, 2 may is required, considering different input parameters. Also, the effectiveness of potential mitigation measures can be examined. Furthermore, the sensitivity analysis of critical factors (i.e. soil resistivity, coating resistivity) facilitates the understanding of DC interference problem on the interfered structures and the assessment of corrosion risk. Finally, it worth mentioned that the impact of coating

holidays is a subject that receives special attention in pipeline systems [96]–[98], [100], [101].

Also, an additional *4th stage* may be introduced for the validation of modelling procedures involving the comparison of calculated results with filed measurements or experimental laboratory tests [98]. For the fine-tuning of numerical models, an adjustment of input parameters may be required in order to converge their calculations with measuring values.

.

References

[1] "Railway applications — Fixed installations — Part 1: Protective provisions relating to electrical safety and earthing," *EN Stand. 50122-1*, 1998.

[2] "Railway applications — Fixed installations —Part 2: Protective provisions aginst the effects of stray currents caused by d.c. traction systems," *EN Stand. 50122-2*, 2013.

[3] "Cathodic Protection of buried or immersed metallic structures- General principles and application for pipelines," *EN Stand. 12954*, 2001.

[4] "Safety of power converters for use in photovoltaic power systems-Part 2: Particular requirements for inverters," *IEC Stand. 62109-2*, 2011.

[5] "Design of earth electrode stations for high-voltage direct current (HVDC) links - General guidelines," *IEC TS 62344*, pp. 1–10, 2013.

[6] Cigre, *General Guidelines For HVDC Electrode Design*. .

[7] "Protection against corrosion by stray current from direct current systems," *EN Stand. 50162*, 2004.

[8] "Electric cables for photovoltaic systems" *EN Stand. 50618*, 2013.

[9] P. R. Roberge, "*Handbook of Corrosion Engineering", McGraw-Hill, New York*. 1999

[10] P. R. Roberge, "*Corrosion Engineering: Principles and Practice*", *McGraw-Hill, New York*, 2008

[11] "Cathodic Protection measurement techniques," *EN Stand. 13509*, 2003.

[12] C. A. Charalambous and P. Aylott, "Dynamic stray current evaluations on cut-and-cover sections of DC metro systems," *IEEE Trans. Veh. Technol.*, vol. 63, no. 8, pp. 3530–3538, 2014, doi: 10.1109/TVT.2014.2304522.

[13] C. A. Charalambous, I. Cotton, and P. Aylott, "Modeling for preliminary stray current design assessments: The effect of crosstrack regeneration supply," *IEEE Trans. Power Deliv.*, vol. 28, no. 3, pp. 1899–1908, 2013, doi: 10.1109/TPWRD.2013.2259849.

[14] C. A. Charalambous, I. Cotton, P. Aylott, and N. D. Kokkinos, "A holistic stray current assessment of bored tunnel sections of DC transit systems," *IEEE Trans. Power Deliv.*, vol. 28, no. 2, pp. 1048–1056, 2013, doi: 10.1109/TPWRD.2012.2227835.

[15] C. A. Charalambos, "Stray Current Control and Corrosion for Dc Mass Transit Systems," vol. 54, no. 2, pp. 722–730, 2005.

[16] A. Dolara, F. Foiadelli, and S. Leva, "Stray current effects mitigation in subway tunnels," *IEEE Trans. Power Deliv.*, vol. 27, no. 4, pp. 2304–2311, 2012, doi: 10.1109/TPWRD.2012.2203829.

[17] "Photovoltaic (PV) arrays – Design requirements Groupes," *IEC Stand. 62548*, 2016.

[18] J. C. Hernández, P. G. Vidal, and A. Medina, “Characterization of the insulation and leakage currents of PV generators: Relevance for human safety,” *Renew. Energy*, vol. 35, no. 3, pp. 593–601, 2010, doi: 10.1016/j.renene.2009.08.006.

[19] M. A. Islam, M. Hasanuzzaman, and N. A. Rahim, “Effect of Different Factors on the Leakage Current Behavior of Silicon Photovoltaic Modules at High Voltage Stress,” *IEEE J. Photovoltaics*, vol. 8, no. 5, pp. 1259–1265, 2018, doi: 10.1109/JPHOTOV.2018.2841500.

[20] M. K. Alam, F. Khan, J. Johnson, and J. Flicker, “A Comprehensive Review of Catastrophic Faults in Mitigation Techniques,” *IEEE J. Photovoltaics*, vol. 5, no. 3, pp. 982–997, 2015.

[21] “Standard for Inverters, Converters, Controllers and Interconnection System Equipment for Use With Distributed Energy Resources,” *Stand. UL-1741*, 2010.

[22] E.E. Stansbury, R.A. Buchanan "*Fundamentials of electrochemical corrosion*" ASM International 2000

[23] W. Von Baeckmann et al., "*Handbook of cathodic corrosion protection: theory and practice of electrochemical protection processes"*, Gulf Proffesional Publishing, 1997

[24] “Assessment of the effectiveness of cathodic protection based on coupon measurements,” *ISO 22426*, 2020.

[25] “Petroleum, Petrochemical and natural gas industries. — Stray Current Interference on Pipeline Systems,” *ISO 21857*, 2019.

[26] B. Brooks, “The Ground-Fault Protection BLIND SPOT: A Safety Concern for Larger Photovoltaic Systems in the United States,” *Sol. Am. Board Codes Stand.*, 2012.

[27] M. C. Falvo and S. Capparella, “Safety issues in PV systems: Design choices for a secure fault detection and for preventing fire risk,” *Case Stud. Fire Saf.*, vol. 3, pp. 1–16, 2015, doi: 10.1016/j.csfs.2014.11.002.

[28] J. C. Hernández and P. G. Vidal, “Guidelines for protection against electric shock in PV generators,” *IEEE Trans. Energy Convers.*, vol. 24, no. 1, pp. 274–282, 2009, doi: 10.1109/TEC.2008.2008865.

[29] “Low-voltage electrical installations – Part 4-41: Protection for safety – Protection against electric shock,” *IEC Stand. 60364-4-41*, 2005.

[30] “Protection against electric shock – Common aspects for installation and equipment,” *IEC Stand. 61140*, 2016.

[31] “Protection against lightning - Part 3: Physical damage to structures and life hazard,” *IEC Stand. 62305-3*, 2011.

[32] “Low-voltage electrical installations - Part 7-712: Requirements for special installations or locations - Photovoltaic (PV) systems,” *IEC Stand. 60364-7-712*, 2016.

[33] “Ground-Fault Circuit- Interrupters,” *Stand. UL-943*, vol. 5, 2016.

[34] J. C. W. W.I. Bower, “Analysis of grounded and ungrounded photovoltaic systems,” 1994, doi: 10.1109/WCPEC.1994.520083.

[35] "Guide for Safety In AC Substation Grounding," *IEEE Stand. 80*, 2000, doi: 10.1109/IEEESTD.2000.91902.

[36] J. Hylský, D. Strachala, P. Vyroubal, P. Čudek, J. Vaněk, and P. Vanýsek, "Effect of negative potential on the extent of PID degradation in photovoltaic power plant in a real operation mode," *Microelectron. Reliab.*, vol. 85, no. September 2017, pp. 12–18, 2018, doi: 10.1016/j.microrel.2018.04.003.

[37] W. Oh, S. Bae, S. Il Chan, H. S. Lee, D. Kim, and N. Park, "Field degradation prediction of potential induced degradation of the crystalline silicon photovoltaic modules based on accelerated test and climatic data," *Microelectron. Reliab.*, vol. 76–77, pp. 596–600, 2017, doi: 10.1016/j.microrel.2017.07.079.

[38] F. Martínez-Moreno, G. Figueiredo, and E. Lorenzo, "In-the-field PID related experiences," *Sol. Energy Mater. Sol. Cells*, vol. 174, no. July 2017, pp. 485–493, 2018, doi: 10.1016/j.solmat.2017.09.037.

[39] A. S. Ayub, W. H. Siew, and F. Peer, "Grounding strategies for solar PV panels," *2018 IEEE Int. Symp. Electromagn. Compat. 2018 IEEE Asia-Pacific Symp. Electromagn. Compat. EMC/APEMC 2018*, pp. 418–422, 2018, doi: 10.1109/ISEMC.2018.8393812.

[40] C. A. Charalambous, N. D. Kokkinos, and N. Christofides, "External lightning protection and grounding in large-scale photovoltaic applications," *IEEE Trans. Electromagn. Compat.*, vol. 56, no. 2, pp. 427–434, 2014, doi: 10.1109/TEMC.2013.2280027.

[41] "Junction boxes for photovoltaic modules - Safety requirements and tests," *IEC Stand. 62709*, 2015.

[42] "National Electrical Code - 2008 Edition," *NFPA 70*, 2008.

[43] Machael Boxwell, *Solar Electricity Handbook*. 2017 Edition.

[44] "Low-Voltage Surge Protective Devices - Surge Protective Devices for Specific Application Including D.C. Part 11: Requirements and Tests for SPDs in Photovoltaic Applications," *EN Stand. 50539-11*, 2013.

[45] C. Shinoda, T. Hashizume, T. Tani, Y. Tanaka, and T. Takada, "Consideration of mechanism of DC leakage current peak in XLPE cables," *Proc. IEEE Int. Conf. Prop. Appl. Dielectr. Mater.*, vol. 1, pp. 402–405, 1997.

[46] H. Muto, J. Furukuwa Electric Co. Ltd., Chiba, and ; Y. Yamashita ; Y. Maruyuma ; Z. Iwata, "A study on leakage current characteristics of field aged XLPE cable," *Proc. 3rd Int. Conf. Prop. Appl. Dielectr. Mater.*, 1991, doi: 10.1109/ICPADM.1991.172105.

[47] K. Suenaga, K. Uchida, and N. Hozumi, "Location of water tree degraded point along XLPE cable line using DC voltage," *Proc. 2008 Int. Conf. Cond. Monit. Diagnosis, C. 2008*, pp. 1224–1227, 2007, doi: 10.1109/CMD.2008.4580509.

[48] "Information technology - Generic cabling systems - Part 1: General requirements," *EN Stand. 50173-1*, 2018.

[49] "Safety of power converters for use in photovoltaic power systems -- Part 1. General requirements," *IEC Stand. 62109-1*, 2014.

[50] F. D. Freijedo *et al.*, "Eliminating Ground Current in a Transformerless Photovoltaic Application," *IEEE Trans. Energy Convers.*, vol. 25, no. 1, pp. 140–147, 2010, doi: 10.1109/tec.2009.2037810.

[51] X. Guo, "Three-phase CH7 inverter with a new space vector modulation to reduce leakage current for transformerless photovoltaic systems," *IEEE J. Emerg. Sel. Top. Power Electron.*, vol. 5, no. 2, pp. 708–712, 2017, doi: 10.1109/JESTPE.2017.2662015.

[52] S. A. Khan, Y. Guo, and J. Zhu, "A high efficiency transformerless PV grid-Connected inverter with leakage current suppression," *Proc. 9th Int. Conf. Electr. Comput. Eng. ICECE 2016*, pp. 190–193, 2017, doi: 10.1109/ICECE.2016.7853888.

[53] "Terrestrial photovoltaic (PV) modules – Design qualification and type approval – Part 1-1: Special requirements for testing of crystalline silicon photovoltaic (PV) modules," *IEC Stand. 61215-1-1*, 2016.

[54] "Terrestrial photovoltaic (PV) modules - Design qualification and type approval - Part 1-2: Special requirements for testing of thin-film Cadmium Telluride (CdTe) based photovoltaic (PV) modules," *EN Stand. 61215-1-2*, 2017.

[55] "Terrestrial photovoltaic (PV) modules - Design qualification and type approval - Part 1-3: Special requirements for testing of thin-film amorphous silicon based photovoltaic (PV) modules," *EN Stand. 61215-1-3*, pp. 1–6, 2017.

[56] "Terrestrial photovoltaic (PV) modules - Design qualification and type approval - Part 1-4: Special requirements for testing of thin-film Cu(In,GA)(S,Se)2 based photovoltaic (PV) modules," *EN Stand. 61215-1-4*, pp. 1–6, 2017.

[57] J. Flicker, J. Johnson, M. Albers, and G. Ball, "Recommendations for CSM and Riso ground fault detector trip thresholds," *2014 IEEE 40th Photovolt. Spec. Conf. PVSC 2014*, pp. 3391–3397, 2014, doi: 10.1109/PVSC.2014.6925659.

[58] G. Ball *et al.*, "Inverter Ground- Fault Detection 'Blind Spot' and Mitigation Methods," *Sol. Am. Board Codes Stand.*, no. June 2013, 2013.

[59] T. D. Eish, F. M. H. Youssef, and S. S. El-Dessouky, "Effect of temperature rise and water contamination of leakage current in underwater used XLPE insulated power cables.," *Conference Record of IEEE International Symposium on Electrical Insulation*, vol. 1988. pp. 343–346, 1988.

[60] Y. Du, P. Geng, J. Song, M. Tian, and D. Pang, "Influence of temperature and frequency on leakage current of XLPE cable insulation," *ICHVE 2016 - 2016 IEEE Int. Conf. High Volt. Eng. Appl.*, no. 2, pp. 1–4, 2016, doi: 10.1109/ICHVE.2016.7800648.

[61] Y. Zhao, J. F. De Palma, J. Mosesian, R. Lyons, and B. Lehman, "Line-line fault analysis and protection challenges in solar photovoltaic arrays," *IEEE Trans. Ind. Electron.*, vol. 60, no. 9, pp. 3784–3795, 2013, doi: 10.1109/TIE.2012.2205355.

[62] M. K. Alam, F. H. Khan, S. L. City, J. Johnson, J. Flicker, and S. N. Laboratories, "PV faults: Overview, modeling, prevention and detection techniques," 2013.

[63] J.-L. Chen, C.-C. Kao, H.-T. Yau, C.-H. Lin, C.-L. Kuo, and S.-J. Chen, "Photovoltaic Energy Conversion System Fault Detection Using Fractional-Order Color Relation Classifier in Microdistribution Systems," *IEEE Trans. Smart Grid*, vol. 8, no. 3, pp. 1163–1172, 2015, doi: 10.1109/tsg.2015.2478855.

[64] Y. Zhao, R. Ball, J. Mosesian, J. F. De Palma, and B. Lehman, "Graph-based semi-supervised learning for fault detection and classification in solar photovoltaic arrays," *IEEE Trans. Power Electron.*, vol. 30, no. 5, pp. 2848–2858, 2015, doi: 10.1109/TPEL.2014.2364203.

[65] J.-L. Chen *et al.*, "DC-side fault detection for photovoltaic energy conversion system using fractional-order dynamic-error-based fuzzy Petri net integrated with intelligent meters," *IET Renew. Power Gener.*, vol. 10, no. 9, pp. 1318–1327, 2016, doi: 10.1049/iet-rpg.2015.0517.

[66] M. J. Albers and G. Ball, "Comparative Evaluation of DC Fault-Mitigation Techniques in Large PV Systems," *IEEE J. Photovoltaics*, vol. 5, no. 4, pp. 1169–1174, 2015, doi: 10.1109/JPHOTOV.2015.2422142.

[67] J. C. Wiles, "Photovoltaic System Grounding," *Sol. Am. Board Codes Stand.*, 2012.

[68] J. Flicker and J. Johnson, "Analysis of fuses for blind spot ground fault detection in photovoltaic power systems," *Sol. Am. Board Codes Stand.*, no. June, 2013.

[69] T. Kerekes, R. Teodorescu, M. Liserre, C. Klumpner, and M. Sumner, "Evaluation of three-phase transformerless photovoltaic inverter topologies," *IEEE Trans. Power Electron.*, vol. 24, no. 9, pp. 2202–2211, 2009, doi: 10.1109/TPEL.2009.2020800.

[70] J. M. Shen, H. L. Jou, and J. C. Wu, "Novel transformerless grid-connected power converter with negative grounding for photovoltaic generation system," *IEEE Trans. Power Electron.*, vol. 27, no. 4, pp. 1818–1829, 2012, doi: 10.1109/TPEL.2011.2170435.

[71] "Electrical Safety in Low Voltage Distribution Systems Up to 1 000 Va.c. and 1 500 V d.c.—Equipment for Testing, Measuring or Monitoring of Protective Measures—Part 8: Insulation Monitoring Devices for IT Systems," *IEC Stand. 61557-8*, 2014.

[72] Karl Schepp, "Patent-Adapted Measuring Pulse EP0654673A1," *Karl Dipl-Ing Walther Bender Co KG GmbH*, 1995.

[73] "Type F and Type B Residual Current Operated Circuit-Breakers With and Without Integral Overcurrent Protection for Household and Similar Uses," *EN Stand. 62423*, vol. 2007, 2009.

[74] Y. Zhao, L. Yang, B. Lehman, J. F. De Palma, J. Mosesian, and R. Lyons, "Decision tree-based fault detection and classification in solar photovoltaic arrays," *Conf. Proc. - IEEE Appl. Power Electron. Conf. Expo. - APEC*, pp. 93–99, 2012, doi: 10.1109/APEC.2012.6165803.

[75] Y. Zhao, B. Lehman, J. F. De Palma, J. Mosesian, and R. Lyons, "Fault analysis in solar PV arrays under: Low irradiance conditions and reverse connections," *Conf. Rec. IEEE Photovolt. Spec. Conf.*, pp. 002000–002005, 2011

[76] V. Salas, E. Olías, M. Alonso, F. Chenlo, and A. Barrado, "DC current injection into the network from PV grid inverters," *Conf. Rec. 2006 IEEE 4th World Conf. Photovolt. Energy Conversion, WCPEC-4*, vol. 2, no. March 2015, pp. 2371–2374, 2007, doi: 10.1109/WCPEC.2006.279668.

[77] M. Tullmin and P. R. Roberge, "Corrosion of Metallic Materials," *IEEE Trans. Reliab.*, vol. 44, no. 2, pp. 271–278, 1995, doi: 10.1109/24.387383.

[78] A. Demetriou, D. Buxton, and C. A. Charalambous, "Stray Current DC Corrosion

Blind Spots Inherent to Large PV Systems Fault Detection Mechanisms: Elaboration of a Novel Concept," *IEEE Trans. Power Deliv.*, vol. 33, no. 1, pp. 3–11, Feb. 2018, doi: 10.1109/TPWRD.2016.2538789.

[79] Safe Engineering Services & Technologies Ltd, "CDEGS Software." Montreal, Quebec, Canada Est. 1978.

[80] BSI Standards Publication, "Petroleum and natural gas industries — External coatings for buried or submerged pipelines used in pipeline transportation systems Part 3: Field joint coatings," *ISO Stand. 21809-3*, 2016.

[81] F. P. Dawalibi, "Study of Influence of Buried Metallic Structure on Soil Resistivity measurements," *Power Trans. Power Deliv.*, vol. 13, no. 2, pp. 356–365, 1998.

[82] A. Pal and P. K. Khare, "Electrical conductivity behaviour of pure and polyblends samples of polyvinyl chloride (PVC) and polymethyl methacrylate (PMMA)," *J. Electrostat.*, vol. 71, no. 6, pp. 976–986, 2013, doi: 10.1016/j.elstat.2013.09.005.

[83] A. Ogunsola, A. Mariscotti, and L. Sandrolini, "Estimation of stray current from a DC-electrified railway and impressed potential on a buried pipe," *IEEE Trans. Power Deliv.*, vol. 27, no. 4, pp. 2238–2246, 2012

[84] "Petroleum, petrochemical and natural gas industries — Cathodic protection of pipeline systems — Part 1: On-land pipelines," *ISO 15589-1*, 2017.

[85] F. P. Dawalibi, D. Mukhedkar, and E. Polytechnique, "Resistance Calculation of Interconnected Grounding Electrodes," *IEEE Trans. Power Appar. Syst.*, no. 1, pp. 59–65, 1977.

[86] F. P. Dawalibi and D. Mukhedkar, "Multi-Step Analysis of Interconnected Grounding Electrodes," *IEEE Trans. Power Appar. Syst.*, vol. PAS-95, pp. 113–119, 1976.

[87] F. P. Dawalibi. and D. Mukhedkar, "Optimum Design of Substation Grounding in Two-Layer Earth Structure - Part III, Study of Grounding Grids Performance and New Electrode Configurations," *IEEE Trans. Power Appar. Syst.*, vol. PAS-94, pp. 267–272, 1975.

[88] F. P. Dawalibi. and D. Mukhedkar, "Optimum Design of Substation Grounding in Two-Layer Earth Structure - Part II, Comparison Between Theoretical and Experimental Results," *IEEE Trans. Power Appar. Syst.*, vol. PAS-94, pp. 262–266, 1975.

[89] F. P. Dawalibi. and D. Mukhedkar, "Optimum Design of Substation Grounding in Two-Layer Earth Structure - Part I, Analytical Study," *IEEE Trans. Power Appar. Syst.*, vol. PAS-94, pp. 252–258, 1975.

[90] F. P. Dawalibi. and D. Mukhedkar, "Ground Electrode Resistance Measurements in Nonuniform Soils," *IEEE Trans. Power Appar. Syst.*, vol. PAS-93, pp. 109–115, 1974.

[91] D. Mukhedkar, Y. Gervais, and F. Dawalibi, "Modelling of potential distribution around a grounding electrode," *IEEE Trans. Power Appar. Syst.*, vol. PAS-92, no. 5, pp. 1455–1459, 1973, doi: 10.1109/TPAS.1973.293689.

[92] F. Dawalibi and A. Pinho, "Computerized Analysis of Power Systems and Gas Pipelines Proximity Effects," *IEEE Trans. Power Deliv.*, vol. 1, no. 4, pp. 40–48,

1986, doi: 10.1109/MPER.1986.5527710.

[93] Sunde, E.D. (1968) Earth Conduction Effects in Transmission Systems. Dover Publications, New York.

[94] I. A. Metwally, H. M. Al-Mandhari, A. Gastli, and Z. Nadir, "Factors affecting cathodic-protection interference," *Eng. Anal. Bound. Elem.*, vol. 31, no. 6, pp. 485–493, 2007, doi: 10.1016/j.enganabound.2006.11.003.

[95] R. A. Holser, G. Prentice, R. B. Pond, and R. J. Guanti, "Current distributions in galvanically coupled and cathodically protected tubes," *Corrosion*, vol. 48, no. 4, pp. 332–340, 1992, doi: 10.5006/1.3315939.

[96] M. E. Orazem, J. M. Esteban, K. J. Kennelley, and R. M. Degerstedt, "Mathematical Models for Cathodic Protection of an Underground Pipeline with Coating Holidays: Part 2 - Case Studies of Parallel Anode Cathodic Protection Systems," *Corros.*, vol. 53, no. 6, pp. 427–436, 1997, doi: 10.5006/1.3280485.

[97] D. P. Riemer and M. E. Orazem, "Application of boundary element models to predict the effectiveness of coupons for accessing cathodic protection of buried structures," *NACE - Int. Corros. Conf. Ser.*, vol. 2000-March, no. August, pp. 794–800, 2000.

[98] S. L. D. C. Brasil, "Simulation of coating failures on cathodically protected pipelines-experimental and numerical results," *Corrosion*, vol. 56, no. 11, pp. 1180–1188, 2000, doi: 10.5006/1.3294402.

[99] M. Purcar, B. Van den Bossche, L. Bortels, J. Deconinck, and P. Wesselius, "Numerical 3-D simulation of a cathodic protection system for a buried pipe segment surrounded by a load relieving U-shaped vault," *Corrosion*, vol. 59, no. 11, pp. 1019–1028, 2003, doi: 10.5006/1.3277520.

[100] L. Bortels and J. Deconinck, "Numerical simulation of the cathodic protection of pipeline networks under various stray current interferences," *Model. Cathodic Prot. Syst.*, vol. 7, pp. 197–224, 2005, doi: 10.2495/1-85312-889-9/08.

[101] R. Weber, "Simulation As an Aid To Steam System Design.," *Proc. Summer Comput. Simul. Conf.*, pp. 218–222.

[102] J. Trevelyan and H. P. Hack, "Analysis of stray current corrosion problems using the boundary element method," *Int. Conf. Bound. Elem. Technol.*, pp. 347–356, 1994.

[103] G. Cui, Z. L. Li, C. Yang, and M. Wang, "The influence of DC stray current on pipeline corrosion," *Pet. Sci.*, vol. 13, no. 1, pp. 135–145, 2016,

[104] Comsol software, COMSOL Multyphysics .https://www.comsol.com

[105] ELSYCA software documentation: CatPro V1.4. July 2004. Available: /http://www.elsyca.com

[106] BEASY software user guide, computational mechanics BEASY Version 10. Southampton, UK, 2005. Available: /http://www. beasy.com

[107] M. N. O. Sadiku and A. F. Peterson, "A comparison of numerical methods for computing electromagnetic fields," *Conf. Proc. - IEEE SOUTHEASTCON*, vol. 1, pp. 42–47, 1990, doi: 10.1109/secon.1990.117766.

List of Publications

Peer-Reviewed Journal Papers resulted from Ph.D. Candidacy.

1. C. A. Charalambous, **A. Dimitriou** and N. D. Kokkinos, "Impact of Photovoltaic-Oriented DC Stray Current Corrosion on Large-Scale Solar Farms' Grounding and Third-Party Infrastructure: Modeling and Assessment," in *IEEE Transactions on Industry Applications*, vol. 51, no. 6, pp. 5421-5430, Nov.-Dec. 2015.

2. **A. Dimitriou**, D. Buxton and C. A. Charalambous, "Stray Current DC Corrosion Blind Spots Inherent to Large PV Systems Fault Detection Mechanisms: Elaboration of a Novel Concept," in *IEEE Transactions on Power Delivery*, vol. 33, no. 1, pp. 3-11, Feb. 2018.

3. **A. Dimitriou** and C. A. Charalambous, "DC Interference Modelling for Assessing the Impact of Sustained DC Faults of Grounded Photovoltaic Systems on Third-Party Infrastructure," in *IEEE Transactions on Industrial Electronics*, vol. 66, no. 4, pp. 2935-2945, April 2019.

Peer-Reviewed Journal Papers in Related Fields:

4. C. A. Charalambous, **A. Dimitriou**, A. Lazari and A. Nikolaidis, "Effects of Electromagnetic Interference on Underground Pipelines caused by the Operation of High Voltage A.C. Traction Systems: The Impact of Harmonics," in *IEEE Transactions on Power Delivery*, doi: 10.1109/TPWRD.2018.2803080, Accepted Feb. 2018

5. C. A. Charalambous, **A. Dimitriou**, N. Kioupis, T. Manolis and N. Kokkinos, "Wall Fusion of Buried Pipelines due to Direct Lightning Strikes: Field, Laboratory and Simulation Investigation of the Damaging Mechanism," in *IEEE Transactions on Power Delivery*, doi: 10.1109/TPWRD.2019.2925622

6. D. Chrysostomou, **A. Dimitriou**, N. Kokkinos, C.A Charalambous, “Short-Term Electromagnetic Interference on a Buried Gas Pipeline Caused by Critical Fault Events of a Wind Park: A Realistic Case Study”, IEEE Transactions on Industry Applications, Accepted January 2020 (DOI: 10.1109/TIA.2020.2965494).

Refereed Conferences:

1. **A. Dimitriou**, C. A. Charalambous and N. Kokkinos, "Integrating the loss of economic value in lightning-related risk assessments of large scale photovoltaic systems participating in regulated and competitive energy markets," *2016 33rd International Conference on Lightning Protection (ICLP)*, Estoril, 2016, pp. 1-6.

2. **A. Dimitriou**, A. L. Lazari and C. A. Charalambous, "Understanding of DC leakage and faults in floating photovoltaic systems: Trojan horse to undermine metallic infrastructure and safety," *2017 IEEE Manchester PowerTech*, Manchester, 2017, pp. 1-6.

3. **A. Dimitriou** and C. A. Charalambous " Interpreting Coating Stress Voltages on Underground Gas Pipelines Due to Lightning Strikes on Adjacent Power Lines," *2018 34th International Conference on Lightning Protection (ICLP)*, Rzersow, 2018

4. **A. Dimitriou** and C. A. Charalambous " Comprehensive Modelling Technique to Allow DC Interference Evaluations on Buried Pipeline Systems near Photovoltaic Installations," *2018 IEEE International Conference on High Voltage Engineering and Application (ICHVE, Athens, 2018)*

5. C. A. Charalambous, **A. Dimitriou** and A. L. Lazari «AC Interference Evaluation of a Cathodically Protected Subsea Structure," *2018 IEEE International Conference on High Voltage Engineering and Application (ICHVE, Athens, 2018)*

6. D. Chrysostomou, **A. Dimitriou**, N. Kokkinos and C. A. Charalambous, "Short-Term Electromagnetic Interference on a Buried Gas Pipeline Caused by Critical Fault Events of a Wind Park: A Realistic Case Study," *2019 IEEE International Conference on Environment and Electrical Engineering and 2019 IEEE Industrial and Commercial Power Systems Europe (EEEIC / I&CPS Europe)*, Genova, Italy, 2019, pp. 1-6.doi: 10.1109/EEEIC.2019.8783794

7. C. A. Charalambous, **A. Dimitriou**, I. Gonos and T. A. Papadopoulos, "Modelling and Assessment of Short-Term Electromagnetic Interference on a Railway System from Pole-to-Ground Faults on HVDC Cable Networks," *2019 IEEE International Conference on Environment and Electrical Engineering and 2019 IEEE Industrial and Commercial Power Systems Europe (EEEIC / I&CPS Europe)*, Genova, Italy, 2019, pp. 1-6. doi: 10.1109/EEEIC.2019.8783289